

Ferrofluid-based deformable robotic sheet with magnetic  
field control

March 2019

Tone Tadayuki

Ferrofluid-based deformable robotic sheet with magnetic  
field control

School of Integrative and Global Majors  
Ph.D. Program in Empowerment Informatics  
University of Tsukuba

March 2019

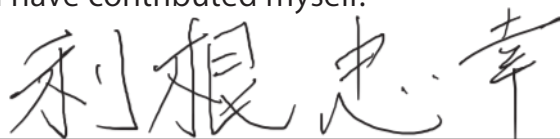
Tone Tadayuki

## Declaration of Authorship

I, Tadayuki TONE, declare that this thesis titled, "Ferrofluid-based deformable robotic sheet with magnetic field control" and the work presented in it are my own. I confirm that:

- This work was done wholly or mainly while in candidature for a research degree at this University.
- Where any part of this thesis has previously been submitted for a degree or any other qualification at this University or any other institution, this has been clearly stated.
- Where I have consulted the published work of others, this is always clearly attributed.
- Where I have quoted from the work of others, the source is always given. With the exception of such quotations, this thesis is entirely my own work.
- I have acknowledged all main sources of help.
- Where the thesis is based on work done by myself jointly with others, I have made clear exactly what was done by others and what I have contributed myself.

Signed:

Handwritten signature in black ink, reading "利根忠幸" (Tone Tadayuki).

Date: February 14th, 2019

---



## *Abstract*

The ferrofluid-based deformable robotic sheet and object manipulation using its deformation characteristics with magnetic field control are described. Through the object manipulation experiment, the applicability to the droplet manipulation field is verified. The robotic sheet has a layered structure of a ferrofluid and thin films and its shape is a sheet-like shape. In the robotic sheet, the ferrofluid freely moves and gathers around a source of magnetic field. A ferrofluid can deform its shape under the influence of a magnetic field generated by the electromagnets. Using this deformation characteristics, the robotic sheet changes its surface shape and a convex appeared on it. An object moves on a downward gradient of the convex. By controlling the activation of the electromagnets, the robotic sheet transports the objects. Two types of the robotic sheet are proposed. One uses the polyethylene films as thin films, and the other uses polytetrafluoroethylene (PTFE) films. The former is used for transporting two balls and a thin plate since the polyethylene films have high robustness against breakage due to contact with the objects. The latter is used for transporting droplets since the PTFE films have a high water and oil repellency. Also, the manipulation methods for a ball, a plate, and a droplet are proposed. Three experiments are conducted: verification of the effect of the thin film on the ferrofluid deformation in the robotic sheet, measurement of the mass range of the object which the robotic sheet lifts up, and measurement of the magnetic responsiveness of the robotic sheet. The object manipulation is also realized using the robotic sheet. In this paper, the robotic sheet is set on a flat and channel-like surface, and the object manipulation was realized. On the flat surface, two balls and a thin plate is transported using the robotic sheet with polyethylene films and a droplet is transported and mixed using the robotic sheet with PTFE films using the proposed methods. Object movements on the robotic sheet are rotation or slides. Therefore, the ball and plate is used as the target object. In the manipulation of a droplet, droplet mixing and droplet transportation are realized. On the channel-like surface, a ball is moved through the channel of the robotic sheet with polyethylene films by changing the inner surface of the channel. The achievement contributes to the technology for soft robotics and advanced control, opening new aspects for fluid-based three-dimensional manipulations.



# *Acknowledgements*

My greatest gratitude is for my supervisor Prof. Kenji Suzuki for giving me the opportunity to be part of his laboratory, for his valuable support, and guidance. He encouraged me to continue pursuing this work even when it seemed there was no hope in succeeding. The work done in this thesis could not have been accomplished without him.

My gratitude is also for Prof. Yoshiyuki Sankai, Prof. Hiromi Mochiyama, Prof. Yasushi Hada, Prof. Kikue Hidaka, and Prof. Shingo Maeda for their valuable supervision and inspiring comments on this work.

I would also like to thank my family and best friends for their friendship, and support.

Also, I would also like to thank all the members of the Artificial Intelligence Laboratory for their friendship, and support.

I was able to do my research thanks to all the predecessors who contributed to development of our civilization and culture. I appreciate them all.





# Contents

<b>Declaration of Authorship</b>	<b>i</b>
<b>Abstract</b>	<b>iii</b>
<b>Acknowledgements</b>	<b>v</b>
<b>1 Introduction</b>	<b>1</b>
1.1 Background . . . . .	1
1.2 Related researches . . . . .	3
1.3 Objective . . . . .	7
1.3.1 Research objectives . . . . .	7
1.3.2 Ferrofluid-based deformable robotic sheet . . .	7
1.4 Dissertation organization . . . . .	8
<b>2 Methodology for manipulation using a ferrofluid deformation</b>	<b>11</b>
2.1 Ferrofluid . . . . .	11
2.2 Ferrofluid-based deformable robotic sheet . . . . .	12
2.3 Modeling . . . . .	13
2.3.1 Ferrofluid . . . . .	13
Deformation . . . . .	13
Specific gravity change of a ferrofluid . . . . .	15
2.3.2 Transportation model . . . . .	16
Manipulation modeling for non-rotating objects	16
Manipulation modeling for rotating objects . . .	17
2.4 Manipulation method . . . . .	18
2.4.1 Flat transportation . . . . .	19
Sphere transportation . . . . .	20
Plate transportation . . . . .	21
2.4.2 Liquid manipulation . . . . .	22
Liquid mixing . . . . .	22
Object detection for liquid manipulation . . . . .	23
Activation of electromagnets for liquid manipulation . . . . .	23
Goal position setting for liquid manipulation . .	24
2.4.3 Channel transportation of a ball . . . . .	25
<b>3 System Overview</b>	<b>27</b>
3.1 Ferrofluid-based deformable robotic sheet . . . . .	27
3.1.1 Ferrofluid-based deformable robotic sheet for solid objects . . . . .	27

3.1.2	Ferrofluid-based deformable robotic sheet for flexible objects . . . . .	28
3.2	Electromagnets . . . . .	30
3.2.1	Electromagnets for solid objects . . . . .	30
3.2.2	Electromagnets for flexible objects . . . . .	31
3.3	Manipulation system . . . . .	32
3.3.1	Flat transportation for solid objects . . . . .	32
3.3.2	Flat transportation for flexible objects . . . . .	33
3.3.3	Channel transportation . . . . .	34
<b>4</b>	<b>Basic characteristics of robotic sheet</b>	<b>35</b>
4.1	Surface deformation . . . . .	35
4.1.1	Shape measurement method . . . . .	36
4.1.2	Experiment procedure . . . . .	37
4.1.3	Result . . . . .	37
4.2	Force of Robotic sheet . . . . .	40
4.2.1	Experiment procedure . . . . .	40
4.2.2	Result . . . . .	41
4.3	Magnetic responsiveness of a robotic sheet . . . . .	42
4.3.1	Displacement with different amount of ferrofluid . . . . .	43
4.3.2	Oscillation amplitude with different amount of ferrofluid . . . . .	44
4.3.3	Displacement with different number of electromagnets . . . . .	45
4.3.4	Oscillation amplitude with different number of electromagnets . . . . .	46
<b>5</b>	<b>Feasibility verification of object manipulation with robotic sheet</b>	<b>47</b>
5.1	Flat transportation of two balls . . . . .	47
5.1.1	Experiment procedure . . . . .	47
5.1.2	Result . . . . .	48
5.2	Flat transportation of a thin plate . . . . .	48
5.2.1	Experiment procedure . . . . .	48
5.2.2	Result . . . . .	48
5.3	Liquid manipulation . . . . .	50
5.3.1	Liquid mixing . . . . .	50
Experiment procedure . . . . .	50	
Result . . . . .	53	
5.3.2	Liquid transportation . . . . .	53
Experiment procedure . . . . .	53	
Result . . . . .	56	
5.3.3	Liquid application . . . . .	57
Experiment procedure . . . . .	57	
Result . . . . .	57	
5.4	Channel transportation . . . . .	59
Experiment procedure . . . . .	59	
Result . . . . .	59	

<b>6</b>	<b>Discussion</b>	<b>61</b>
6.1	Surface deformation . . . . .	61
6.2	Force of the robotic sheet . . . . .	62
6.3	Responsiveness of the robotic sheet . . . . .	62
6.4	Flat transportation . . . . .	63
6.5	Liquid mixing experiment . . . . .	63
6.6	Liquid manipulation experiment . . . . .	64
6.7	Channel transportation . . . . .	66
6.8	Ferrofluid-based deformable robotic sheet . . . . .	67
6.9	Limitation of a ferrofluid-based deformable robotic sheet	68
<b>7</b>	<b>Conclusion and Future Directions</b>	<b>71</b>
7.1	Contribution of this work . . . . .	72
7.1.1	Contribution to Soft Robotics . . . . .	72
7.1.2	Contribution to Human Informatics . . . . .	74
7.2	Future Directions . . . . .	74



# List of Figures

1.1	Concept of a ferrofluid-based deformable robotic sheet. The characteristics of the robotic sheet can allow it to move the flexible object as well as mix and separate the droplets based on deformation control. . . . .	6
2.1	Ferromagnetic particles with a surfactant are dispersed in a ferrofluid. The particles repel each other owing to the surfactant and thermal motion. Subject to the influence of a magnetic field, a ferrofluid gathers around the source of the magnetic field, including the convexity loci at the interface. [ Tone et al., [92], p.2 ] . . . . .	11
2.2	The concept of a ferrofluid-based deformable robotic sheet. This robotic sheet is consist of thin film and a ferrofluid. In this robotic sheet, a ferrofluid can freely move and gather around the source of a magnetic field. According to the ferrofluid deformation, this robotic sheet can change its shape. Even if this robotic sheet is set three-dimensionally, a ferrofluid can move to the magnetic field against gravitational force. . . . .	12
2.3	Ferrofluid or a ferrofluid-based deformable robotic sheet surface with magnetic field imposed to it. [ Tone et al., [92], p.5 ] . . . . .	14
2.4	Behavior of a ferrofluid in the (a) absence and (b) in presence of a magnetic field gradient. When a magnetic field gradient is applied to the fluid (b), its apparent specific weight changes and this makes it possible for a non-magnetic object to float on the fluid. [ Tone et al., [92], p.6 ] . . . . .	15
2.5	Geometric representation of the slope and the acting forces over the transported object such as a plate. [ Tone et al., [92], p.6 ] . . . . .	16
2.6	Geometric representation of the slope and the acting forces over the transported object such as a ball. . . . .	17
2.7	Schematic diagram of the flat transportation system. This system mainly composed of the robotic sheet and electromagnets. By controlling activation of each electromagnet, the surface of Robotic sheet is controlled. [ Tone et al., [92], p.3 ] . . . . .	19

2.8	Image showing the behavior of the surface in the presence of a magnetic field (left picture) and at the time of degaussing the magnetic field (right picture). $F$ and $F'$ indicate the normal force. [ Tone et al., [92], p.4 ] . . .	19
2.9	Transportation method for a sphere. First, the system generates three convexities for making the concave region and traps the transport object. Next, the system degausses two of the electromagnets and rolls the objects in the intended direction. [ Tone et al., [92], p.4 ] . . . . .	20
2.10	Transportation method for a thin circle plate. An oscillating slope is generated along to the direction of the transportation route with three electromagnets. [ Tone et al., [92], p.4 ] . . . . .	21
2.11	The schematic image of mixing droplets. By vibrating the surface of a robotic sheet using a pulsed magnetic field generated from electromagnets, combined droplets are stirred and mixing are realized. . . . .	22
2.12	Processed target object using a web camera mounted above the robotic sheet. The rightmost image is the enlarged image. The coordinates of the electromagnet were acquired beforehand. [ Tone et al.,[91], p.2816 ] . .	23
2.13	Transportation method for an object. Using three activated electromagnets, the surface is lifted, and the object descends along the slope, moving the object. [ Tone et al., [91], p.2817 ] . . . . .	24
2.14	Goal position setting near the boundary of the electromagnets area. [ Tone et al., [91], p.2817 ] . . . . .	24
2.15	Top view of the channel transportation system. The system activates the two electromagnets facing each other and generates two convexities to push the object. By controlling the electromagnets and moving the convexities, the channel ferrofluid-based robotic sheet moves the object. [ Tone et al., [92], p.5 ] . . . . .	25
3.1	A ferrofluid-based deformable robotic sheet for solid objects. Polyethylene films are used as the thin film and a ferrofluid is wrapped with the films. [ Tone et al., [92], p.3 ] . . . . .	27
3.2	The ferrofluid-based deformable robotic sheet for flexible objects. Polytetrafluoroethylene films are used as the thin film and a ferrofluid is wrapped with the films. [ Tone et al., [91], p.2816 ] . . . . .	28
3.3	By activating several electromagnets, the surface can be deformed along with the number of electromagnets. [ Tone et al., [91], p.2816 ] . . . . .	29
3.4	Arrangement of electromagnets used for transporting solid objects. . . . .	30

3.5	Structure of an electromagnet for solid objects and distribution of a magnetic field. [ Tone et al., [92], p.3 ] . . .	30
3.6	Arrangement of electromagnets used for transporting flexible objects. [ Tone et al., [91], p.2816 ] . . . . .	31
3.7	Structure of an electromagnet for small objects and distribution of a magnetic field. [ Tone et al., [91], p.2816 ] . . . . .	31
3.8	Overall system of the ferrofluid-based deformable robotic sheet for solid objects. [ Tone et al., [92], p.3 ] . . . . .	32
3.9	Overall system of the ferrofluid-based deformable robotic sheet for flexible objects. . . . .	33
3.10	Schematic diagram of the robotic sheet. [ Tone et al., [91], p.2815 ] . . . . .	33
3.11	Schematic diagram of the channel transportation system. [ Tone et al., [92], p.3 ] . . . . .	34
4.1	Appearance of the equipment used in the surface deformation. This equipment is simple version of the robotic sheet, and the thickness of the ferrofluid is measured using 3D-CT by changing the thickness of the polyethylene sheet: 0.1, 0.2, 0.3, 0.4, and 0.5 mm. [ Tone et al., [92], p.7 ] . . . . .	35
4.2	Tomographic image. The red square is the electromagnet and the white object over the electromagnet is the ferrofluid in the glass dish. There are black lines on each images due to the electromagnet. [ Tone et al., [92], p.7 ] . . . . .	36
4.3	Result of the shape measurement. The number at the upper left corner of each image indicates the thickness of the polyethylene sheet. In the first figure "0.0" means the sheet is not on the fluid. The red lines on each picture represent the interface of the ferrofluid. [ Tone et al., [92], p.7 ] . . . . .	38
4.4	Thickness of the ferrofluid. Horizontal axis represents the length from the center of the convexity. Vertical axis represents the thickness of the ferrofluid. The legend represents the thickness of the polyethylene sheet on the ferrofluid. "0.0" implies "without the sheet". [ Tone et al., [92], p.8 ] . . . . .	39
4.5	Relationship between the thicknesses of the polyethylene sheet and the ferrofluid in the simple version of the robotic sheet at the center of the convexity ( $X = 0$ ). The horizontal axis represents the thickness of the polyethylene sheet and the vertical axis represents the thickness of the ferrofluid in the robotic sheet. [ Tone et al., [92], p.8 ] . . . . .	39

4.6	Schematic image of this experiment. The simple version of the robotic sheet is used. A sphere object is put on the robotic sheet. The mass of the object is changed and the displacement change is measured using a laser positioning sensor. . . . .	40
4.7	Blue dots shows the top of the convex surface of the robotic sheet when a magnetic field is applied to it. Red dots shows the top of the surface of the robotic sheet without a magnetic field. . . . .	41
4.8	Experimental setup for verification of magnetic responsiveness of a robotic sheet. [ Tone et al., [91], p.2817 ] . .	42
4.9	The process of lifting up the surface of the robotic sheet. The three types of the robotic sheet including a ferrofluid with mass of 19.8, 43.9, and 69.8 are used. Reference indicates that there is no large noise. Each result shows the average value measured seven times. [ Tone et al., [91], p.2818 ] . . . . .	43
4.10	The process of declining the surface of the robotic sheet. The electromagnets are demagnetized 30 s after the saturation displacement. Reference indicates that there is no large noise. Each result shows the average value measured seven times. [ Tone et al., [91], p.2818 ] . . . .	44
4.11	Peak-to-peak amplitude of the robotic sheet versus the frequency of the pulsed magnetic field. [ Tone et al., [91], p.2818 ] . . . . .	45
4.12	Response speed of a robotic sheet with different number of electromagnets: 3, 4, 5, 7, and 9 electromagnets. [ Tone et al., [91], p.2818 ] . . . . .	45
4.13	A peak-to-peak amplitude of a robotic sheet by replacing the number of activating electromagnets: 3, 4, 5, 7, and 9 electromagnets. [ Tone et al., [91], p.2819 ] . . . .	46
5.1	Conceptual transportation route of two balls. The red line indicates the route of "Object A", and the green line indicates the route of "Object B". [ Tone et al., [92], p.8 ] . . . . .	47
5.2	A thin plate transportation results on the two-dimensional surface. The red line shows the trajectory of object A, and the green line shows the trajectory of object B. The elapsed time is shown at the top left corner. [ Tone et al., [92], p.9 ] . . . . .	49
5.3	Conceptual transportation route of a thin plate transported from right to left. [ Tone et al., [92], p.9 ] . . . . .	50
5.4	A thin plate transportation result on the two-dimensional surface. The red line shows the trajectory of the object transport. The elapsed time is shown at the top left corner. [ Tone et al., [92], p.9 ] . . . . .	51



5.5 Method of quantifying a mixing process. The leftmost picture shows the state in which red and white droplets are combined. The rightmost picture shows the result of the droplet mixing. By using the saturation of the picture, the mixing result is quantified. [ Tone et al., [91], p.2819 ] . . . . . 52

5.6 Standard deviation of saturation of colored liquid during mixing. The robotic sheet with 43.9 g of ferrofluid is used and frequency of a pulsed magnetic field is 5, 10, 15, 20, 25, and 30 Hz. [ Tone et al., [91], p.2819 ] . . . 53

5.7 The robotic sheet continues to move the object so as to turn around three preset goals sequentially. This graph shows one of the experiment results. The average transportation speed is derived from the total transport distance of a droplet. The accuracy of a droplet transportation is obtained from the mean and standard deviation of the distance of each round. "Start" and "Stop" indicate the position of the droplet at the start or end of the transport experiment, respectively. "Goal" shows the preset goals. [ Tone et al., [91], p.2820 ] 54

5.8 The average velocity of the droplets. [ Tone et al., [91], p.2820 ] . . . . . 54

5.9 The trajectories of the droplet with a volume of 0.186, 0.396, 0.693, and 1.114ml. In each graph, gray dots are the trajectory, orange dots are the goal, black dot is the start point, and red dot is the point in which the target droplet stops after 300 s. . . . . 55

5.10 The average and standard deviation of the distance of one round of the transported droplet with a volume of 0.297, 0.495, 0.693, and 0.990 ml. [ Tone et al., [91], p.2820 ] . . . . . 56

5.11 Initial state of the liquid application experiment. Transportation and mixing are conducted in one sequence. At first, a white droplet moves to a red droplet. After these droplet are combined, the combined droplet are mixed using oscillation. The mixed droplet moves to blue powder, and the droplet and powder is mixed. . . 57

5.12 Liquid transport results. The upper left in each picture shows the experiment time. [ Tone et al., [90], p.780 ] . . 58

5.13 Channel transportation route. The robotic sheet is set on channel-like surface. By activating the electromagnets and changing the inner surface of the channel, the ball is moved from right to left. [ Tone et al., [92], p.9 ] . 59

5.14 Ball transportation result through the channel ferrofluid-based robotic sheet. The frames are sequential, starting at "(1)" and ending at "(6)". [ Tone et al., [92], p.10 ] . . . . . 60

6.1	Left schematic image shows the system state at Step: $t$ . Right schematic image shows the system state at Step: $t+1$ . . . . .	65
6.2	Object movement on the convex surface of the robotic sheet . . . . .	65
6.3	Schematic diagram of deformation of the robotic sheet	67

# List of Tables

3.1	Ferrofluid in the ferrofluid-based deformable robotic sheet for solid objects . . . . .	28
3.2	Ferrofluid in the ferrofluid-based deformable robotic sheet for droplets . . . . .	29
3.3	System specifications of the robotic sheet for solid objects	33
3.4	System specifications of the robotic sheet for flexible objects. . . . .	34



*This work is dedicated to my parents, Toshio and Shoko Tone, my brother, Yoshinori Tone, my pets, Tama and Kotama.*

*They have always been on the side of me and supported me.*

*I dedicate this dissertation to my grandparents, Yoshisuke and Matuwe Sudo.*

*They have always loved and cheered me up.*

*I dedicate this work to my best friends, Yuki Tokunaga (Oshima), Teruaki Saito, and Yutaro Okuda.*

*Thanks to them being my best friend, I have been able to overcome many difficulties.*



# Chapter 1

## Introduction

### 1.1 Background

What is a robot? The terminological definition of a robot is defined in Oxford Dictionaries [1] as follows:

1. (especially in science fiction) A machine resembling a human being and able to replicate certain human movements and functions automatically.
2. A machine capable of carrying out a complex series of actions automatically, especially one programmable by a computer.

These definitions show that we consider that robots are machines which automatically achieve the tasks that we require. As representative robots that automatically perform our work, there are manipulators and conveyors. Manipulators and conveyors have been used for grasping, transporting, and assembling objects in factories [2, 3]. These robots had a low computing speed and their size was difficult to be made small. Therefore, they were dangerous to be used with people around and built on the premise of use in isolated environments. Along with the development of robot technologies, such as computing speed and controls, and miniaturization of robot components, robots based on the premise that people are around them have been appearing. Pepper, Aibo, LOVOT, and Roomba receive customers, heal our feelings, watch children, and clean up our house automatically [4–7]. Owing to these robots, we can save our time and reduce difficult or unnecessary tasks. The development of artificial intelligence technologies, such as machine learning, improves robot performance. Considering the human history, by developing engineering systems and using it in several field, human has pursued rationalization and improved labor productivity per unit time. Since the industrial revolution that occurred in the UK in the late 18th century, industrial machines were introduced to industries such as production sites. Then, importance was placed on the rationality of the task, and the production capacity sharply improved. Along with the development of industrial machinery, the robotics field also developed. These technologies were applied to home appliances. Household appliances were introduced in our daily life and automated

housework we had to do in our daily life. Pepper, Aibo, LOVOT, and Roomba show that robot technologies begin to automatically achieve tasks that were difficult to automate until a while ago. From this, it is considered that the robot is further needed in daily life [8]. Moreover, due to the increase in elderly people and lack of number of their care workers, demand for robots aiming to care the elderly people and reduce the burden on caregivers and compensate for the number of caregivers is increasing [9–11]. Assuming that, in the future, robots are routinely used in the same space with us like consumer electronics, such as home appliances and smart phones.

However, in order to enable robots to work in the same space with us, the problem of contact between robots and people should be considered. As described in the above, robots are required to carry out tasks. An incident of unintentional contact between a person and a robot increase. Unintentional contact may cause injuries or damage to people, robots, and surrounding environment of the robots. In order to solve this problem, collision avoidance systems have been researched [12–14]. These researches showed a method to avoid collision between the robot and surrounding objects by grasping objects around the robot using multiple sensors. However, in everyday life, there are many obstacles to the movement of robots. Also, the environment in which the robot can move is restricted, and the robot can not always avoid the object. Therefore, even if robots uses the collision avoidance systems, it is very difficult to avoid collision completely between robots and people or objects. Therefore, even if the robot collides with surrounding people or objects, a system that reduces the effects of injury and damage is required. As a new field of robotics aiming to increase affinity to the surroundings, Soft Robotics has attracted attention recently.

Soft Robotics is a robotics field aiming at improving the affinity with the environment and the target object by using its own flexibility and geometric characteristics without requiring exact position, attitude and force control [15–17]. In Soft Robotics, the flexibility and softness of living creatures such as humans are used as a reference for robot motion [18–21]. In addition, Soft Robotics aims at a robot that gives the user a sense of security and has a high adaptability to the environment by utilizing the high degree of freedom associated with the flexibility of the robot. Such a deformable and inflatable robot is called a soft robot, and soft robots are composed of flexible materials that have not been used in existing robots [22]. Therefore, it is not possible to use conventional development and control methods.



## 1.2 Related researches

Soft robots have been studied by combining various fields such as mechanical engineering, material science, and biology for developing robots using flexible materials, constructing new control methods, and searching for application fields. The components of soft robots have been widely researched, and soft robots using flexible materials such as elastomers and gels, or a robot combining a fluid and an elastic membrane have been proposed [23–29]. Araromi et al. developed a flexible manipulator using casted silicone as the dielectric elastomer [23]. By changing a voltage applied to this dielectric elastomer, this manipulator can grasp a target materials. Tolley et al. and Shepherd et al. realized locomotive robots which composed of soft materials such as silicone elastomer and small air compressor [24, 25]. The movement of this robot is inspired by animals, and by elevating pressure inside the elastomer with the compressor, the legs of the robot was actuated. Also, this robot could hold a payload on its body while moving. Daehoon et al. developed a robot using electroactive hydrogels [26]. The electroactive hydrogels largely deform in response to electric field. They realized 3D-printed fabrication methods for electroactive hydrogels and enabled the electroactive hydrogel robots to grasp and move an object and walk by controlling electric field. Laschi et al. proposed a soft robot arm inspired by the octopus [27]. They focused that the octopus changes its stiffness and realizes its grasping and locomotion by using its structure, named a muscular hydrostat [30]. They developed artificial muscular hydrostats with longitudinal actuators made of Ultra High Molecular Weight Polyethylene synthetic fibers and transverse actuators using shape memory alloys, and showed the basic movement with their proposed octopus-like arm. Glick et al. introduced a surface layer of gecko-inspired adhesives to an elastomer actuator [28]. Gecko has a unique structure on the surface of their feet [31]. Gecko's feet have dense setae and maximize the effect of van der Waals forces by increasing the adhesion area. Also, Gecko changes its angle of setae and controls its effect. Therefore, Gecko can freely stick to and leave a vertical wall. By using gecko-inspired adhesives, they succeeded in increasing the mass of the object that the manipulator can lift. Brown et al. introduced jamming transition effect to robotic gripper and made it grasp several shape objects [29]. Jamming transition is the property of granules whose overall viscosity increases as the density of powdery grains increases [32]. Using this physical property, the robotic gripper adapts its shape to the shape of a target object and grasp it. As shown in these examples, new soft robots have been researched using various flexible materials, development methods, and control methods.

Among these materials for soft robots, functional fluids have been gaining increased attention [33–37]. Functional fluids are fluids to

which functions, such as viscosity changes, are artificially added by dispersing micro-particles reacting to external stimuli in a solvent [38]. The elicited characteristics of functional fluids are according to the changes in its external environment, such as the presence of magnetic or electric fields. This type of fluid can be applied to any shape and exhibits relevant characteristics even if a small quantity is used. The fluid can thus simplify and downsize system mechanisms. Magnetorheological fluids (MR fluids) and electrorheological fluids (ER fluids) are examples of functional fluids, for which the viscosity changes in the presence of magnetic or electric field [39, 40]. These fluids have already been applied to engineering equipment, such as in dampers and clutches [41, 42]. A ferrofluid is also an example of functional fluids, and can change its shape in addition to its viscosity under the presence of a magnetic field [43]. These unique properties have attracted many researchers in several field, such as the engineering and art fields.[36, 37, 43–63]. Among them, Chen et al., Leon-Rodriguez et al, and Tanaka et al. developed soft robots using a ferrofluid. Chen et al. focused on deformation and magnetic characteristics of a ferrofluid, and developed the spherical robot with ferrofluid encapsulated in a hollow polymer rubber [36]. This robot moves toward the source of a magnetic field. Also, since this robot is flexible, it can also pass through a hole smaller than its own size. Leon-Rodriguez et al. developed the ferrofluid soft robots inspired by an amoeba [37]. This robot is consist of a ferrofluid and polyethylene films, and moves like an amoeba by controlling a magnetic field. Tanaka et al. succeeded in conveying paper and water in one direction by controlling ferrofluid deformation and revealed that a ferrofluid transfers mechanical energy to objects that are in contact with it [61–63]. A ferrofluid is flexible and can be deformed optimally to the shape of the object. Therefore, it can handle any shape of objects in addition to paper and water. By using flexibility of a ferrofluid, a robot system using a ferrofluid can transport both of solids or flexible objects. Moreover, a ferrofluid shape can be varied by changing a location where a magnetic field is generated. Since a ferrofluid has both fluid and magnetic properties, it has properties of freely aggregating with respect to the source of a magnetic field. By using electromagnets as the magnetic field source and controlling their activation, a ferrofluid aggregates according to the position of the electromagnets, and objects can move along with a downward gradient generated by the ferrofluid aggregation. Therefore, Based on the previous researches related to the soft robots using a ferrofluid, it is possible to develop a new soft robot technology which three-dimensionally manipulates objects including the operations of transport and coalescence of objects on the robot. In recent years, other studies were published which used flexible membranes as the upper layer with pneumatic/inflatable actuators [64–69] or liquid metals [70, 71], and

handled the target object by controlling its deformable surface. Conversely, this study proposes to use a ferrofluid as a component of a soft robot.

Also, this research is related to the field of morphological computing [72–74]. A new technology is used to change the morphological features using the surface deformation of a flexible membrane filled with ferrofluid is one of the main contributions to soft robotics. Morphological computing is a research field that uses the geometric properties of the system to control the system. Muller et al. stated that the morphological computing can be distinguished three fields: morphology that facilitates control, morphology that facilitates perception, and morphology itself used as a calculation [74]. In the first morphology, by utilizing morphological features of robots, reduction of calculation cost in the robot control is realized. The coffee balloon gripper is composed of coffee powder and balloon and grabs any shape object using the flexibility and the jamming transition of the coffee powder [29, 32]. In the conventional robotics and control methods, dynamical shape changes due to flexible characteristics were avoided since it was difficult to make them into computational parameters. Instead of controlling the dynamic shape changes, by leaving motion such as grasping of object to them, it is possible to realize complicated robot motions while suppressing calculation cost. In the second morphology, by implementing a characteristic morphology into sensors of robots, data obtained by sensing can be easily processed. Floreano et al. developed the devices referring to compound eyes of flies [75]. Compound eyes are visual organs possessed by insects such as flies, and have structures in which individual eyes composed of lenses and photoreceptor cells are organized [76]. By imitating compound eyes, it is possible to enlarge the viewing angle and to construct a system that efficiently acquires object information and reconstructs it. In the third morphology, the morphological characteristics themselves have functions as computing like the Recurrent Neural Network. The proposed system is related to the first morphology. As the proposed system uses a ferrofluid as its component, it actively changes its shape and passively adapts its shape to the shape of target objects. The shape of the proposed system is not calculated and is decided with the deformation characteristics of a ferrofluid. Therefore, the proposed system realizes its motion using simple algorithm. Also, due to the flexibility of the ferrofluid, the system automatically adapts its shape to the target object without complex calculation.

Fig. 1.1 is the concept of the proposed system. Assuming that the proposed system can be used in new systems that control reagent reactions in biological analyses, such as droplet manipulations and chemical analyses [77–81]. In the field of thdroplet manipulation, it is desired to speed up the analysis, reduce precious reagents, and

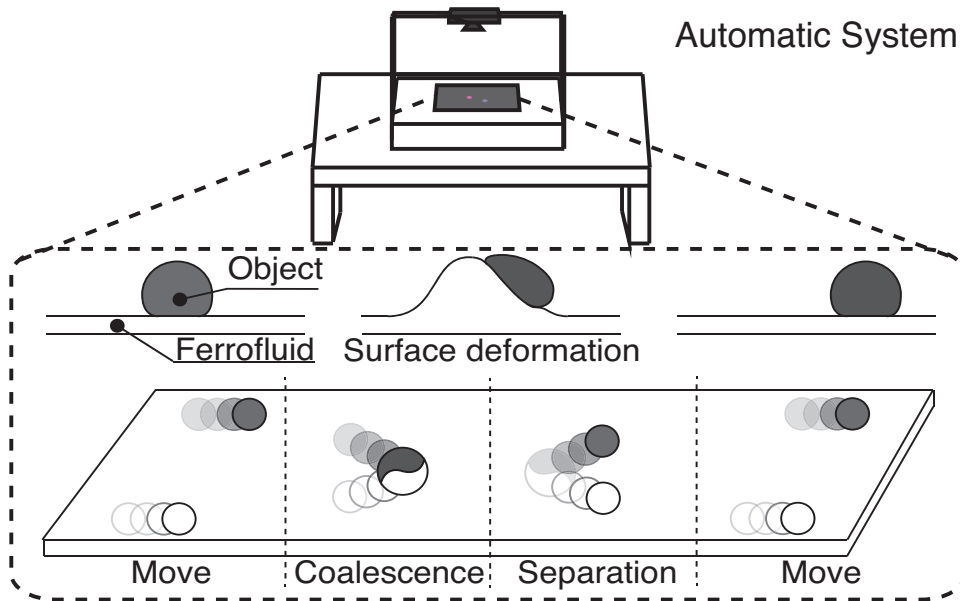


FIGURE 1.1: Concept of a ferrofluid-based deformable robotic sheet. The characteristics of the robotic sheet can allow it to move the flexible object as well as mix and separate the droplets based on deformation control.

reduce the burden on the subjects. The purpose of the droplet manipulation is to reduce the amount of reagent [82] and analysis time by using a small amount of reagent and automating the process of moving and mixing reagents. Conventional studies realized to manipulate and analyze a reagent with a size of approximately a few centimeters or less with only one piece of equipment. A reagent can be moved in channels on a plate by controlling the repellency of the plate surface or by adding additives such as electrolytes or magnetic powder to the reagent and using magnetic or electric fields [83–87]. The proposed method does not require channels or additives and moves liquids and solid objects; therefore, users can freely move a reagent and choose the mixing and analysis area. Users can manipulate solid reagents as well as liquids without considering the effect of the additives on the reagent. In addition, since the main components of the proposed system are ferrofluid and electromagnets, simple mechanism for making the surface deformation can be achieved. With the proposed method, it is easy to reduce the system size and the control system can thus be simplified. It is possible to develop a simple sorting robot that can handle objects with sizes less than 1 mm.

## 1.3 Objective

### 1.3.1 Research objectives

The research objective is to develop new soft robot and realize object manipulation using deformation characteristics of a ferrofluid by magnetic field control. The requirements of the robot to be developed are as follows:

1. The robot has a layered structure in which a ferrofluid is wrapped with thin films.
2. The robot shape follows the shape of the ferrofluid and can be controlled by a magnetic field.
3. The robot can perform object manipulation on its surface using its deformation.

Also, solid objects and flexible objects are used as transport objects. Balls and flat plates are used as solid objects, and droplets are used as flexible objects. Manipulation includes a plurality of motions such as grasping, transporting, combining, tearing and pushing objects. In this research, transportation is focused on among the manipulation motions. In manipulation of droplets, transportation and mixing are conducted.

### 1.3.2 Ferrofluid-based deformable robotic sheet

In this research, a ferrofluid-based deformable robotic sheet is proposed as a robot fulfilling these requirements. The ferrofluid-based deformable robotic sheet is defined as the robot which is a sheet-type shape, which is consist of a ferrofluid and thin films, which deforms its shape using a magnetic field, and in which the ferrofluid freely moves. Due to its sheet-type shape and flexibility, the robotic sheet can adapt its shape to its surrounding environment. Therefore, the robotic sheet can be set on not only a flat surface but also a non-flat surface, such as a channel. Moreover, under the influence of a magnetic field, the ferrofluid inside the robotic sheet gathers around the magnetic field and the surface of the robotic sheet is deformed. An object moves along with the downward gradient on the robotic sheet.

A ferrofluid-based deformable robotic sheet enclosing a ferrofluid with a thin film as a new manipulation system has already been proposed [88]. The mechanism based on which the robotic sheet can move two balls and a plate on its surface by deforming its shape and by performing alternate tasks by changing its configuration to the channel shape was realized [89]. Also, transportation of a droplet on the robotic sheet was realized and the effect of the volume of the ferrofluid inside the robotic sheet and the number of activated electromagnets on the deformation speed and oscillation amplitude of

the robotic sheet was clarified [90, 91]. The deformation characteristics of the robotic sheet using 3D-CT was verified and the process of object transportation was validated [92].

## 1.4 Dissertation organization

In this paper, the contents of these proceedings and papers are systematically summarized. At first, a ferrofluid-based deformable robotic sheet and its methodology are proposed in Chapters 2 and 3. Chapter 2 describes characteristics of the robotic sheet and models of the ferrofluid characteristics and object transportation with the robotic sheet. In this research, a ball, plate, and droplet are used as target objects and their motions are rotation or slide. The object transport models focus on these moving objects and the transportable conditions of these objects are derived. Then, the transportation method for these target objects are proposed. After that, object transportation with the proposed robotic sheet are realized. Chapter 3 shows the developed robotic sheets according to the methodology.

Chapters 4 and 5 show the verification of characteristics of a robotic sheet and the feasibility verification of object transportations. The shape of a robotic sheet depends on the shape of a ferrofluid and characteristics of a thin film. By elucidating the effect of a thin film on a ferrofluid shape, the shape model of a robotic sheet can be derived. Then, in order to verify this effect, the deformation of the robotic sheet are measured using 3D-CT. Moreover, in the robotic sheet, the movement and mixing of the objects depends on the magnetic responsiveness of the robotic sheet. When a magnetic field is applied to the robotic sheet, high deformation speed is required to move a target object properly to the destination, and a large oscillation amplitude is required to mix the liquids. The influence on the magnetic responsiveness depends on the number of electromagnets, amount of ferrofluid inside the robotic sheet, ferrofluid characteristics such as the viscosity and saturation, distribution and size of the magnetic field generated by the electromagnet, and Young's modulus of the thin films wrapping the ferrofluid. By clarifying the effect of these parameters, this magnetic responsiveness can be estimated, and the system can be developed according to a required analysis condition in the future. Among these parameters, this paper concentrates on the amount of the ferrofluid and the number of electromagnets, and these effects are verified. Then, the effect of the amount of the ferrofluid and the number of electromagnets on the magnetic response is clarified and the effect of the oscillation amplitude and frequency on liquid mixing is explained. In the feasibility verification, two balls and a thin circular plate are transported along a pre-defined path using the proposed method. A droplet is automatically transported using a visual feedback and the transportable volume range, velocity, and transport accuracy of droplet using the automatic transportation

method are clarified. Also, mixing of two types of droplets is quantitatively verified.

Chapters 6 shows the discussion of these experiments and a ferrofluid-based deformable robotic sheet. Chapters 7 summarizes this study and explains contributions and future directions of this study.





## Chapter 2

# Methodology for manipulation using a ferrofluid deformation

### 2.1 Ferrofluid

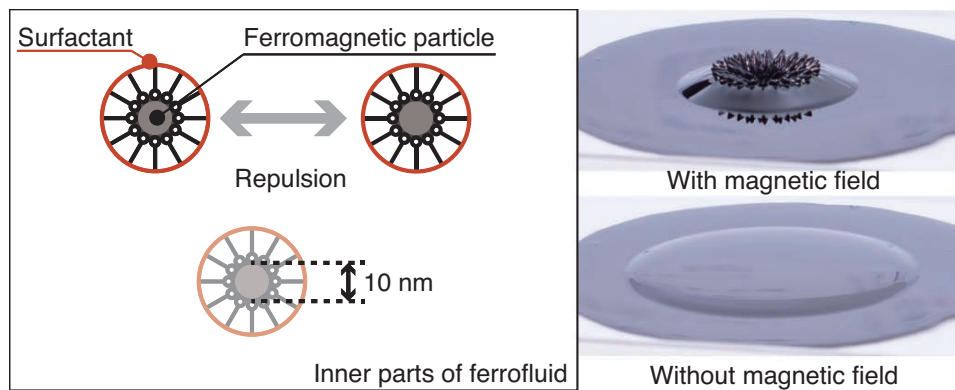


FIGURE 2.1: Ferromagnetic particles with a surfactant are dispersed in a ferrofluid. The particles repel each other owing to the surfactant and thermal motion. Subject to the influence of a magnetic field, a ferrofluid gathers around the source of the magnetic field, including the convexity loci at the interface. [ Tone et al., [92], p.2 ]

A ferrofluid is used as a component of our proposed system. This fluid contains ferromagnetic particles with diameters of 10 nm or less, which are covered with a surfactant and dispersed in a solvent, as shown in Fig. 2.1. Owing to the surfactant, the surface of the particles is charged negative, and particles repel each other because of electrostatic repulsion. Also, these particles are very small so that they are affected by thermal motion and eventually disperse in the solvent. Subject to the influence of a magnetic field, the particles gather around the source of the magnetic field. The structural configuration of the ferrofluid changes, the shape of the ferrofluid changes, and convexity appears on its interface, as shown in Fig. 2.1. Some spikes also appear on the deformed surface because of the instability of the fluid interface [43]. The apparent density of the ferrofluid also increases because it is affected by the magnetic force in addition to

the gravitational force, and its internal pressure increases owing to the magnetic field. Therefore, under the influence of the magnetic field, the objects with a higher density will still float on the surface of the ferrofluid. The shape of the ferrofluid the distribution of the magnetic field, and a force is generated according to the magnetic field gradient [43, 44]. A ferrofluid does not exhibit hysteresis, unlike other magnetic materials [43]. The particles in a ferrofluid have a single magnetic domain structure. Under the presence of a magnetic field, each magnetic moment is oriented in the direction of the magnetic field, thus leading to the magnetization of the ferrofluid. After the magnetic field vanishes, the particles immediately spread owing to the thermal motion and electrostatic repulsion, and the magnetization of the ferrofluid becomes zero.

## 2.2 Ferrofluid-based deformable robotic sheet

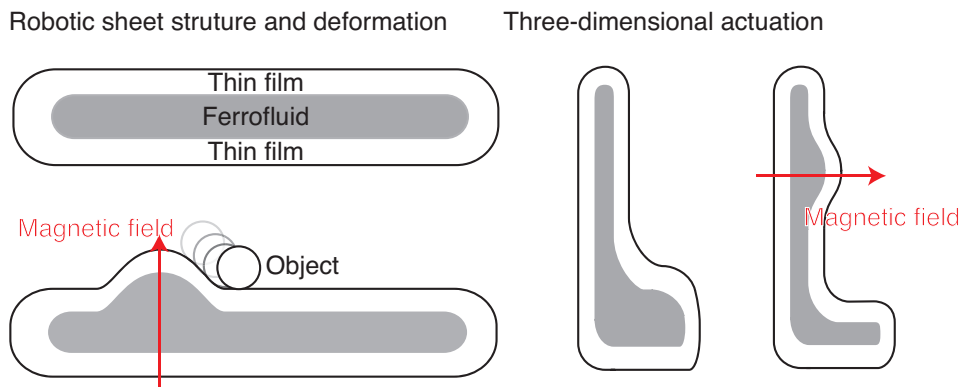


FIGURE 2.2: The concept of a ferrofluid-based deformable robotic sheet. This robotic sheet is consist of thin film and a ferrofluid. In this robotic sheet, a ferrofluid can freely move and gather around the source of a magnetic field. According to the ferrofluid deformation, this robotic sheet can change its shape. Even if this robotic sheet is set three-dimensionally, a ferrofluid can move to the magnetic field against gravitational force.

Fig. 2.2 shows the concept of a ferrofluid-based deformable robotic sheet. In this research, the ferrofluid-based deformable robotic sheet satisfying the requirements shown in the objective section are proposed. The robotic sheet is a sheet-shaped robot in which a ferrofluid is enclosed in a thin film as shown in the left figures of Fig. 2.2. This robotic sheet has a layered structure. By wrapping the ferrofluid with the thin film, it is possible to prevent direct contact between an object and the ferrofluid. The shape of the ferrofluid depends on a magnetic field distribution, and the shape of the robotic sheet also depends on it and the thin films and is convex. When an object is placed on the

surface of the robotic sheet, due to the friction between the object and the films, the object can stop on the surface. Moreover, the object can be moved using the difference height generated by the surface deformation of the robotic sheet.

As shown in the right figure of Fig. 2.2, owing to the sheet shape, even if the robotic sheet is set three-dimensionally, the robotic sheet can change its shape. For any configuration of the robotic sheet, the ferrofluid always stays at the bottom of the bag, as long as a magnetic field is not applied to it. Under the influence of a magnetic field, the ferrofluid moves and gathers around the source of the magnetic field in the robotic sheet and the surface deforms according to the location of the activated electromagnet.

## 2.3 Modeling

In this section, the characteristic models of deformation and specific gravity change of a ferrofluid and the object transport models of the robotic sheet are explained.

### 2.3.1 Ferrofluid

#### Deformation

The deformation model of a ferrofluid are described. The properties and fluid model of a ferrofluid have already been verified by Rovensweig et al. [43] and T.B Jones [44]. Eq.2.1 represents the equation of motion of a ferrofluid.

$$\rho_o \frac{Du}{Dt} = -\nabla P + \eta \nabla^2 u + \rho_o g + F_m \quad (2.1)$$

This equation is derived from the Navier stokes equation.  $\rho_o$  is the density of the ferrofluid,  $\frac{Du}{Dt}$  is a material derivative,  $P$  is the pressure in the ferrofluid,  $u$  is the fluid velocity,  $t$  is the time (second),  $\eta$  is the coefficient of viscosity,  $g$  is the gravitational acceleration, and  $F_m$  is the magnetic dipole force. In the ferrofluid, the force  $F_m$  derived from the magnetic dipole force is added to the equation because the fluid is affected by a magnetic field. The fluid in the experiment is non conducting fluid with no magnetic monopole; thus, Eq.(2.1) satisfies Eqs.(2.2) and (2.3).

$$\nabla \times H = 0 \quad (2.2)$$

$$\nabla \cdot B = 0 \quad (2.3)$$

$H$  is the magnetic field and  $B$  is the magnetic flux density. Assuming that the magnetization in the fluid is parallel to the magnetic field,

and the magnetic field is expressed through Eq.(2.4). Moreover, magnetic flux density in the fluid is expressed through Eq.(2.5).

$$M = \chi H \quad (2.4)$$

$$B = \mu_o(H + M) \quad (2.5)$$

$$F_m = \mu_o M \nabla H \quad (2.6)$$

$M$  is magnetization of the fluid through Eq.(2.4) and  $\mu_o$  is the permeability of free space through Eqs.(2.5) and (2.6). From Eq.(2.1), the thickness of the ferrofluid is obtained when a magnetic field is applied to it, shown in Fig. 2.3. In this model, the instability such as

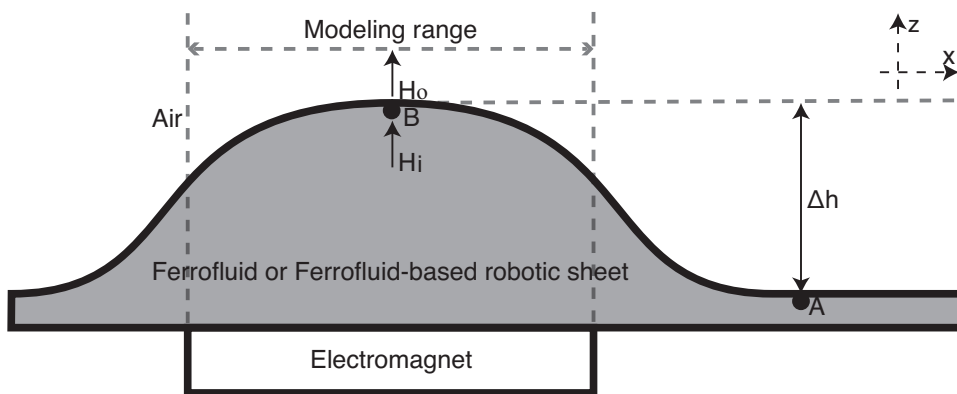


FIGURE 2.3: Ferrofluid or a ferrofluid-based deformable robotic sheet surface with magnetic field imposed to it. [ Tone et al., [92], p.5 ]

spikes on the fluid interface is not considered, as shown in Fig. 2.1. Also, assuming that the fluid is in a state of equilibrium after the deformation stopped, and the viscosity term in Eq.(2.1) is ignored. The fluid satisfies Eq.(2.7) because it is an incompressible fluid.  $F_m$  is written using the potential function  $\psi_m$  as  $F_m = \nabla \psi_m$ .  $\psi_m$  is written as in Eq.(2.8)[44]. Owing to these conditions, the Bernoulli equation is expressed as in Eq.(2.9).

$$\nabla \cdot u = 0 \quad (2.7)$$

$$\psi_m = \mu_o \int_0^H M(H') dH' \quad (2.8)$$

$$\rho \frac{u^2}{2} + P + \rho g z - \psi_m = const. \quad (2.9)$$

$z$  is the  $z$ -axis displacement in Fig. 2.3.  $\rho$  is the density of the ferrofluid. When the point A is defined as the reference point in Fig. 2.3, the thickness is expressed as  $\delta h$ . The points A and B are set at the interface, as shown in Fig. 2.3. At point A, magnetic field is sufficiently decreased; thus, the magnetic field at A is regarded as 0, and the pressure is equal to the external pressure  $P_o$ . At point B, a pressure jump is experienced between the external and internal fluid

[44], [45], and the magnetic fields inside and outside of the fluid are different, as shown in Eq.(2.10), and are expressed through  $H_{in}$  and  $H_o$ , respectively.

$$\mu_o H_o = \mu_o (H_{in} + M(H_{in})) \quad (2.10)$$

The pressure jump is written as follows:

$$P_{in} - P_o = -\frac{\mu_o}{2} (\hat{n} \cdot \overline{M})^2 \quad (2.11)$$

$P_{in}$  is a pressure in the ferrofluid at point B through Eq.(2.11). By considering these equations and the fluid velocity and by substituting the parameter for Eq.(2.9), the thickness of the fluid expressed as follows is obtained:

$$\delta h = \frac{\mu_o}{\rho g} \left( \int_0^{H_{in}} M(H') dH' + \frac{1}{2} M(H_{in})^2 \right) \quad (2.12)$$

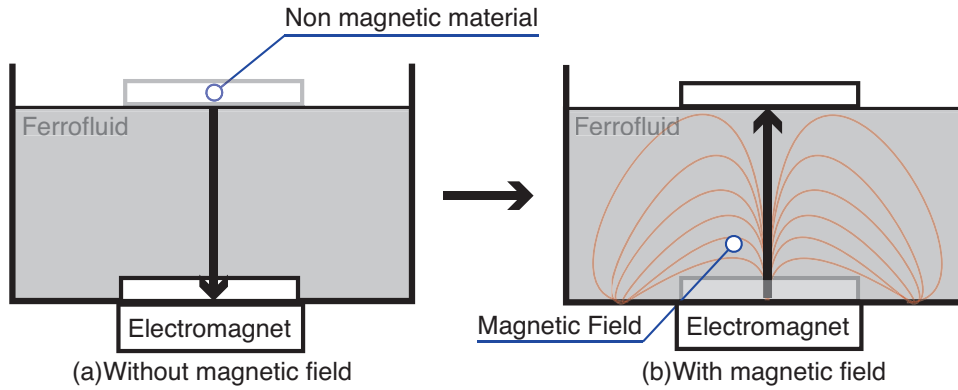


FIGURE 2.4: Behavior of a ferrofluid in the (a) absence and (b) in presence of a magnetic field gradient. When a magnetic field gradient is applied to the fluid (b), its apparent specific weight changes and this makes it possible for a non-magnetic object to float on the fluid.

[ Tone et al., [92], p.6 ]

### Specific gravity change of a ferrofluid

To achieve object transportation, the following two conditions must be satisfied simultaneously: i) the transportation object cannot sink into the magnetic fluid as shown in Fig. 2.4, and ii) the underlying interface must be convex in shape. To satisfy the first condition, the force exerted on the object by the ferrofluid must be proportional to the volume of the fluid displaced by the nonmagnetic object due to Archimedes' principle. Assuming that the direction of motion of the fluid interface is positive along the  $z$ -axis, and the other components are removed. The equation for the force of the ferrofluid on the non-magnetic object is defined as in Eq.(2.13). The equation of motion of

the nonmagnetic object is derived in Eq.(2.14).

$$F = \left( \rho_f - \frac{\mu_o M}{g} \frac{dH}{dz} \right) g V_f \quad (2.13)$$

$$m \frac{d^2 z}{dt^2} = F - \rho_o g V_o \quad (2.14)$$

In these equations,  $g$  is the force of gravity,  $F$  is the force applied by the ferrofluid,  $\frac{dH}{dz}$  is the gradient of the magnetic field along the  $z$ -axis,  $M$  is the magnetization of ferromagnetic particles in the ferrofluid,  $\rho_f$  and  $\rho_o$  are the specific weights of the ferrofluid and transported object, respectively,  $\frac{d^2 z}{dt^2}$  is the vertical acceleration of the object, and  $m$  is its mass.  $V_f$  is the volume of the magnetic fluid displaced by the object and  $V_o$  is its volume. To guarantee that the non-magnetic object does not sink into the ferrofluid, its specific weight should lie within the following range:

$$0 < \rho_o < \left( \rho_f - \frac{\mu_o M}{g} \frac{dH}{dZ} \right) \frac{V_f}{V_o} \quad (2.15)$$

### 2.3.2 Transportation model

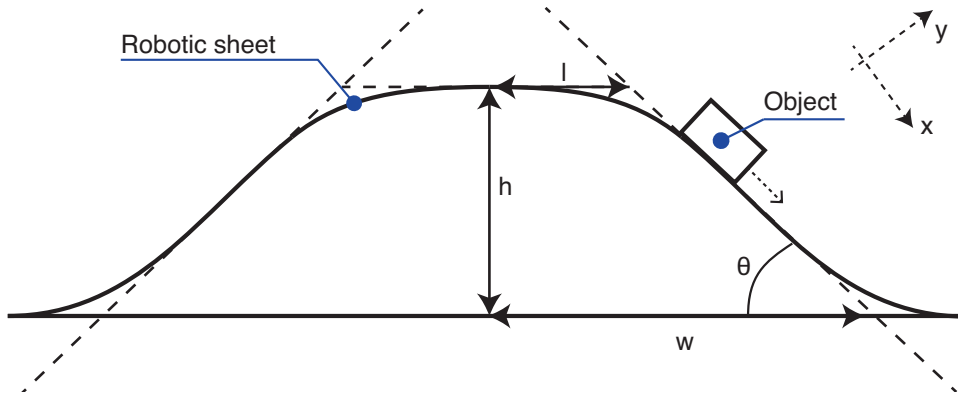


FIGURE 2.5: Geometric representation of the slope and the acting forces over the transported object such as a plate. [ Tone et al., [92], p.6 ]

#### Manipulation modeling for non-rotating objects

The second condition is related to the friction coefficient and the angle of the slope generated when a magnetic field is applied to the robotic sheet. Fig. 2.5 shows the schematic view of the force acting on the object when it is placed over a convex shape generated by the application of a magnetic field. In Fig. 2.5, the  $x$ -axis is a horizontal axis parallel to the surface, and the  $y$ -axis is a vertical axis perpendicular to the convexity. To simplify the computations, the

curved surface can be approximated by using a straight line and a convex surface as a rigid body. The motion of the object is governed by Eqs.(2.16) and (2.17).

$$m \frac{d^2 X}{dt^2} = mg \sin \theta - F \alpha \quad (2.16)$$

$$m \frac{d^2 Y}{dt^2} = F - mg \cos \theta \quad (2.17)$$

In these equations,  $\alpha$  is the coefficient of the thin film,  $m$  is the mass of the object,  $\theta$  is the slope angle,  $g$  is the force of gravity, and  $F$  is the force applied by the ferrofluid. If the right side of Eq.(2.16) is greater than 0, then the object moves along the slope. Eq.(2.17) can be omitted because of the normal forces acting on the fluid surface; thus, assuming that in Fig. 2.5, the only direction in which the object can move is in the  $x$ -direction. It is possible to determine the minimum value of angle  $\theta$  from Eqs.(2.18) and (2.19) to ensure the generation of a convex shape that can be used as a propulsor to move the object along the robot surface. By satisfying Eq.(2.19), the object can slide or rotate on a convex surface.

$$\theta = \arctan \frac{h}{w-l} \quad (2.18)$$

$$\frac{h}{w-l} > \alpha \quad (2.19)$$

$l$  and  $w$  are the displacement of the upper and the bottom side of the convexity, and  $h$  is the height of the convexity as shown in Fig. 2.5.

### Manipulation modeling for rotating objects

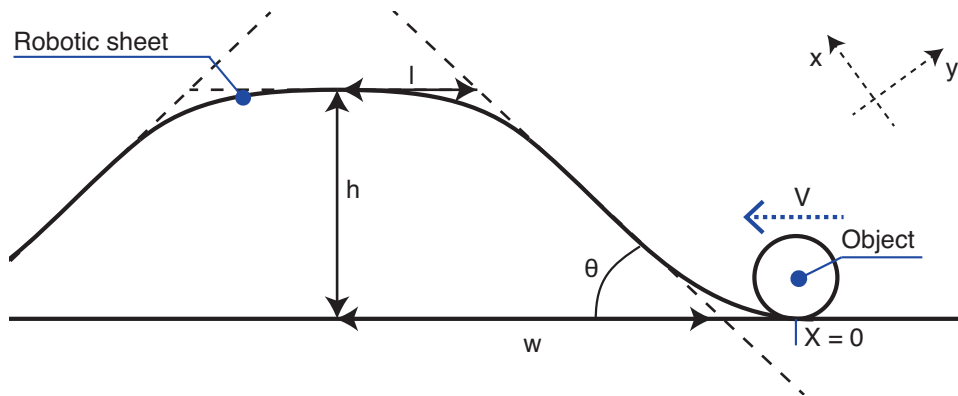


FIGURE 2.6: Geometric representation of the slope and the acting forces over the transported object such as a ball.

The second condition is also related to the object velocity and the angle of the slope generated when a magnetic field is applied to the

robotic sheet. Fig. 2.6 shows the schematic view of the force acting on the spherical object when it moves to the convex surface generated by the application of a magnetic field. The x-axis is a horizontal axis parallel to the surface, and the y-axis is a vertical axis perpendicular to the convexity. The spherical object easily moves on the slope. However, the velocity also easily increases and it is difficult for the system to stop the movement of the object using the convex surface. Then, the velocity range in which the object can stop due to the surface deformation is derived. The convex surface is regarded as a trapezoid, and the condition that the motion stops is that the velocity of the object becomes 0 on the convex slope. By satisfying this condition, the robotic sheet can control the velocity of the object and transport it to a designated goal. The motion of the object is governed by Eqs.(2.20) and (2.17).

$$m \frac{d^2 X}{dt^2} = -mg \sin \theta - F s \quad (2.20)$$

$$F s = \frac{I}{R^2} \frac{d^2 X}{dt^2} \quad (2.21)$$

$$I = \frac{2}{5} m R^2 \quad (2.22)$$

$m$  is the mass of the object,  $g$  is the force of gravity,  $R$  is the radius of the object,  $F s$  is the friction between the object and the robotic sheet, and  $I$  is the moment of inertia. From these equations, the moving distance of the object is defined as Eq.(2.23). If the object stops and its velocity is 0 on the slope of the convex, the object movement can be controlled by our proposed system. This condition is expressed as Eq.(2.24). From these equations, the velocity is shown as Eq.(2.25).

$$X = V t - \frac{t^2}{2(m + \frac{I}{R^2})} m g \sin \theta \quad (2.23)$$

$$X \leq \sqrt{(w - l)^2 + h^2} \quad (2.24)$$

$$V \leq \sqrt{\frac{10gh}{7}} \quad (2.25)$$

$l$  and  $w$  are the displacement of the upper and the bottom side of the convexity, and  $h$  is the height of the convexity as shown in Fig. 2.6.

## 2.4 Manipulation method

In this section, methods of the flat transportation and channel transportation are explained. In the flat transportation, the robotic sheet is set on the flat surface and transports objects on the surface of the robotic sheet. In the channel transportation, the robotic sheet is set on the channel-shape surface and moves a spherical object through its channel.



### 2.4.1 Flat transportation

Fig. 2.7 shows the schematic of the flat transportation using the robotic sheet. An object transportation is realized by making the

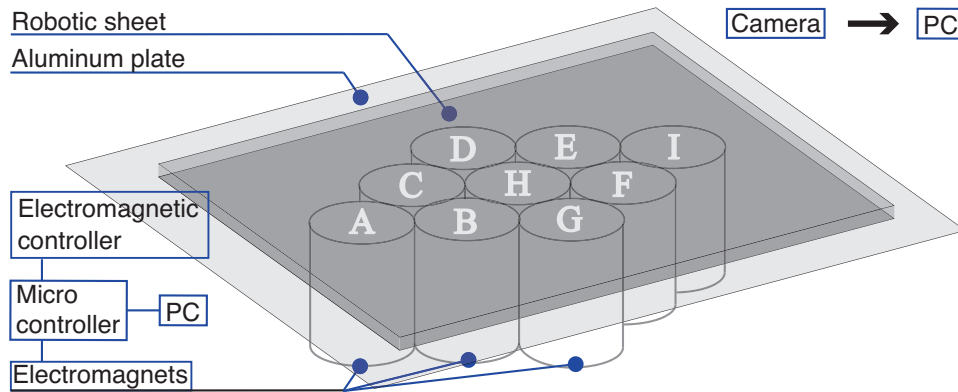


FIGURE 2.7: Schematic diagram of the flat transportation system. This system mainly composed of the robotic sheet and electromagnets. By controlling activation of each electromagnet, the surface of Robotic sheet is controlled. [ Tone et al., [92], p.3 ]

object slide or roll down along a surface gradient pointing downwards. This surface gradient is generated from the concave region made from one or several convexities. When a target object cannot move due to friction even if a thin film with a low friction coefficient is used, oscillation is used to reduce the friction between the target object and the film. First, the principle of the oscillating transporta-

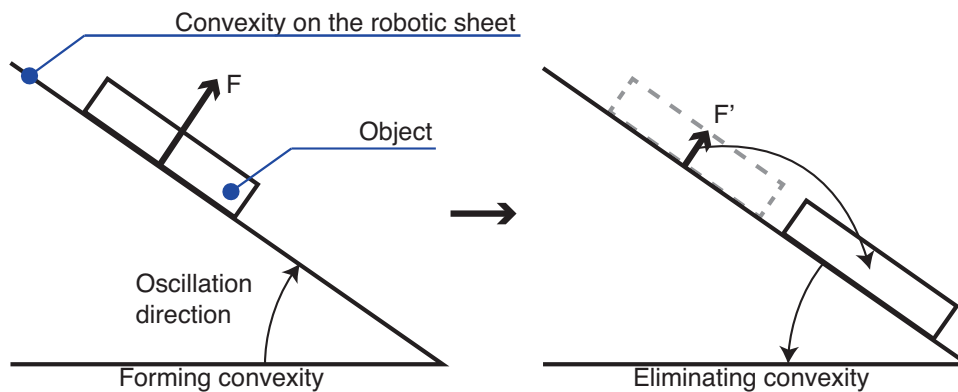


FIGURE 2.8: Image showing the behavior of the surface in the presence of a magnetic field (left picture) and at the time of degaussing the magnetic field (right picture).  $F$  and  $F'$  indicate the normal force. [ Tone et al., [92], p.4 ]

tion method is introduced. Fig. 2.8 shows the schematic explaining the method of oscillating transport. When an electromagnet is activated, an object moves in the direction perpendicular to the surface

of the convexity. At this moment, a force supporting the convexity is applied to the object, and the object clings to the surface because of the static friction between the object and surface. After the magnetic field disappears, the power vanishes, and the surface begins to fall. The normal force to the object drastically decreases, decreasing the static friction; therefore, by oscillating the surface, the friction can be decreased, and the object moves horizontally along the surface.

### Sphere transportation

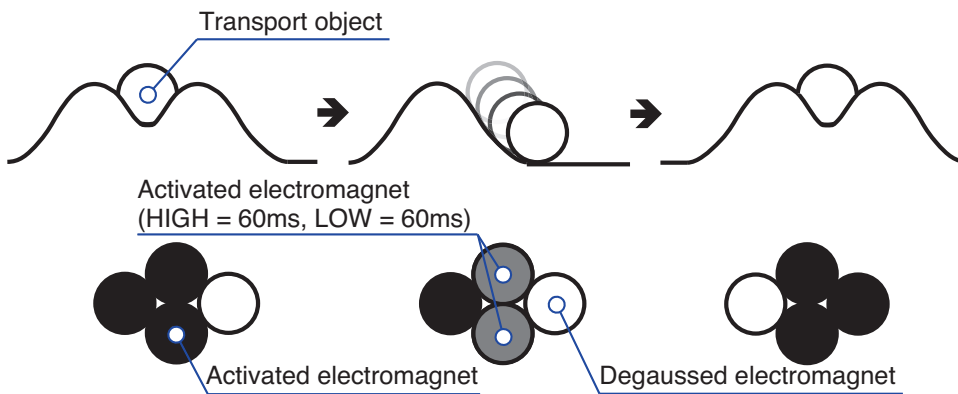


FIGURE 2.9: Transportation method for a sphere. First, the system generates three convexities for making the concave region and traps the transport object. Next, the system degausses two of the electromagnets and rolls the objects in the intended direction. [ Tone et al., [92], p.4 ]

Fig. 2.9 shows the transport method for the two spheres. The robotic sheet moves the object by controlling three adjacent electromagnets. When these electromagnets are activated, three convexities appear and a concave region is formed between them on the interface to trap the object. Then, the system degausses the two electromagnets with the intended direction. A slope is formed due to the remaining convexity, causing the object to roll down along the surface gradient. When the movement of the objects is slow or stopped at this concave region, the signal for the two electromagnets with the intended direction as HIGH and LOW = 60 ms within 5 s is set. In the transportation experiment, the robotic sheet oscillated its surface for 1 s. By using the signal, the surface vibrates and the friction between the object and surface reduces. As a result, the object moves faster with the oscillation than without it. After the object moves, the robotic sheet again generates a concave region by using three other electromagnets and traps the object to prevent it from straying out of the transport route due to the surface crease or the object excessive speed.

When the robotic sheet moves several objects, there is a high possibility that the electromagnets are shared, and a race condition occurs from the transportation algorithms interfering with each other. To avoid this problem, all the operations of the robot are synchronized when sharing the electromagnets for the same behavior. By repeating activation and demagnetization of the electromagnets, the robotic sheet transports an object along the transportation route.

### Plate transportation

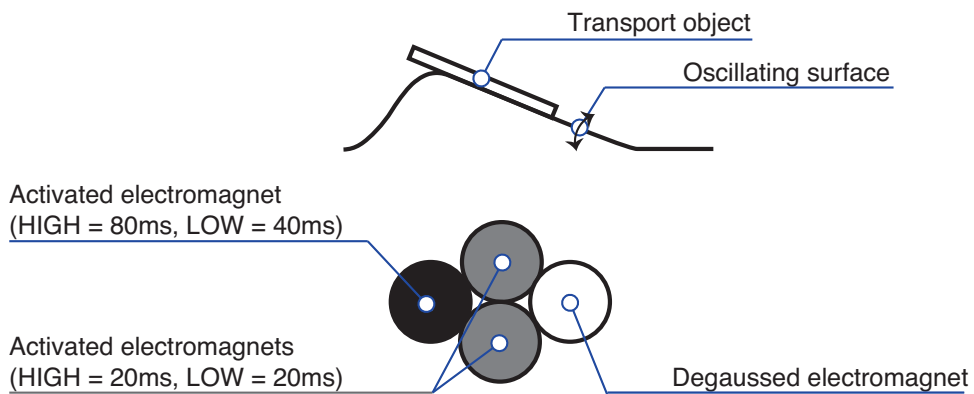


FIGURE 2.10: Transportation method for a thin circle plate. An oscillating slope is generated along to the direction of the transportation route with three electromagnets. [ Tone et al., [92], p.4 ]

In the case of a plate transportation, by using a thin film with a low friction coefficient, it is possible to transport with a concave region generated from a convex, like the flat transportation of a ball. However, in the case of an object with a large mass or a high friction coefficient, the friction between the sheet and the object is increased and the plate cannot move along the surface gradient. Then, this method assumes a case where the object can not move with friction.

In order for the robotic sheet to move a plate in a desired direction, the system creates a slope and oscillates it using three adjacent electromagnets. The oscillation starts at the same time the surface deformation starts, and its signal of one of the electromagnets is set as HIGH = 80 ms and LOW = 40 ms and that of two of the electromagnets is set as HIGH and LOW = 20 ms, as shown in Fig. 2.10. When  $HIGH > LOW$ , the height of the convexity at the peak electromagnet is higher than at the other electromagnets due to the viscosity of the ferrofluid, and a surface gradient is generated in the intended direction. The period of one downward movement is in the range of 5 to 20 s, and the oscillation continues during the period. In the transportation experiment, the period of one downward movement was fixed to 17 s. By repeating these operations, the robotic sheet transports the plate along the transportation route.

## 2.4.2 Liquid manipulation

As a target object in liquid manipulation, a droplet is used in this study. In addition, as liquid manipulation methods, methods of mixing droplets and transporting droplets are described. When the robotic sheet moves a droplet on its surface, the entire system including the robotic sheet uses a visual-feedback methods for controlling the droplet movement. Therefore, as the droplet transport method, the methods of the object detection, the activation of the electromagnets, and Goal Position Setting are explained.

### Liquid mixing

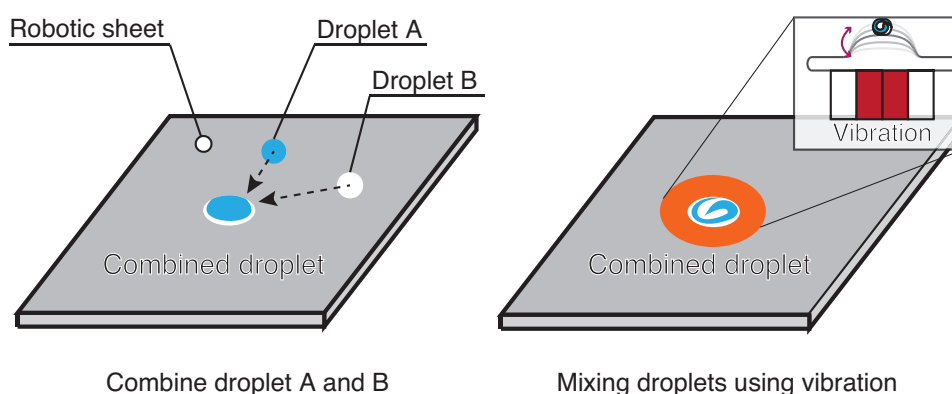


FIGURE 2.11: The schematic image of mixing droplets. By vibrating the surface of a robotic sheet using a pulsed magnetic field generated from electromagnets, combined droplets are stirred and mixing are realized.

Mixing droplets is realized using vibration. This vibration is occurred by applying pulsed magnetic fields from the electromagnets to the robotic sheet, and its frequency can be also controlled. The control unit applies a rectangular voltage with duty ratio of 0.5 to the electromagnets, and the electromagnets generate pulsed magnetic fields depending on the frequency of the pulsed magnetic field. The voltage applied to the electromagnets is 24 V at HIGH and 0 V at LOW. When the pulsed magnetic field is generated from multiple electromagnets, these electromagnets are synchronized and the robotic sheet surface to which the pulsed magnetic field is applied vibrates.

### Object detection for liquid manipulation

As shown in Fig. 2.12, the entire system detects and handles a target object using a visual feedback method using a camera with a frequency of 30 Hz. The position of the target liquid is recognized with the camera by setting the pixel red-green-blue (RGB) values on an area other than the target liquid to 0 and extracting the RGB values

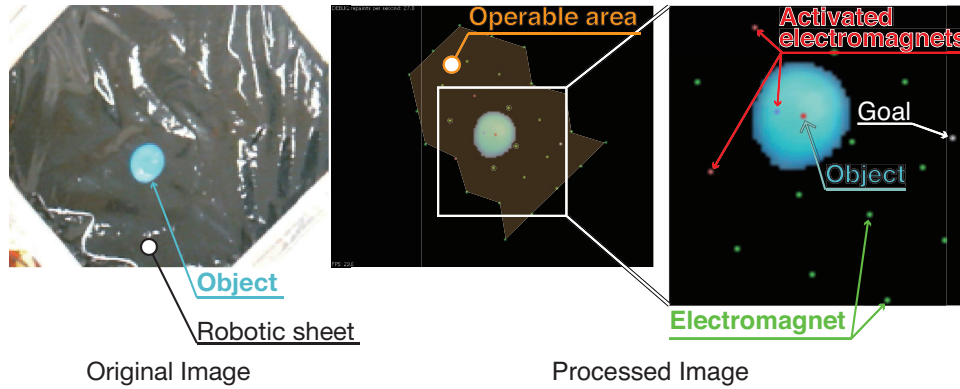


FIGURE 2.12: Processed target object using a web camera mounted above the robotic sheet. The rightmost image is the enlarged image. The coordinates of the electromagnet were acquired beforehand. [ Tone et al.,[91], p.2816 ]

of the target liquid. Some reflecting lights on the robotic sheet cause noise. The color of the robotic sheet is black and the reflecting light is white. The noise is mainly grey, and the dispersion of RGB values of noise is much smaller than that of colored target liquid. Therefore, when the difference between each of the RGB values and the average value obtained by combining these values is 30 or less, the RGB value of this place is set to 0. By this process, the proposed system can extract only the target object. A target position is obtained by calculating the mean of X and Y coordinates of the target liquid at its center. The position of each electromagnet is obtained in advance and set to the proposed system.

### Activation of electromagnets for liquid manipulation

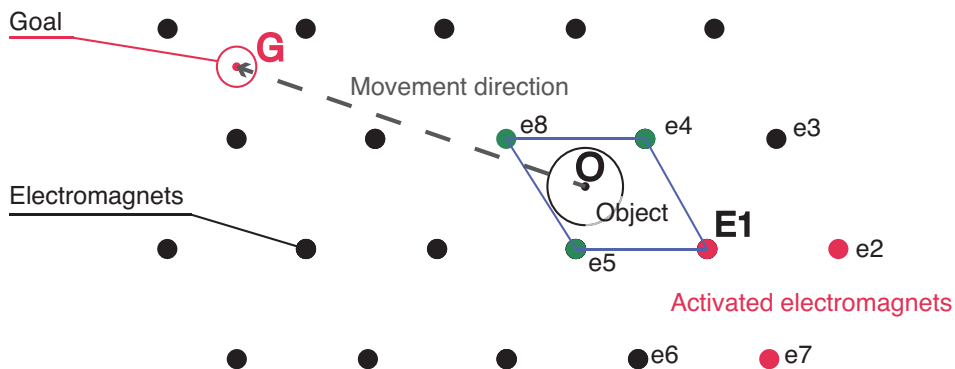


FIGURE 2.13: Transportation method for an object. Using three activated electromagnets, the surface is lifted, and the object descends along the slope, moving the object. [ Tone et al., [91], p.2817 ]

An automatic liquid manipulation is realized by activating three adjacent electromagnets, creating a downward slope, and moving a target liquid along it. Fig. 2.13 is a schematic image of the proposed system. An area where the target object is always surrounded by four adjacent electromagnets is defined as an operable area, as shown in Fig. 2.12. The object within the operable area is always surrounded by four electromagnets, E1, e4, e5, e8, as shown in Fig. 2.13. Electromagnet E1 is selected, which is farthest from the goal. Among six electromagnets: e2, e3, e4, e5, e6, e7 adjacent to E1, the two electromagnets: e2, e7, which are farthest from the goal are selected. After that, the surface is lifted up by activating three adjacent electromagnets and the target liquid is moved toward the defined goal due to the downward slope. If the droplet sits on one of the electromagnets, by activating three adjacent electromagnets near the electromagnet, the proposed system moves the droplet slightly from the position of the electromagnet. By repeating this algorithm, the proposed system automatically moves the target liquid to the goal discretely. If the object moves around the boundary of the operable area, and there are only one or two adjacent electromagnets to be activated, the proposed system activates these electromagnets.

### Goal position setting for liquid manipulation

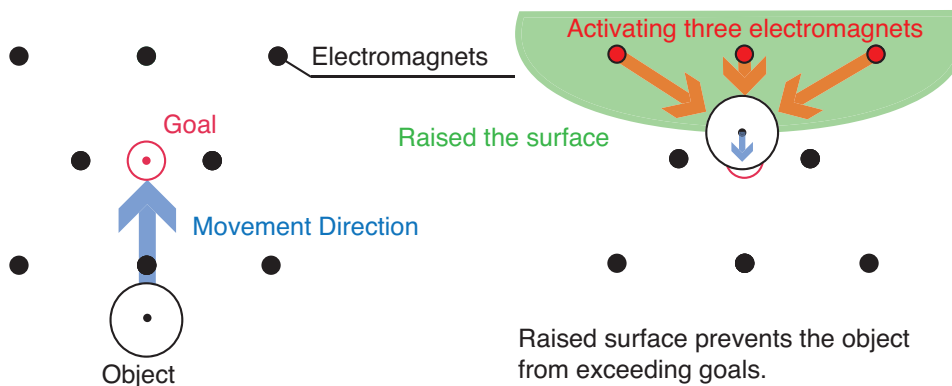


FIGURE 2.14: Goal position setting near the boundary of the electromagnets area. [ Tone et al., [91], p.2817 ]

A goal position should be set in order to prevent the liquid from exceeding that goal and operable area. The method for setting a goal position is proposed as shown in Fig. 2.14. When the object arrives at the goal, by activating the three electromagnets on the opposite side of the object with respect to the destination and lifting up the surface of the robotic sheet to stop the object moving, the proposed system prevents the object from exceeding the goal and operable area.

### 2.4.3 Channel transportation of a ball

In channel transportation, the robotic sheet is set on a channel surface and transports a ball through its channel. Fig. 2.15 shows the transport method. When the robotic sheet moves the ball, two elec-

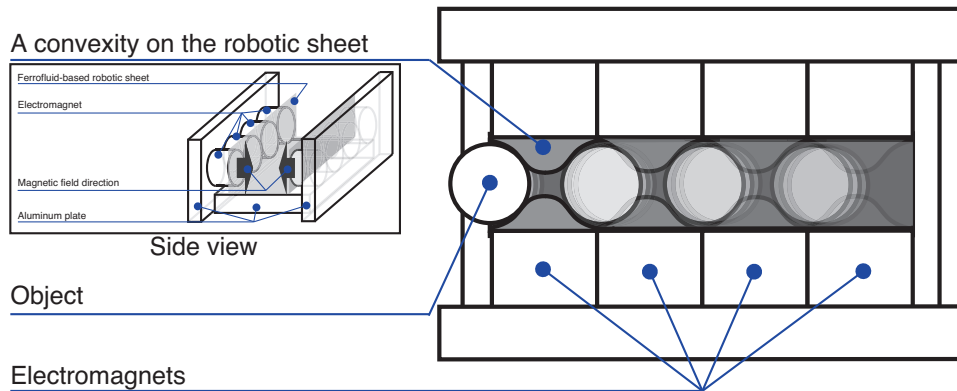


FIGURE 2.15: Top view of the channel transportation system. The system activates the two electromagnets facing each other and generates two convexities to push the object. By controlling the electromagnets and moving the convexities, the channel ferrofluid-based robotic sheet moves the object. [ Tone et al., [92], p.5 ]

tromagnets are activated in the opposite directions and a convexity is generated on each side. The ferrofluid in the robotic sheet moves toward the source of the magnetic field against the gravity and gathers around it. Therefore, the channel width of the robotic sheet locally decreases and the height of the bottom increases. The ball is pushed by the two convexities and moves on the slope formed by the height difference of the bottom of the channel. By switching the electromagnets with the pre-defined direction, the robotic sheet moves the object within the channel.





# Chapter 3

## System Overview

### 3.1 Ferrofluid-based deformable robotic sheet

Two type of ferrofluid-based deformable robotic sheets are used in this research. One is used for solid objects such as balls and plates, and the other is used for flexible objects such as droplets. Some wrinkles with a height of about a few mm or less appears on the robotic sheets to be explained, so that a ferrofluid deformation is not prevented by the thin film. Because of the wrinkles of the sheets, the distribution of the ferrofluid is not uniform. However, the ferrofluid can freely move and gather to the source of the magnetic field.

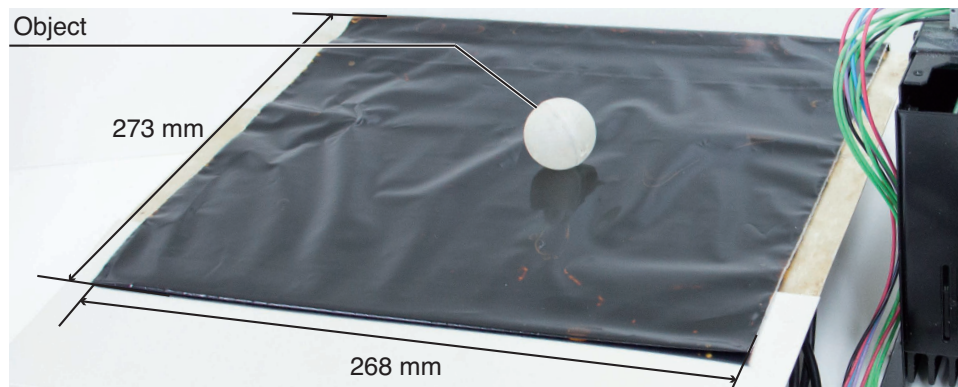


FIGURE 3.1: A ferrofluid-based deformable robotic sheet for solid objects. Polyethylene films are used as the thin film and a ferrofluid is wrapped with the films. [ Tone et al., [92], p.3 ]

#### 3.1.1 Ferrofluid-based deformable robotic sheet for solid objects

This ferrofluid-based deformable robotic sheet is used for transporting solid objects such as balls and plates. Fig. 3.1 shows the appearance of this robotic sheet. This robotic sheet is quadrilateral shape and its four sides are thermally compressed. It has a layered structure and uses polyethylene film as the thin film since the polyethylene film has a high robustness against damage caused by

TABLE 3.1: Ferrofluid in the ferrofluid-based deformable robotic sheet for solid objects

Name	DS-50 Sigma Hi-Chemical Inc.
Solvent	Isoparaffin
Ferromagnetic particle	Magnetite
Surfactant	Oleic acid
Saturation magnetization	50.0 mT
Specific gravity	1.4
Mass	71.4 g
Viscosity (293.15 K)	50.0 mPa·s

contact with the target objects. Furthermore, an unbreakable and easy processing material is preferable. A ferrofluid is wrapped with the polyethylene film.

The size of this polyethylene film is 273 mm × 268 mm × 0.15 mm (thickness), and that of the robotic sheet is 273 mm × 268 mm × 1.8 mm (thickness). The maximum height of the convexity of the robotic sheet is 4.7 mm, and its diameter is approximately 60 mm. By controlling the electromagnets, moving the position of the convexity, and oscillating the surface of the robotic sheet according to the transportation route, the system can move the balls and plates on the surface. The ferrofluid used in this robotic sheet is shown as Table 3.1.

### 3.1.2 Ferrofluid-based deformable robotic sheet for flexible objects



FIGURE 3.2: The ferrofluid-based deformable robotic sheet for flexible objects. Polytetrafluoroethylene films are used as the thin film and a ferrofluid is wrapped with the films. [ Tone et al., [91], p.2816 ]

This ferrofluid-based deformable robotic sheet is used for transporting flexible objects such as droplets. Fig. 3.2 shows the appearance of this robotic sheet. This robotic sheet is quadrilateral shape and its four sides are thermally compressed. This robotic sheet also

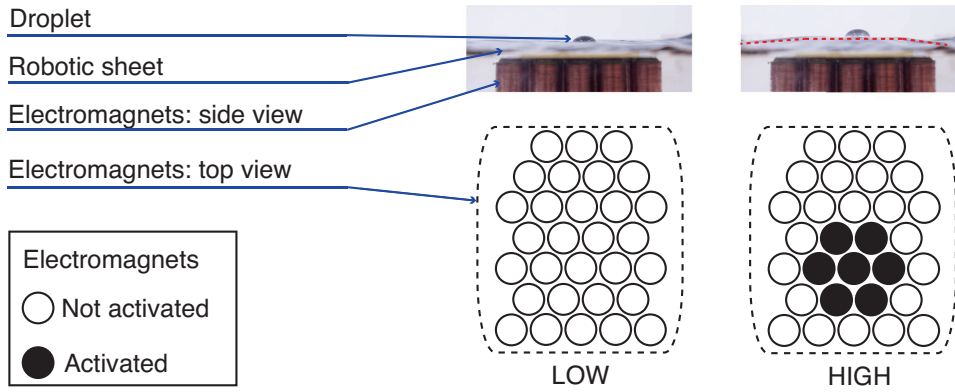


FIGURE 3.3: By activating several electromagnets, the surface can be deformed along with the number of electromagnets. [ Tone et al., [91], p.2816 ]

TABLE 3.2: Ferrofluid in the ferrofluid-based deformable robotic sheet for droplets

Name	DS-50 Sigma Hi-Chemical Inc.
Solvent	Isoparaffin
Ferromagnetic particle	Magnetite
Surfactant	Oleic acid
Saturation magnetization	46.6 mT
Specific gravity	1.4
Mass	43.9 g
Viscosity (293.15 K)	88.0 mPa·s

has a layered structure and a ferrofluid is wrapped with polytetrafluoroethylene films as the thin film. Thin films with a high water and oil repellency are suitable for droplet manipulation. The films should be easy to process and also minimize the inhibition of ferrofluid deformation. Hence, I use a polytetrafluoroethylene (PTFE) film.

Fig. 3.3 shows the surface deformation with the electromagnets activated. By activating several electromagnets adjacent to each other, the surface to which the magnetic field is applied is lifted up. When a droplet spreads on the surface of the robotic sheet as the volume increases, a magnetic field is generated from multiple electromagnets to raise the surface of the robotic sheet, where the droplet and robotic sheet are in contact since the droplet shape changes during its moving and

The size of the PTFE film is  $130 \text{ mm} \times 121 \text{ mm} \times 0.025 \text{ mm}$  (thickness), and that of the robotic sheet is  $130 \text{ mm} \times 121 \text{ mm} \times 2 \text{ mm}$  (thickness). The maximum height of the convexity of the robotic sheet is 3.5 mm, and its diameter is approximately 30 mm. By controlling the electromagnets automatically according to the position of the droplets and the goal using the camera, the robotic sheet can move droplets on the surface. The ferrofluid used in this robotic sheet is shown as Table 3.2.

## 3.2 Electromagnets

### 3.2.1 Electromagnets for solid objects



FIGURE 3.4: Arrangement of electromagnets used for transporting solid objects.

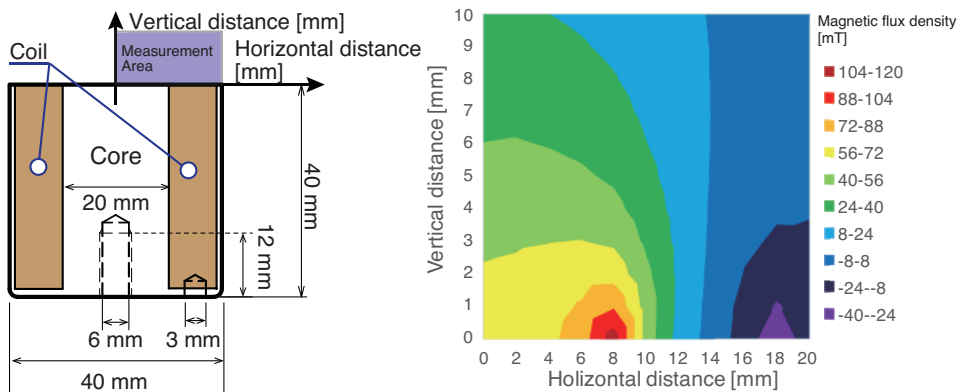


FIGURE 3.5: Structure of an electromagnet for solid objects and distribution of a magnetic field. [ Tone et al., [92], p.3 ]

The nine electromagnets (K.K Fujita, FSGP-40D) are arranged adjacent to each other to reduce the space between the electromagnets as shown in Fig. 3.4. A magnetic field is generated by electromagnets, which are supplied with DC 24 V and 0.24 A from a power supply (K.K Fujita, FSC-2403-P13). The structure and magnetic field of each electromagnet are shown in Fig. 3.5. The electromagnet has an iron core, and its coil is surrounded by iron connected to the core; thus, magnetic flux from the core gathers on the iron at the side of the electromagnet. At the edge of the electromagnet, the magnitude of the magnetic field drastically decreases. At this part on the robotic sheet, the surface of the robotic sheet curves downwards. The proposed system moves an object using this downwards part.

### 3.2.2 Electromagnets for flexible objects

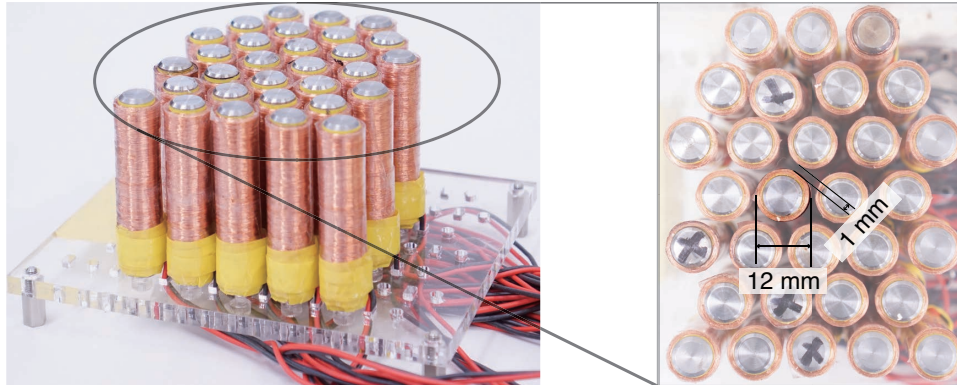


FIGURE 3.6: Arrangement of electromagnets used for transporting flexible objects. [ Tone et al., [91], p.2816 ]

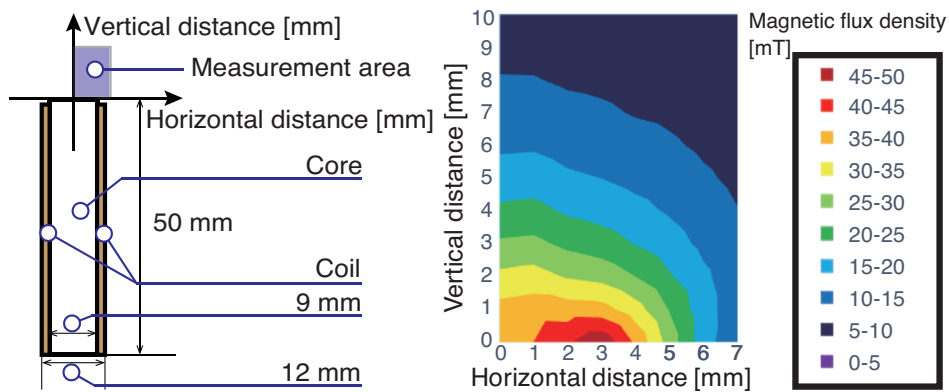


FIGURE 3.7: Structure of an electromagnet for small objects and distribution of a magnetic field. [ Tone et al., [91], p.2816 ]

The 30 electromagnets (K.K Gigateco, TMB-1209G) are arranged adjacent to each other to reduce the space between the electromagnets as shown in Fig. 3.6. A gap of 1 mm is set between electromagnets to avoid interference from both the conducting wire extending from the electromagnet and the adjacent electromagnet. As shown in Fig. 3.7, the diameter of the electromagnets is 12 mm. A DC voltage of 24 V and a current of 0.192 A are supplied to each electromagnet, and a control unit controls the power supply (K.K Fujita, FSC-2403-P13). The magnetic field at the center of this electromagnet is 39.9 mT.

At the edge of the electromagnet, the magnitude of the magnetic field drastically decreases. At this part on the robotic sheet, the surface of the robotic sheet curves downwards. The robotic sheet moves an object using this downwards part. In this research, the diameter of the target droplet is a few centimeters or less. The diameter of the convex on the ferrofluid sheet is about 3 cm, and the size of the convex generated by an electromagnet is enough to move the droplet to



an area where a convex is generated by an adjacent electromagnet. 30 electromagnets are used, but if the feasibility of moving and mixing objects is established by this experiment, scaling it for other intended uses is possible in the future. It is also possible to increase the resolution by downsizing the electromagnet. When a droplet spreads on the surface of the robotic sheet as the volume increases, a magnetic field is generated from multiple electromagnets to raise the surface of the robotic sheet, where the droplet and robotic sheet are in contact.

### 3.3 Manipulation system

#### 3.3.1 Flat transportation for solid objects

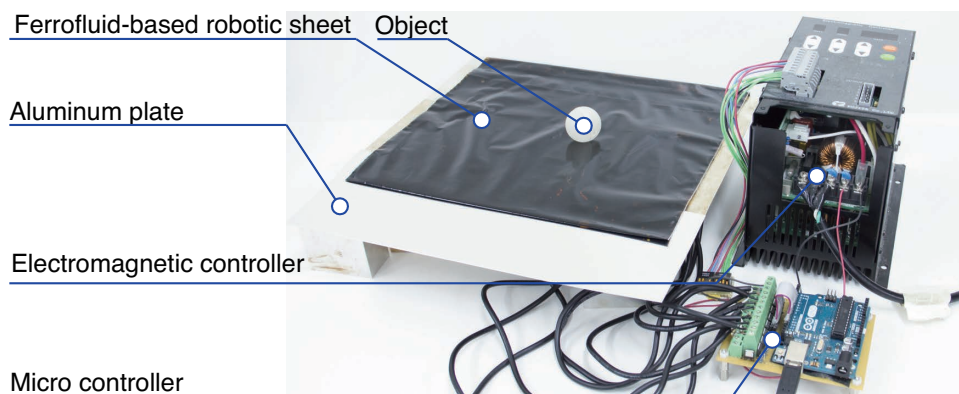


FIGURE 3.8: Overall system of the ferrofluid-based deformable robotic sheet for solid objects. [ Tone et al., [92], p.3 ]

Table 3.3 shows the system specifications. The entire system consists of the ferrofluid-based deformable robotic sheet for solid objects, electromagnets, power supply, micro-controller (Atmega328P-PU), PC, and camera, as shown in Fig. 3.8. The activation and deactivation of each electromagnet is controlled using a microcontroller. There are two configurations of transport methods for this robot: flat transportation, in which the robotic sheet is set on a flat surface and the robot transports the object on its surface, and channel transportation, in which the robotic sheet is curled up and the object moves through it. In the flat transportation, between the robotic sheet and the electromagnets, there are 0.5 mm thick aluminum plates to support the robotic sheet flat on the electromagnets. This plate is not affected by the magnetic field because it is non magnetic. The camera located above the robot tracks the position of the transport object and sends the data to a PC. Currently, the camera is just used to record the object movement.

TABLE 3.3: System specifications of the robotic sheet for solid objects

Power	DC24 V, 2.16 A
Polyethylene film [mm]	273 × 268 × 0.15 (Thick)
Robotic sheet [mm]	273 × 268 × 1.8 (Thick)
Electromagnet [mm]	40 × 40 (D × H)

### 3.3.2 Flat transportation for flexible objects

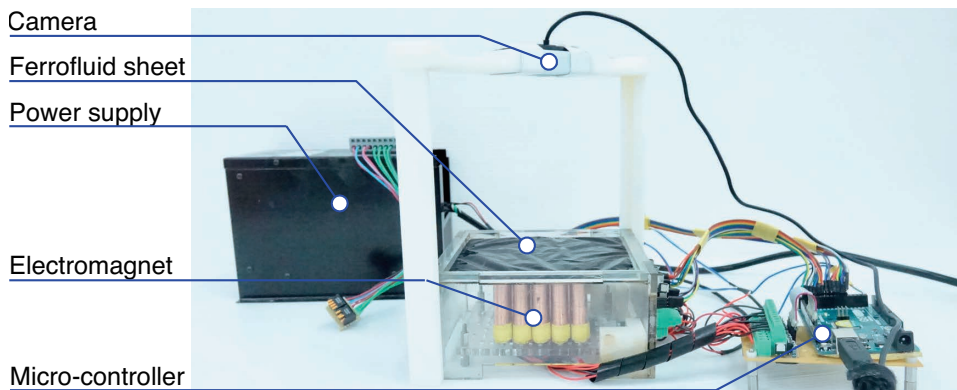
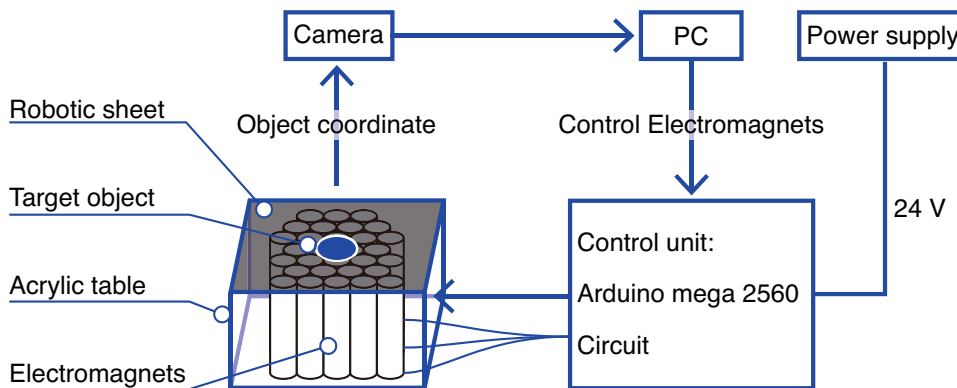


FIGURE 3.9: Overall system of the ferrofluid-based deformable robotic sheet for flexible objects.

FIGURE 3.10: Schematic diagram of the robotic sheet.  
[ Tone et al., [91], p.2815 ]

As shown in Fig. 3.9, the overall system is composed of the ferrofluid-based deformable robotic sheet for flexible objects, electromagnets (K.K Gigateco, TMB-1209G), microcontroller (Arduino Mega 2560), power supply (K.K Fujita, FSC-2403-P13), PC, and web camera (Logitech Co Ltd., C615). Fig. 3.10 is the schematic diagram of the system. A visual feed-back method is introduced to droplet manipulation. The frequency of the feedback loop is 30 Hz.

Table. 3.4 shows the system specifications. The frequency of the feedback loop is 30 Hz. The robotic sheet is installed on an acrylic table, and the electromagnets are set beneath it to apply a magnetic

TABLE 3.4: System specifications of the robotic sheet for flexible objects.

Power	DC24 V, 2.16 A
Polyethylene bag [mm]	131 × 120 × 0.02 (Thick)
Ferrofluid sheet [mm]	131 × 120 × 2.0 (Thick)
Electromagnet [mm]	40 × 12 (D × H)

field to the bottom of the robotic sheet. A 2 mm gap is maintained between the electromagnets and the acrylic board with a thickness of 1 mm, to prevent the electromagnets from transmitting heat to the robotic sheet. A control unit including a microcontroller and circuit controls the activation of the electromagnets.

### 3.3.3 Channel transportation

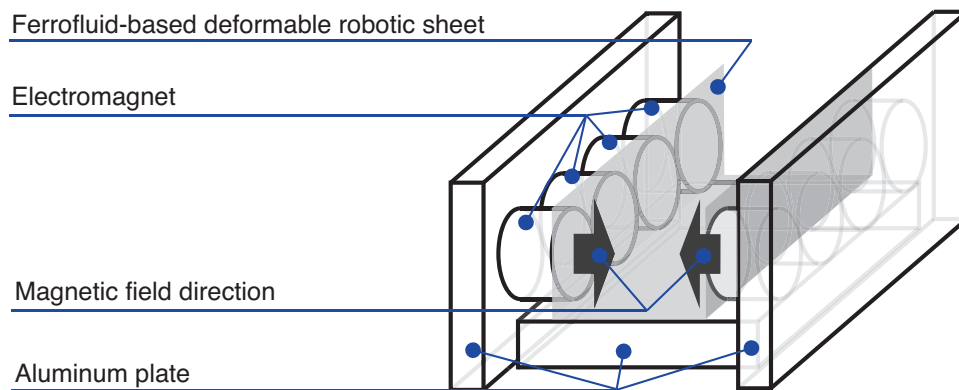


FIGURE 3.11: Schematic diagram of the channel transportation system. [ Tone et al., [92], p.3 ]

Fig. 3.11 shows an overview of the channel transportation. The robotic sheet for solid objects is curled up, and eight electromagnets are symmetrically placed on the sides of the robotic sheet. The electromagnets are fixed to an aluminum block. The channel width is 33 mm in the absence of a magnetic field. Firstly, the ferrofluid in the robotic sheet stays on the bottom of the channel owing to gravitational force. Under the presence of a magnetic field, the ferrofluid moves and gathers around the source of the magnetic field, creating a convexity on the inner side of the channel. The convexity changes the channel width and pushes the sides of the object in the robotic sheet and moves it through the channel. This transport method mimics the bionic movement, such as that of an esophagus.



## Chapter 4

# Basic characteristics of robotic sheet

In this research, the characteristics of the ferrofluid-based deformable robotic sheets are verified and the object manipulation using it are realized. The characteristics of a ferrofluid have already been elucidated. However, the robotic sheet is composed of the ferrofluid enclosed by the polyethylene or PTFE films, and these films affect the deformation, the output force, and magnetic responsiveness of the ferrofluid. Therefore, in this chapter, these effects are elucidated.

### 4.1 Surface deformation

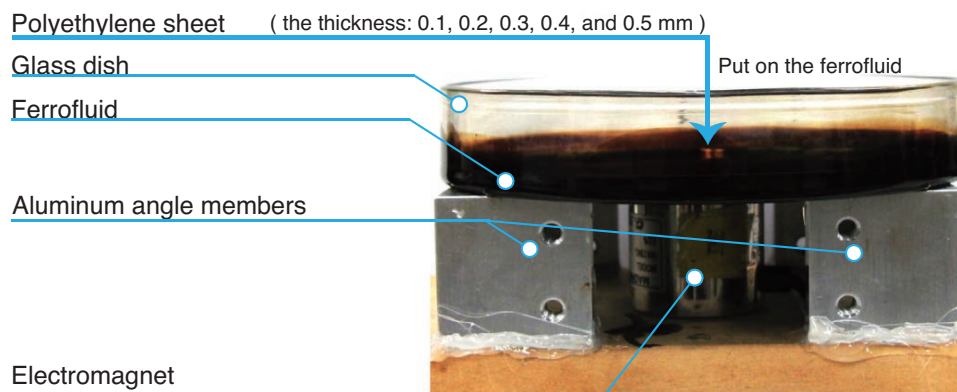


FIGURE 4.1: Appearance of the equipment used in the surface deformation. This equipment is simple version of the robotic sheet, and the thickness of the ferrofluid is measured using 3D-CT by changing the thickness of the polyethylene sheet: 0.1, 0.2, 0.3, 0.4, and 0.5 mm. [ Tone et al., [92], p.7 ]

The verification of the effect of the polyethylene sheets on the shape of the ferrofluid in the robotic sheet under the influence of a magnetic field is explained. This verification was conducted to obtain the knowledge required to formulate the shape model of the robotic sheet. In this experiment, simple version of a robotic sheet instead of the proposed robotic sheets were used for changing the thickness of the polyethylene sheet on the ferrofluid, as shown in

Fig. 4.1. This equipment consisted of polyethylene films and a ferrofluid with a volume of 51.6 mL in a glass dish with a height of 28 mm, an inner diameter of 148 mm, and a bottom thickness of 1.8 mm. Without the magnetic field, the thickness of the ferrofluid in the dish was 2.1 mm. The electromagnet used for transportation of solid objects was set under the dish, and the center axis of the electromagnet and the dish were aligned. The magnetic field generated from the electromagnet was sufficiently reduced at the edge of the dish, and the edge did not affect the fluid shape. Four aluminium angle members were set under the dish for supporting it. The height of the members was the same as that of the electromagnet, and these members were hardly affected by the magnetic field because aluminum is non-magnetic material. Moreover, these members were more than 10 mm away from the electromagnet, and the magnetic fields were sufficiently reduced at the points. The polyethylene sheet used in this experiment was developed by piling up a polyethylene film with 0.02 mm thickness. The thickness of the polyethylene sheet was initially 0.5 mm and reduced by every 0.1 mm whenever the fluid shape was measured. The shape of the ferrofluid without the sheet was also measured.

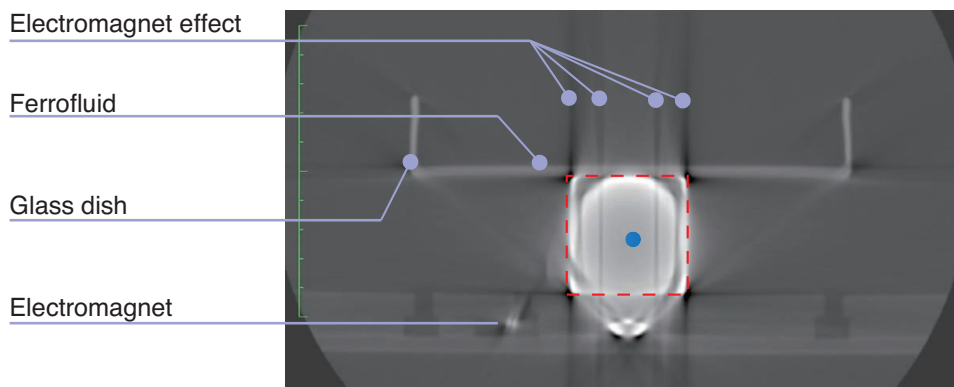


FIGURE 4.2: Tomographic image. The red square is the electromagnet and the white object over the electromagnet is the ferrofluid in the glass dish. There are black lines on each images due to the electromagnet. [ Tone et al., [92], p.7 ]

### 4.1.1 Shape measurement method

3D-CT was used to measure the thickness of the ferrofluid under the polyethylene sheet [93]. By using the 3D-CT, the measurement accuracy could be maintained and the shape of the ferrofluid was measured by using a magnetic field applied through a non contact method. The 3D-CT uses an X-ray to take tomographic images of the subject at 0.5 mm intervals. An X-ray is provided to the subject

from an X-ray tube bulb; a part of the X-ray is absorbed by the subject, and the radiation detector on the other side of the X-ray tube bulb measures the absorbed rate. The X-ray tube bulb and the radiation detector quickly revolve around the subject. As shown in Fig. 4.2, the tomographic image could be obtained because the image was reconstructed based on the X-ray obtained through Fourier transformation. The white parts on the image represent the subject while the other part represents the background. The obtained image was analyzed through OsiriX (Pixmeo). The field of view of the 3D-CT is 240 mm, and the pixel matrix of the tomographic image is a  $512 \times 512$  pixel matrix. The length of a pixel side is 0.46875 mm. Each pixel has a pixel value derived from the X-ray absorption rate of the object and is expressed as light and shade on the image. Based on the difference in the light and shadow areas, I detected the boundary of the object and measured the thickness of the ferrofluid.

### 4.1.2 Experiment procedure

The thickness of the sheet was initially 0.5 mm and was reduced by 0.1 mm after the tomographic image was taken; this process was repeated until the thickness was 0.0. The tomographic image was taken more than 20 s after the electromagnet was activated because it took more than 20 s for the ferrofluid deformation to stop under the presence of the ferrofluid. The ferrofluid boundary was extracted from the tomographic images through the canny edge detection [94] after the edges were emphasized.

### 4.1.3 Result

Fig. 4.2 shows the tomographic image taken through 3D-CT. The red square represents the electromagnet and the white object over it is the ferrofluid in the glass dish. Fig. 4.2 shows four black lines, which occurred because the absorption rate of the electromagnet including iron was higher than that of the other objects, and this effect was maximum at the edge of the electromagnet. The two inside lines in Fig. 4.2 express the inner edge of the coil in the electromagnet, and the other lines express the outside edge. I extracted the thickness of the ferrofluid by considering this effect.

Fig. 4.3 shows the experimental result when a magnetic field was applied to the ferrofluid. The number at the upper left corner of each image represents the sheet thickness, and the red line represents the fluid interface. The maximum thickness of the ferrofluid with the sheet was lower than without the sheet, and the width of the convexity with the sheet was wider than without the sheet. The maximum thickness of the ferrofluid decreased with the increasing sheet thickness. As the thickness of the ferrofluid reached 0.0, two saliencies appeared on the fluid interface around the top of the convexity; these

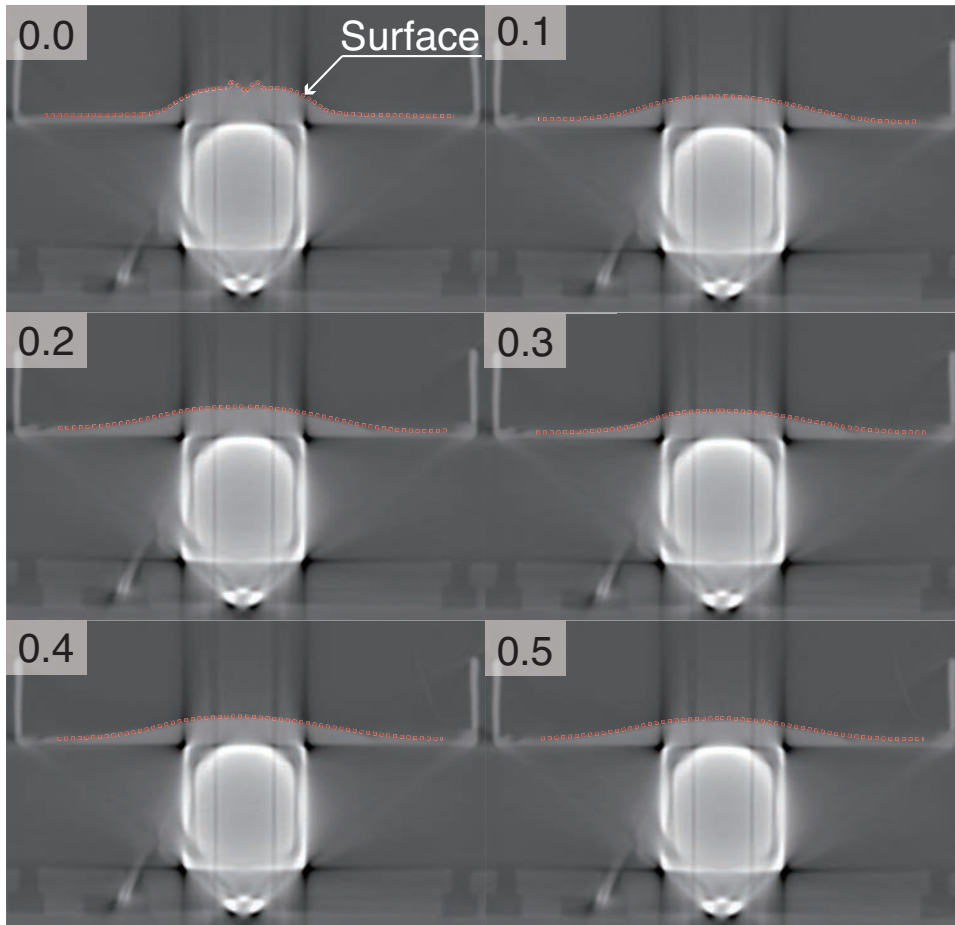


FIGURE 4.3: Result of the shape measurement. The number at the upper left corner of each image indicates the thickness of the polyethylene sheet. In the first figure "0.0" means the sheet is not on the fluid. The red lines on each picture represent the interface of the ferrofluid. [ Tone et al., [92], p.7 ]

appeared as spikes caused by the instability of the ferrofluid [43], as shown in Fig. 2.1. I extracted the fluid thickness on each sheet within 40 mm horizontally from the center of the electromagnet.

Fig. 4.4 shows the extracted data. This data includes the bottom thickness of the glass dish. The black line represents the fluid shape without the sheet, while other lines represent the fluid with the sheet. At approximately  $X = 4$  mm, the black line suddenly changed. This part is represented by the spike on the ferrofluid. The application of the sheet on the fluid caused the spike to disappear. The fluid thickness decreased with increase of the sheet thickness. At approximately  $X = 22$  mm, the black line went below the other lines. The effect of the magnetic field reduced sufficiently over  $X = 20$  mm because the radius of the electromagnet was 20 mm; thus, the

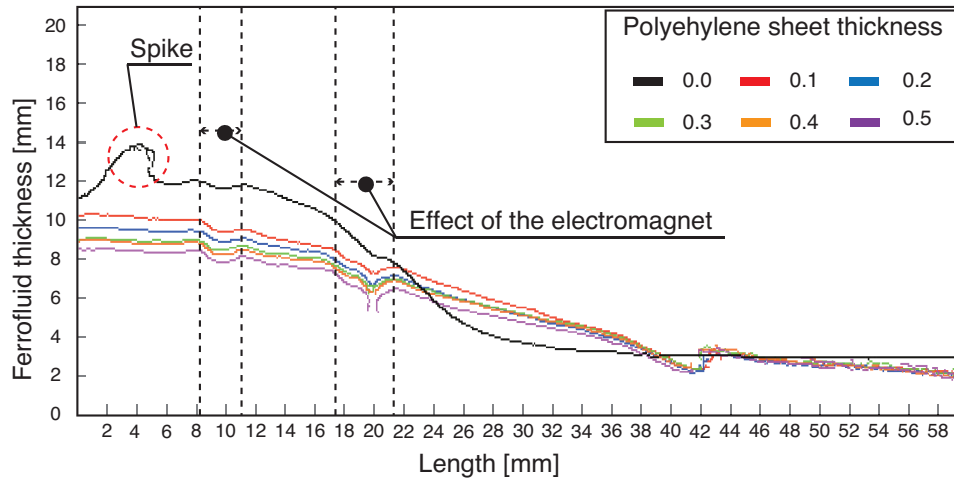


FIGURE 4.4: Thickness of the ferrofluid. Horizontal axis represents the length from the center of the convexity. Vertical axis represents the thickness of the ferrofluid. The legend represents the thickness of the polyethylene sheet on the ferrofluid. "0.0" implies "without the sheet". [ Tone et al., [92], p.8 ]

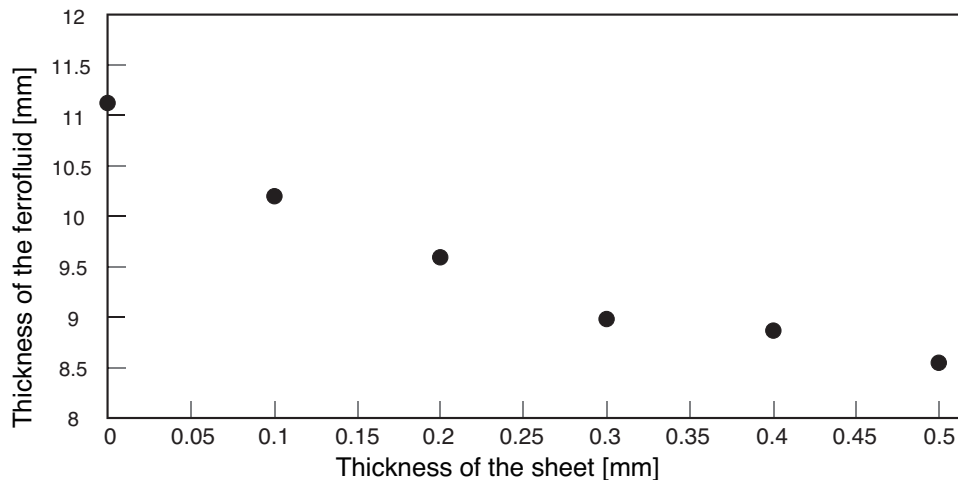


FIGURE 4.5: Relationship between the thicknesses of the polyethylene sheet and the ferrofluid in the simple version of the robotic sheet at the center of the convexity ( $X = 0$ ). The horizontal axis represents the thickness of the polyethylene sheet and the vertical axis represents the thickness of the ferrofluid in the robotic sheet. [ Tone et al., [92], p.8 ]

thickness of the ferrofluid without the sheet decreased sharply. However, when the sheet was placed on the ferrofluid, the internal pressure increased because the fluid thickness at the deformed portion decreased according to the weight of the sheet, and the fluid thickness increased over 20 mm. As the distance increases horizontally from the center of the electromagnet, it was confirmed that there was

no difference in thickness of the ferrofluid inside the robotic sheet caused by the difference in thickness of the film. Over  $X = 37$  mm, the thickness of the ferrofluid with the sheet sharply changed because a bubble was inserted between the sheet and ferrofluid interface. Fig. 4.5 shows the relationship between the thicknesses of the polyethylene sheet and ferrofluid at  $X = 0$ . The ferrofluid thickness gradually decreased around the center of the convexity.

## 4.2 Force of Robotic sheet

The purpose of this experiment is to clarify the mass range of the object which the robotic sheet lifts up and the relationship between the mass range and the displacement of the convex surface of the robotic sheet. The robotic sheet moves the object using the surface gradient of the convex surface generated by its deformation. As shown in Eq. 2.14, as the mass of the object on the convex surface of the robotic sheet increases, its displacement decreases.  $F$  in Eq. 2.14 includes  $\frac{dH}{dz}$  as shown in Eq. 2.13, and  $\frac{dH}{dz}$  increases as the distance between the object and the source of the magnetic field decreases. It is difficult to achieve the theoretical value of the mass range of the object due to its non-linear relationship. Then, by measuring the relationship between the mass of the object and the displacement of the convex surface, the mass range of the object is elucidated. Also, it is verified whether the relationship can be approximated linearly or not.

### 4.2.1 Experiment procedure

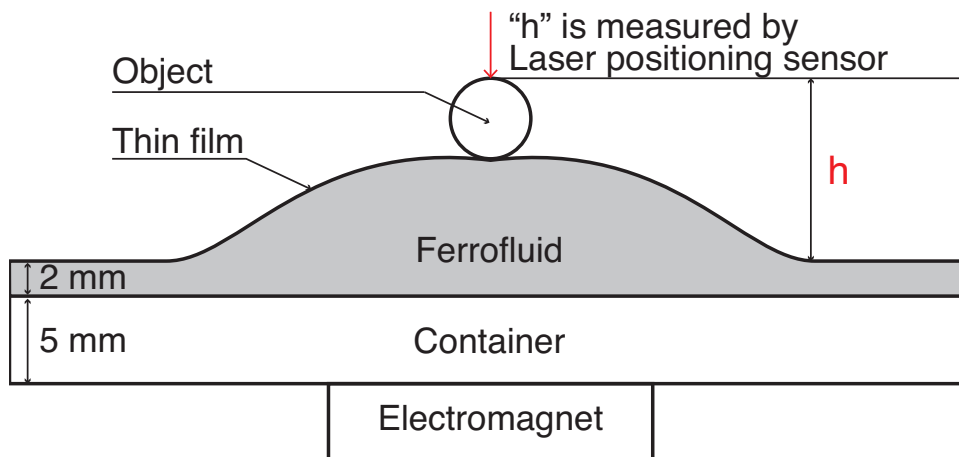


FIGURE 4.6: Schematic image of this experiment. The simple version of the robotic sheet is used. A sphere object is put on the robotic sheet. The mass of the object is changed and the displacement change is measured using a laser positioning sensor.

Fig. 4.6 shows the experimental setup. In this experiment, the simple version of the robotic sheet was used, in which a ferrofluid was placed in a glass container with a bottom thickness of 5 mm and a polyethylene sheet was placed on the interface of the ferrofluid. The thickness of the ferrofluid from the bottom of the container was 2 mm. Under the glass container, the same electromagnet used for solid objects was set. As the object used in this experiment, a capsule ball with a diameter of 30 mm was used. The mass of this capsule ball was changeable between 3 g and 11 g. As shown in Fig. 4.6, the capsule ball was placed right above the electromagnet. The indicator of this experiment was the displacement before and after the deformation of the robotic sheet in the state where the capsule ball was installed. The displacement was measured by irradiating the laser to the apex of the capsule sphere from the laser positioning meter (Hokuyo Automatic Co., Ltd., PDA-25KT). The measurement was carried out ten times with respect to each mass of the capsule ball.

#### 4.2.2 Result

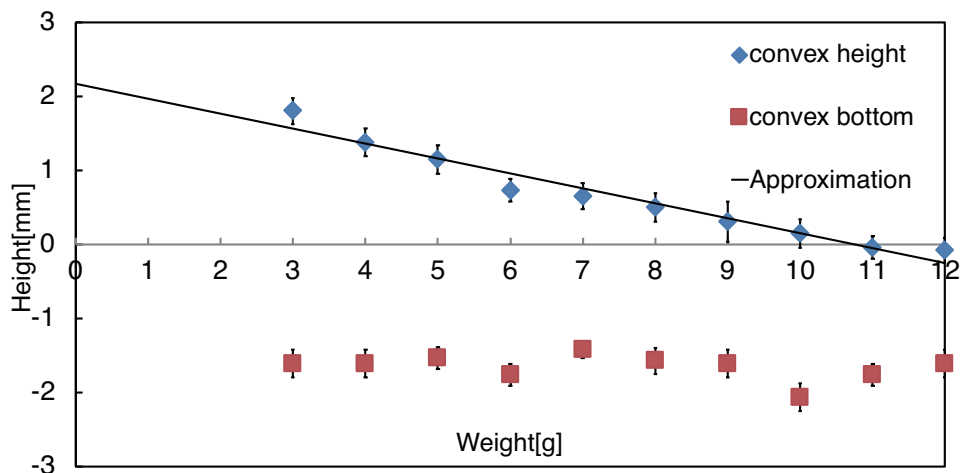


FIGURE 4.7: Blue dots shows the top of the convex surface of the robotic sheet when a magnetic field is applied to it. Red dots shows the top of the surface of the robotic sheet without a magnetic field.

Fig. 4.7 shows the result of this experiment. In this result, "0" shows the surface of the robotic sheet when the object was not installed and the magnetic field was not applied to it. The blue diamonds in the graph indicate the displacement of the robotic sheet when the magnetic field was applied to it and the object was put on the convex surface. The red quadrangles in the graph show the displacement of the robotic sheet when the magnetic field was not applied to it and the object was put on the surface. Without the magnetic field, the magnetic force in the ferrofluid was not generated as shown in Eq. 2.6, and the object on the surface of the robotic sheet

sunked as shown in the red quadrangles. Then, the measured displacement was less than 0. With the magnetic field, the mass of the object and the displacement of the convex surface of the robotic sheet were in a linear relationship as shown in the blue diamonds in Fig. 4.7. Moreover, it was elucidated that the displacement was less than 0 when the weight of the object to be installed exceeded 10 g. It was found that the object with the mass of more than 10 g can be raised with the shape change of the robotic sheet.

### 4.3 Magnetic responsiveness of a robotic sheet

The purpose of this experiment is to clarify the effect of the amount of the ferrofluid and the number of electromagnets on the magnetic response of the robotic sheet by measuring the displacement of the robotic sheet with respect to time. In this experiment, the quantity

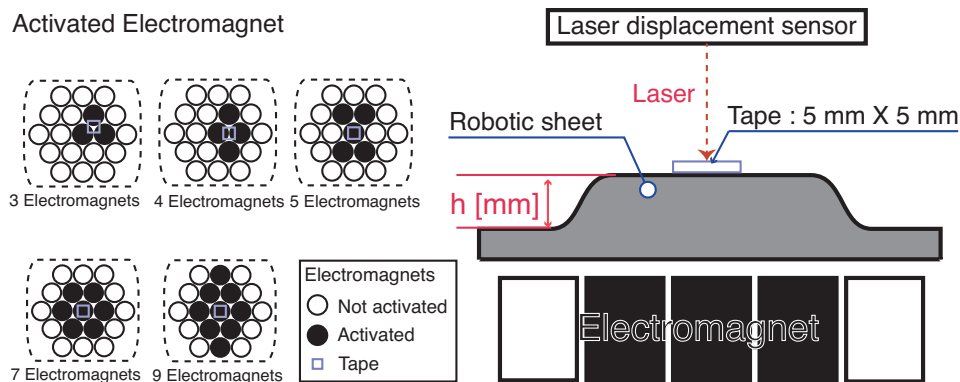


FIGURE 4.8: Experimental setup for verification of magnetic responsiveness of a robotic sheet. [ Tone et al., [91], p.2817 ]

inside the robotic sheet and the number of electromagnets to activate were changed, and the influence of these on the deformation and oscillation amplitude of the robotic sheet were clarified. The robotic sheet with PTFE films was used. The deformation of the robotic sheet was measured using a laser positioning meter with a sampling frequency of 500 Hz (OPTEx FA Co. Ltd., CD1-100N(J)) with a resolution of 30  $\mu\text{m}$ , as shown in Fig. 4.8. "h" in Fig. 4.8 is the indicator of this experiment, which shows the displacement before and after the deformation. The ferrofluid could not sufficiently reflect laser light. Thus, white tape with dimensions 5 mm  $\times$  5 mm was attached to the part of the PTFE film which was at the center of the deformed surface due to activation of the electromagnets. In the verification of displacement, the deformation was measured for 2000 ms from the start of activating electromagnets and from the start of demagnetizing electromagnets 30 s after the electromagnet was activated. Thirty



seconds was required to wait for saturation displacement. High deformation speed was required for object manipulation using the proposed system, so the displacement was measured for 2000 ms. It was verified whether noise affected the measurement, and this result is shown as "Reference" in the results. In the verification of the oscillation amplitude, it was measured 30 seconds after the pulsed magnetic fields were applied. The mean and the standard deviation of 40 peak-to-peak amplitudes were calculated.

### 4.3.1 Displacement with different amount of ferrofluid

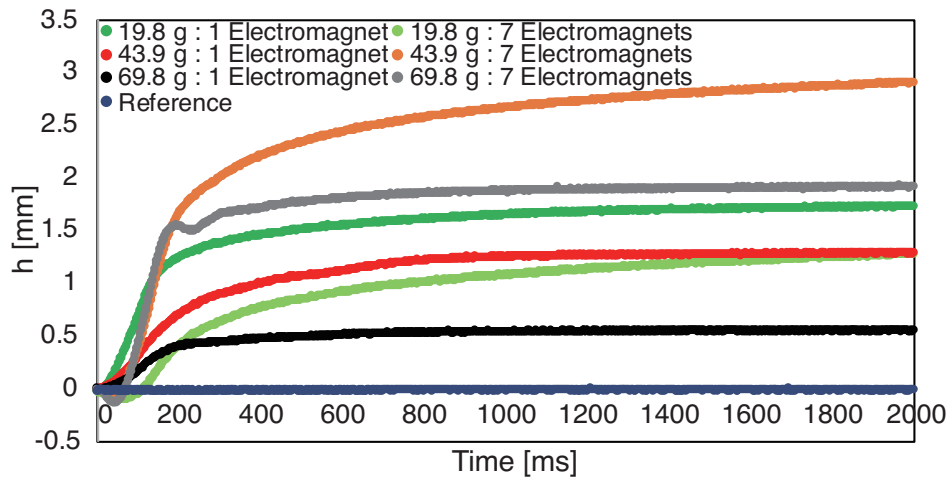


FIGURE 4.9: The process of lifting up the surface of the robotic sheet. The three types of the robotic sheet including a ferrofluid with mass of 19.8, 43.9, and 69.8 are used. Reference indicates that there is no large noise. Each result shows the average value measured seven times. [ Tone et al., [91], p.2818 ]

The three types of robotic sheets were used. The amount of ferrofluid contained in each robotic sheet was 19.8 g, 43.9 g, and 69.8 g, and the thickness of the robotic sheet was about 1 mm, 2 mm, and 3 mm, respectively. Displacement was measured with respect to time for each robotic sheet by activating one or seven electromagnets. The number of measurements in each condition was seven times, and the mean result is shown in Figs. 4.9 and 4.10. The robotic sheet lifted up and declined its surface drastically within 200 ms after the deformation started. By activating one electromagnet, the response speed and deformation increased as the volume of the ferrofluid in the robotic sheet decreased. Conversely, by activating seven electromagnets, even if the response speed of the robotic sheet with 69.8 g of ferrofluid was highest, the deformation of the robotic sheet with 43.9 g of ferrofluid was largest. This result indicates that the PTFE film prevented the deformation of the ferrofluid due to a lack of the

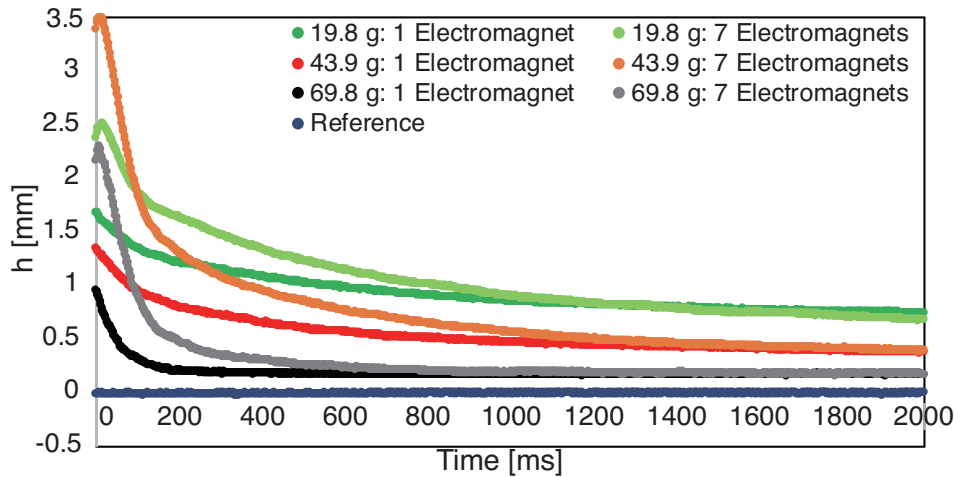


FIGURE 4.10: The process of declining the surface of the robotic sheet. The electromagnets are demagnetized 30 s after the saturation displacement. Reference indicates that there is no large noise. Each result shows the average value measured seven times. [ Tone et al., [91], p.2818 ]

wrinkles. In the declining result with one electromagnet, as the volume of the ferrofluid in the robotic sheet increased, the deformation speed increased. In the declining result with seven electromagnets, the deformation speed of 43.9 g and 69.8 g of the robotic sheet was similar. Although the displacement of 43.9 g of the robotic sheet was largest, the deformation speed increased as the amount of the ferrofluid increased. There are deviations in the declining result. This deviation decreased as the amount of the ferrofluid increased. When the content of ferrofluid is high, the thickness of the ferrofluid inside the robotic sheet increases, and the dispersion of ferrofluid is fast according to Hagen-Poiseuille flow.

### 4.3.2 Oscillation amplitude with different amount of ferrofluid

The same three types of robotic sheets were used, and the peak-to-peak amplitude was measured by applying a pulsed magnetic field with a frequency of 2, 5, 8, 10, 15, 20, 25, and 30 Hz to each robotic sheet from the seven adjacent electromagnets. The mean and the standard deviation of 40 peak-to-peak amplitudes for each frequency and robotic sheet is shown in Fig. 4.11. Until 8 Hz of the pulsed magnetic field, the peak-to-peak amplitude changed dynamically, and from 8 Hz, the peak-to-peak amplitude hardly changed.

By considering this and previous results, since high deformation speed and large deformation are required for a transportation, and large peak-to-peak amplitude is also required for mixing liquid on

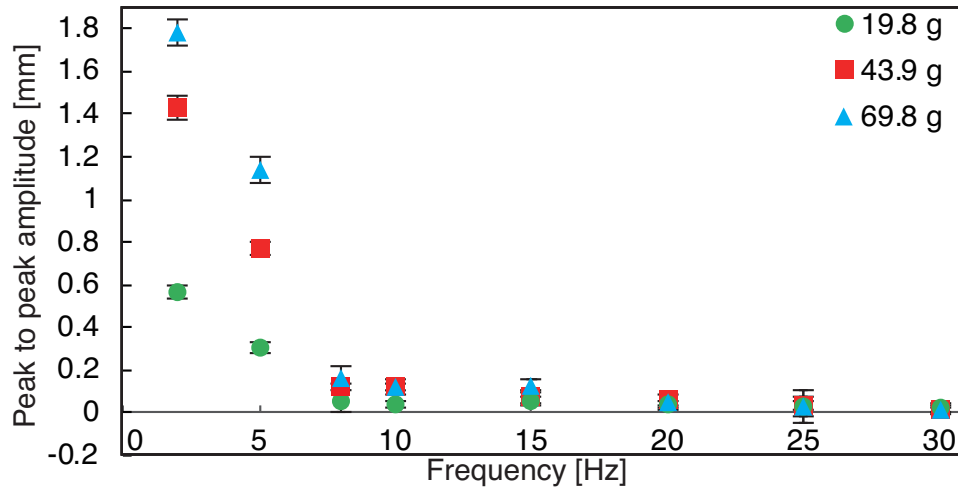


FIGURE 4.11: Peak-to-peak amplitude of the robotic sheet versus the frequency of the pulsed magnetic field. [ Tone et al., [91], p.2818 ]

the surface, the robotic sheet with 43.9 g of ferrofluid should be used for a liquid manipulation.

### 4.3.3 Displacement with different number of electromagnets

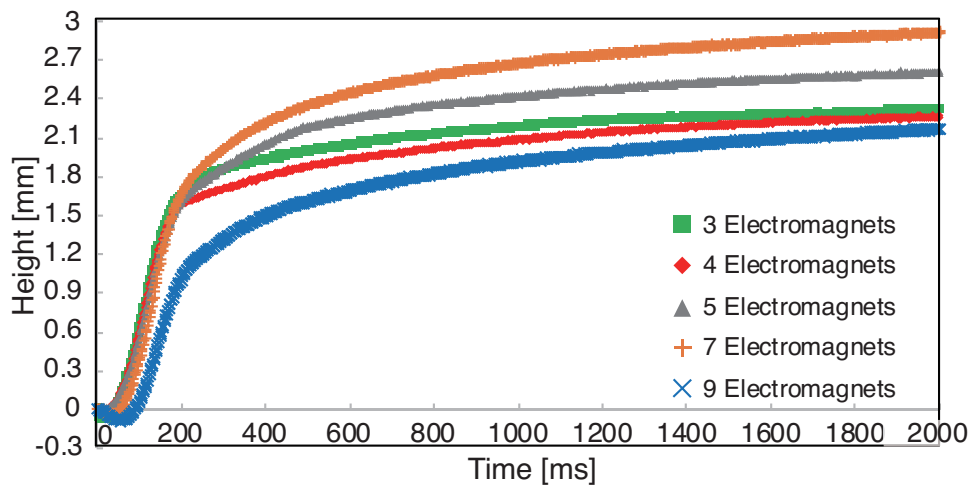


FIGURE 4.12: Response speed of a robotic sheet with different number of electromagnets: 3, 4, 5, 7, and 9 electromagnets. [ Tone et al., [91], p.2818 ]

The deformation speed of the robotic sheet was determined with 43.9 g of ferrofluid by changing the number of activating electromagnets: 3, 4, 5, 7, and 9 electromagnets. The deformation process was measured for 2000 ms and 7 times for each electromagnet configuration. The mean result is shown in Fig. 4.12. As the number of activating electromagnets decreased, the response speed increased.

The deformation speed with the 3 adjacent electromagnets was highest, and the displacement with 7 adjacent electromagnets was largest. When the proposed system moves an object, the surface should be immediately lifted up when magnetic fields are applied, and a high deformation speed of the robotic sheet is required. Therefore, in the proposed transport method, moving an object using three adjacent electromagnets is ideal.

#### 4.3.4 Oscillation amplitude with different number of electromagnets

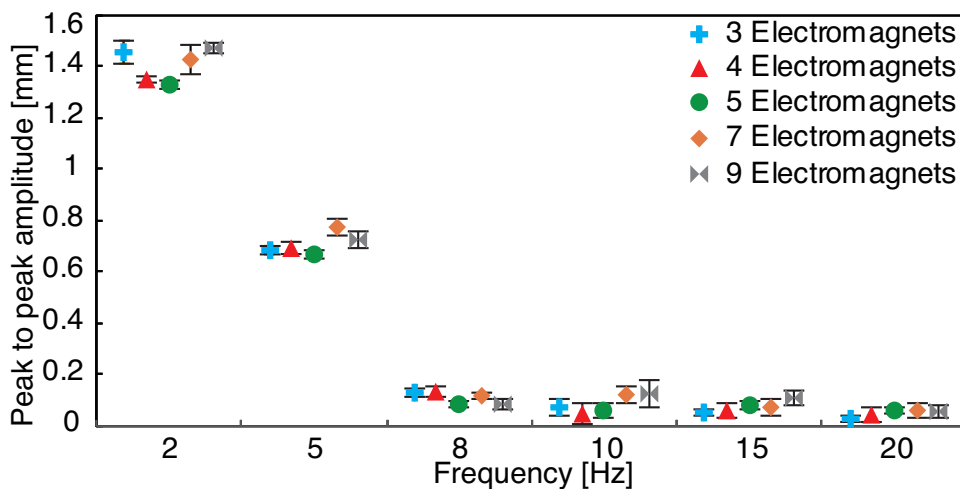


FIGURE 4.13: A peak-to-peak amplitude of a robotic sheet by replacing the number of activating electromagnets: 3, 4, 5, 7, and 9 electromagnets. [ Tone et al., [91], p.2819 ]

The peak-to-peak amplitude of the robotic sheet with 43.9 g of ferrofluid was found by changing the numbers of activating electromagnets: 3, 4, 5, 7, and 9 electromagnets. The mean and the standard deviation of 40 peak-to-peak amplitudes for each frequency is shown in Fig. 4.13. After 20 Hz, since there was no difference in amplitude, further amplitude increase was omitted. Even if the frequency of a pulsed magnetic field changes, there was no large difference on each peak-to-peak amplitude. From this result, even if the proposed system mixes some droplets and increases the number of activating electromagnets according to the size of a droplet to be mixed, a similar mixing result can be obtained.

## Chapter 5

# Feasibility verification of object manipulation with robotic sheet

In this chapter, object manipulation is realized using the robotic sheet. At first, using the robotic sheet with polyethylene films, two balls and a thin circular plate are transported. Next, using the robotic sheet with PTFE films, liquid manipulation is realized. In this liquid manipulation, a water droplet is used as the target object, and droplet transportation and mixing are conducted. Finally, the robotic sheet with polyethylene films is placed like a groove shape and a ball is moved within its inner surface. It is elucidated that the robotic sheet can move the target object in the several environment.

### 5.1 Flat transportation of two balls

#### 5.1.1 Experiment procedure

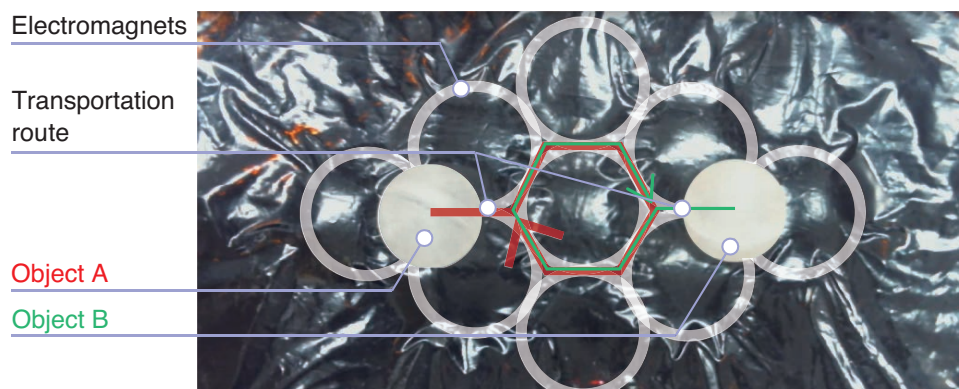


FIGURE 5.1: Conceptual transportation route of two balls. The red line indicates the route of "Object A", and the green line indicates the route of "Object B". [ Tone et al., [92], p.8 ]

The transportation of two spheres was verified by using the robotic sheet with polyethylene films. The robotic sheet was set on the aluminum plate, and the nine electromagnets were set under this plate.

Above the robotic sheet, the web camera was placed for recording the object transportation. Fig. 5.1 shows the planned path whose length was 280 mm. Two polystyrene balls (Object A and Object B in Fig. 5.1) with a diameter of 30 mm and mass of 2.9 g were used. These balls were simultaneously moved using the proposed method. The surface of the ball was rubbed with sandpaper to prevent the ball from clinging to the surface of the robotic sheet.

### 5.1.2 Result

The result of this experiment is shown in Fig. 5.2. Both the objects were transported in 11.9 s. The red and green lines show each object trajectory which are the trajectories of the center of each object and added to the video using an image processing. The robotic sheet completed the object transportation by repeating the proposed method. It was confirmed that the balls moved straight along with the direction of the downward slope when the downward slope was generated as shown in Fig. 5.2.(1.7s). Also, in the proposed method, each ball was hold with concave region generated by three adjacent convex surface during transportation, and it was confirmed that each ball stopped and changed its moving direction at the concave region. The results elucidated that the robotic sheet can transport an object which can be rotated such as a ball by deforming its shape.

## 5.2 Flat transportation of a thin plate

### 5.2.1 Experiment procedure

The transportation of a thin plate is verified by using the robotic sheet with polyethylene films. As the previous experiment, the robotic sheet was set on the aluminum plate, and the nine electromagnets were set under this plate. Above the robotic sheet, the web camera was set for recording the object transportation. Fig. 5.3 shows the planned path whose length was 200 mm. A thin circular plate with a diameter of 40 mm, depth of 3 mm, and weight of 15.2 g is used. With the height and slope of the convex surface on the robotic sheet, the plate cannot rotate. Also, due to the friction between the plate and the robotic sheet, the plate cannot slide on it. This plate was transported by using the proposed method.

### 5.2.2 Result

This experimental result is shown in Fig. 5.4. The robotic sheet transported the pate in 97 s along the planned path. The trajectory of the pate is represented as a red line which were the trajectory of the center of the plate and added to the video using an image processing. The plate almost moved along the transport path by using oscillation



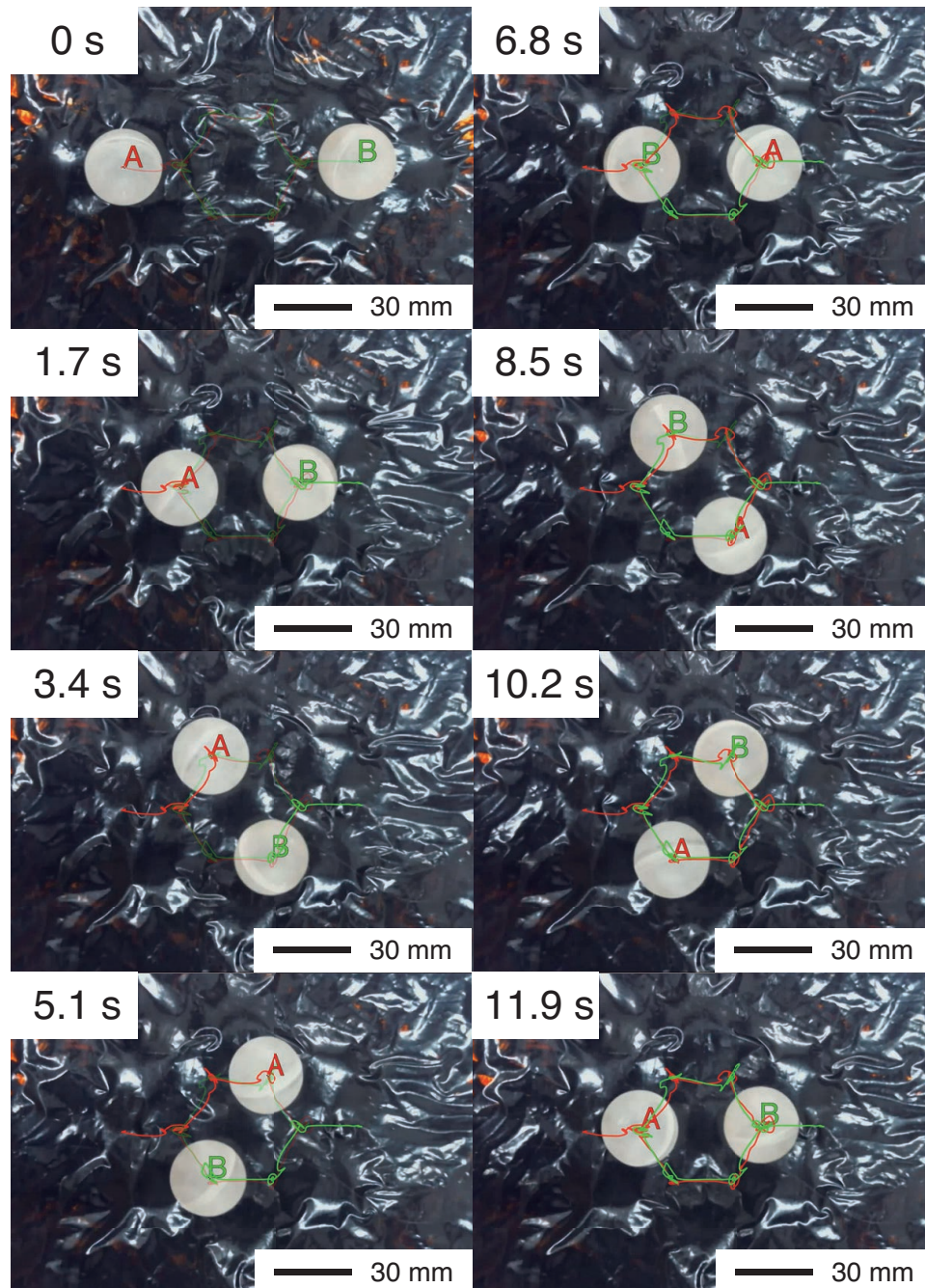


FIGURE 5.2: A thin plate transportation results on the two-dimensional surface. The red line shows the trajectory of object A, and the green line shows the trajectory of object B. The elapsed time is shown at the top left corner. [ Tone et al., [92], p.9 ]

of the robotic sheet and reducing the friction. In this experiment, the robotic sheet prevented the plate from veering off the path, and this operation can be shown at 56 s. It was confirmed that the movement direction of the plate was changed as shown in Fig. 5.4.(14s, 42s, 56s, and 70s), and the plate was moved along with the planned path by repeating the proposed method.

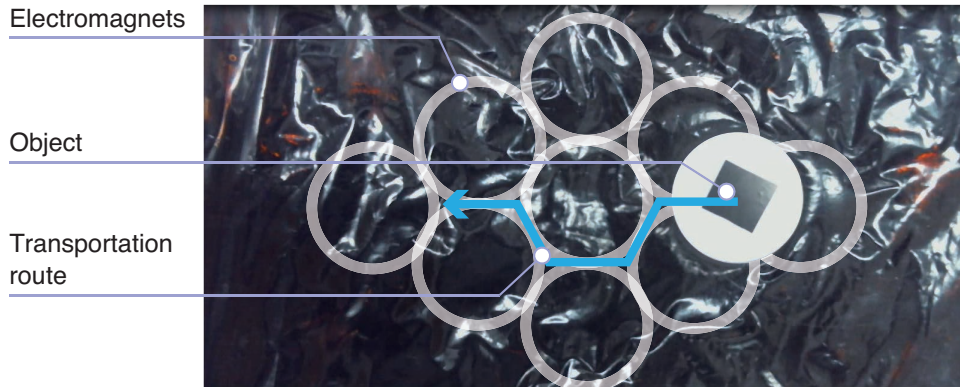


FIGURE 5.3: Conceptual transportation route of a thin plate transported from right to left. [ Tone et al., [92], p.9 ]

This and the previous results show that by vibrating and deforming the shape of the robotic sheet, the robotic sheet can transport objects whose motion is rotation or slide.

## 5.3 Liquid manipulation

In this section, as liquid manipulation, a droplet mixing and droplet transportation on the robotic sheet are realized. In the droplet manipulation field, droplets of reagents are moved and mixed for analyzing the chemical reaction. Therefore, the mixing and transportation are focused on among the droplet manipulation methods.

### 5.3.1 Liquid mixing

#### Experiment procedure

An effect of the oscillation amplitude and frequency of the robotic sheet containing 43.9 g of the ferrofluid on the result of the liquid mixing by changing the oscillation frequency: 5, 10, 15, 20, 25, and 30 Hz is verified. In this experiment, a process for liquid mixing is quantified and the mixing result and the peak-to-peak amplitude are compared. As the target liquids, water colored with either blue or white paint was used. The viscosity of water is about 1 mPa·s at 293.15 K. The volume ratio of water and paint was 100 : 1. Blue water with a mass of  $0.2027 \text{ g} \pm 0.0154 \text{ g}$  and white water with a mass of  $0.2042 \text{ g} \pm 0.0152 \text{ g}$  were used. The video of the mixing process is taken by a camera (Sony,  $\alpha 6000$ ) and the 7 adjacent electromagnets generate pulsed magnetic fields for oscillating the surface. When these fluids are combined, each fluid is localized in the combined liquid and the deviation of the saturation is significant. As the robotic sheet mixes these fluids, the deviation of the saturation decreases, as shown in Fig. 5.5. The RGB data of the target liquid is extracted from the video



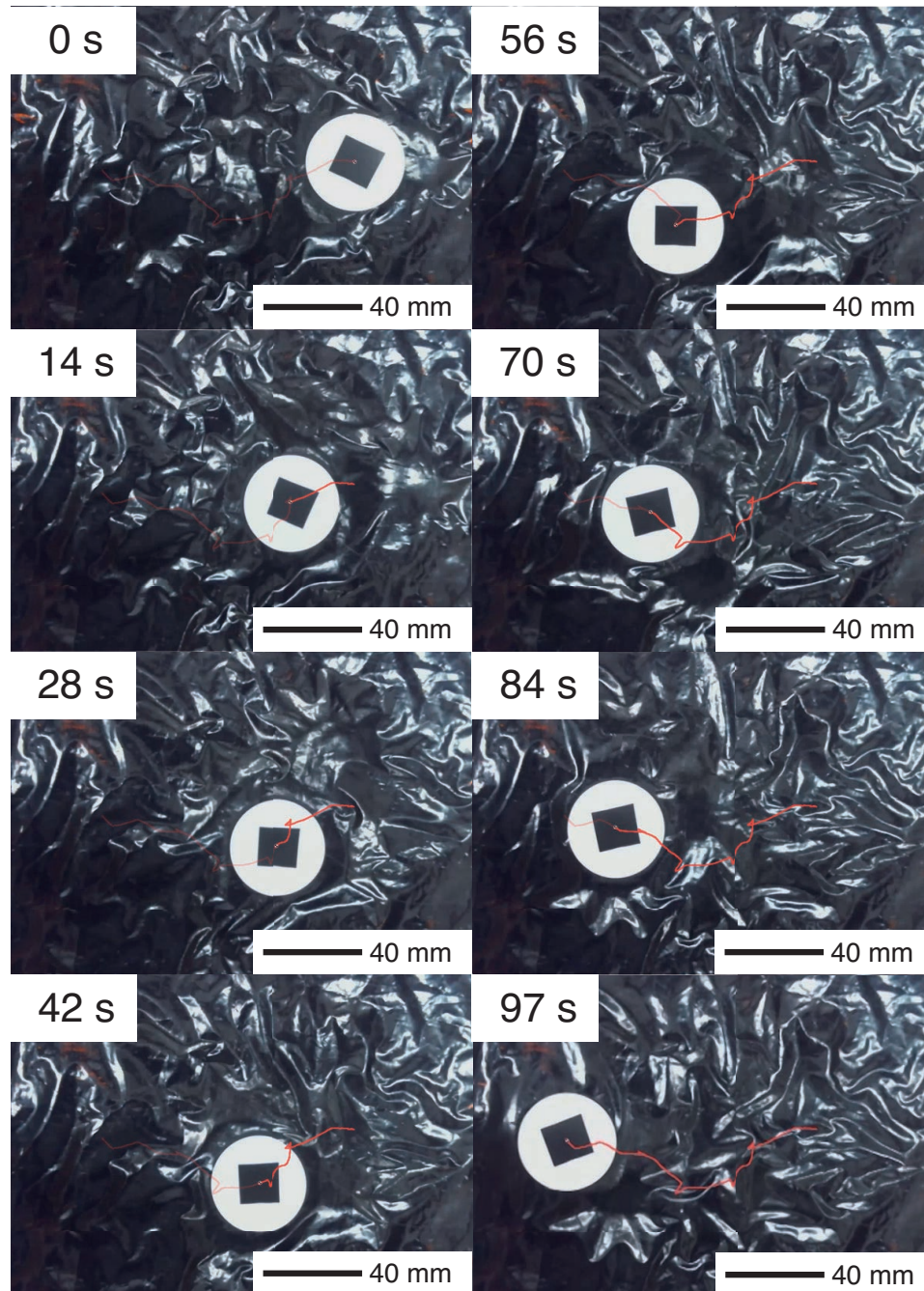


FIGURE 5.4: A thin plate transportation result on the two-dimensional surface. The red line shows the trajectory of the object transport. The elapsed time is shown at the top left corner. [ Tone et al., [92], p.9 ]

and it is converted to the HSV model. In the experiment of droplet mixing, in order to quantify the mixing process of droplets, the mixing degree of color is used as this experiment indicator. In this experiment, a white liquid droplet and a blue liquid droplet are mixed to be a light blue liquid. In order to quantify this process, the blue dispersion value is used. However, since the brightness of light affects the color of the droplet acquired by the camera, the RGB value varies



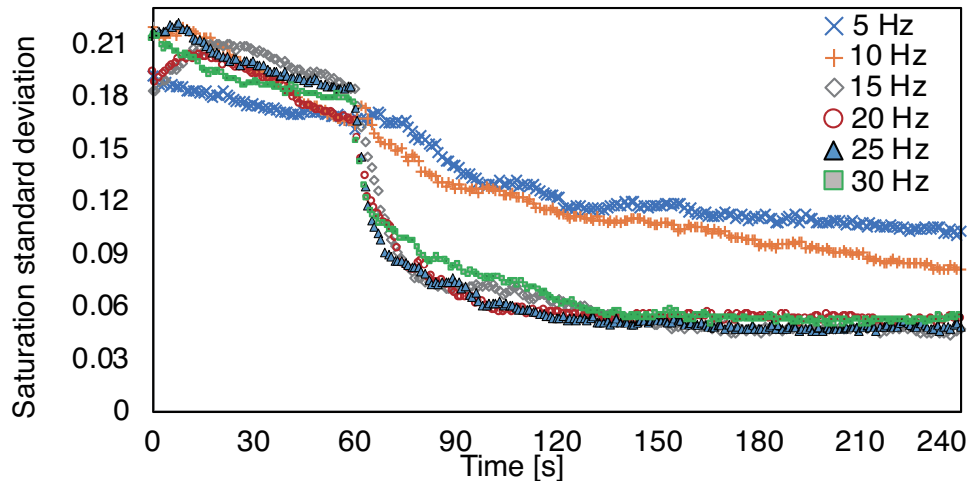


FIGURE 5.6: Standard deviation of saturation of colored liquid during mixing. The robotic sheet with 43.9 g of ferrofluid is used and frequency of a pulsed magnetic field is 5, 10, 15, 20, 25, and 30 Hz. [ Tone et al., [91], p.2819 ]

## Result

Fig. 5.6 shows the mean result of 7 measurements for each frequency, in which the combined value of the standard deviations of the saturations for each frequency are exhibited. At zero second, the white and blue water were combined on the robotic sheet, and until 60 seconds, the droplet remained combined. After that, the robotic sheet oscillated its surface and continued to mix until 240 seconds. In the oscillation frequency of 5 and 10 Hz, there was no difference in the way of decreasing the standard deviation before and after oscillation start. In the oscillation frequency from 15 to 30 Hz, the standard deviation of the saturation dramatically changed after 60 seconds, and the standard deviation of the saturation for each frequency is similar. Compared to Fig. 4.13, the 10 Hz amplitude is similar to the amplitude behavior at frequencies after 15 Hz but was found to be insufficient for mixing. It was clarified that the mixing of water used in the robotic sheet has a dominant influence on the mixing result rather than the amplitude.

### 5.3.2 Liquid transportation

#### Experiment procedure

The transportable volume range and velocity of droplets and the influence of the droplet volume on the accuracy of droplet transportation using the proposed method are clarified. As shown in Chapter. 2, the proposed system transports droplet by using a visual feedback method. Since the shape of the droplet is changed during the movement, the position of the center of gravity of the droplet moves.

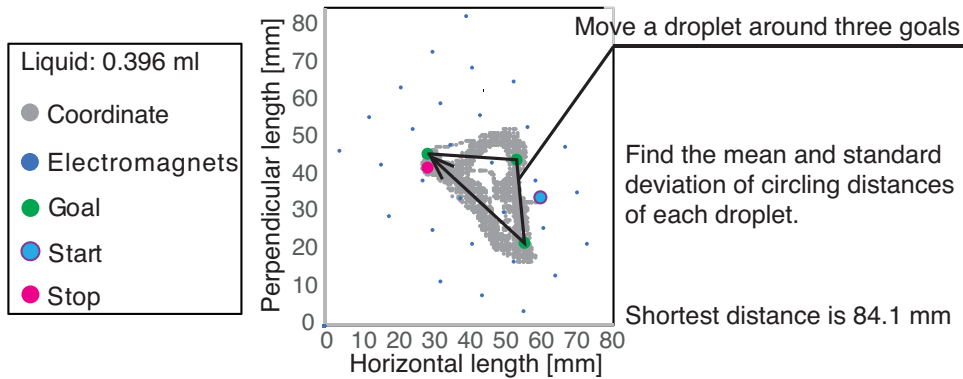


FIGURE 5.7: The robotic sheet continues to move the object so as to turn around three preset goals sequentially. This graph shows one of the experiment results. The average transportation speed is derived from the total transport distance of a droplet. The accuracy of a droplet transportation is obtained from the mean and standard deviation of the distance of each round. "Start" and "Stop" indicate the position of the droplet at the start or end of the transport experiment, respectively. "Goal" shows the preset goals. [ Tone et al., [91], p.2820 ]

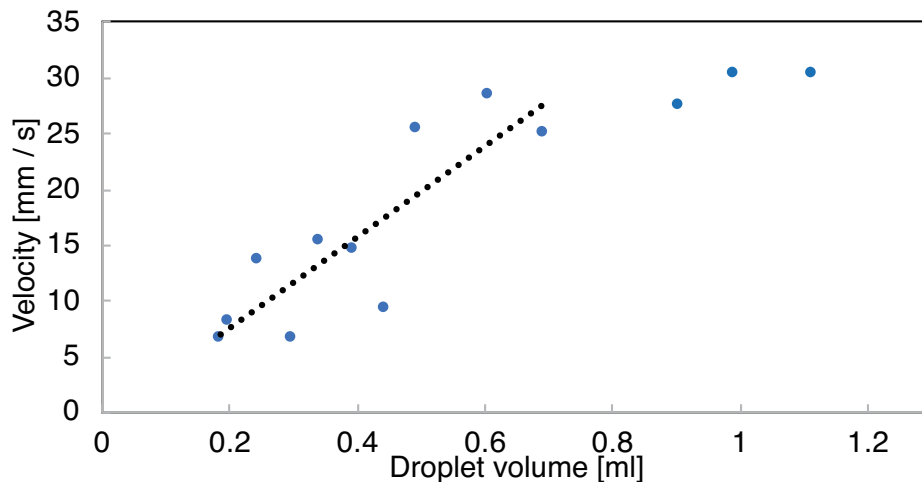


FIGURE 5.8: The average velocity of the droplets. [ Tone et al., [91], p.2820 ]

Even if the same droplet moves on the same slope, the droplet does not always move in the same direction. By using a visual feedback method, the robotic sheet activated the proper electromagnets along with the position of the droplet and moves it to the goals.

At first, the transportable volume range and velocity of the liquid was detected by using the volume of 0.174, 0.186, 0.198, 0.246, 0.297, 0.343, 0.396, 0.446, 0.495, 0.607, 0.693, 0.903, 0.990, 1.114, and 1.211



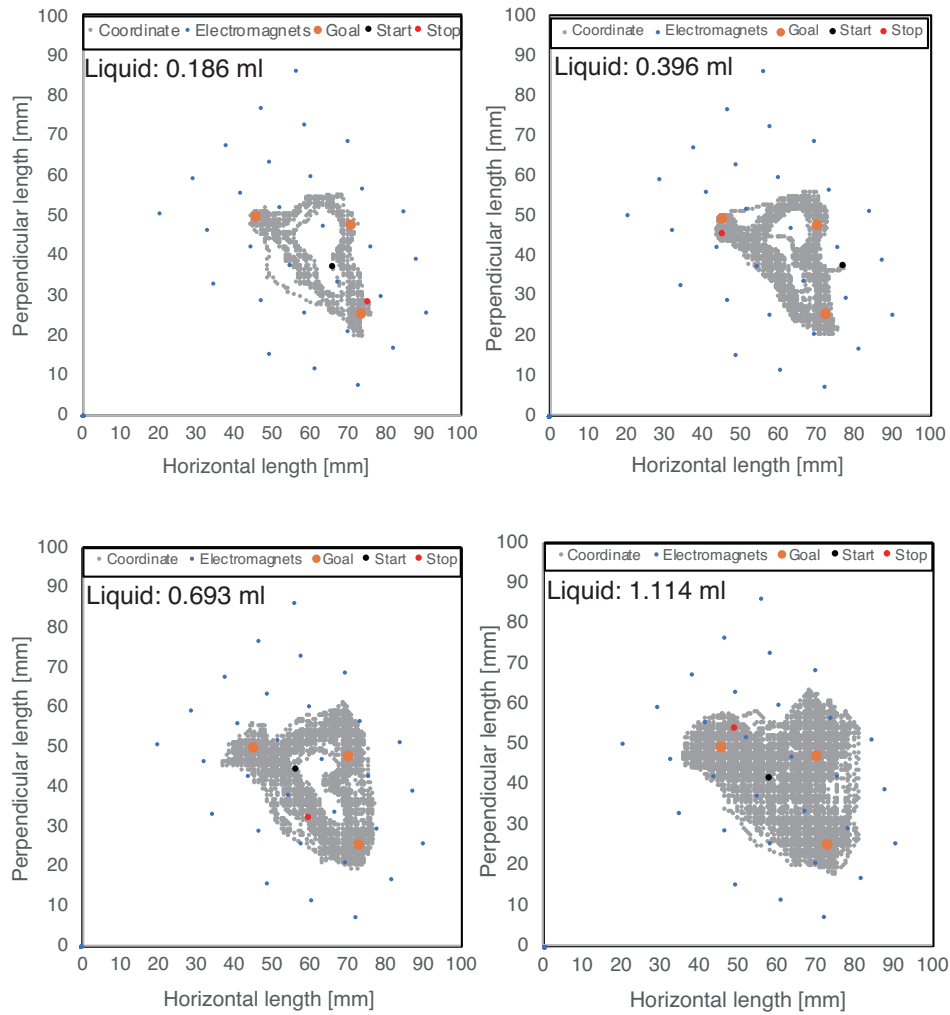


FIGURE 5.9: The trajectories of the droplet with a volume of 0.186, 0.396, 0.693, and 1.114ml. In each graph, gray dots are the trajectory, orange dots are the goal, black dot is the start point, and red dot is the point in which the target droplet stops after 300 s.

ml of a blue colored liquid, the same as the one used in the previous experiment. The volume of the droplet was converted from the mass of water obtained by subtracting the mass of the paint contained in the droplet from the mass of the colored droplet after measuring the mass of the colored droplet. The velocity was calculated by dividing the transportation length by the transportation time. The robotic sheet transported the droplet for 300 s. Three goal positions were set, and the system continued to move the droplet to all of the goal position for 300 s. The transportable volume and velocity of droplets were obtained through this experiment, as shown in Fig. 5.7. Then, the accuracy of the droplet transportation was clarified by using the volume of 0.297, 0.495, 0.693, and 0.990 ml of the same blue colored water, as shown in Fig. 5.7. The robotic sheet moved each droplet so as to turn around three preset goals sequentially for 180 s. This

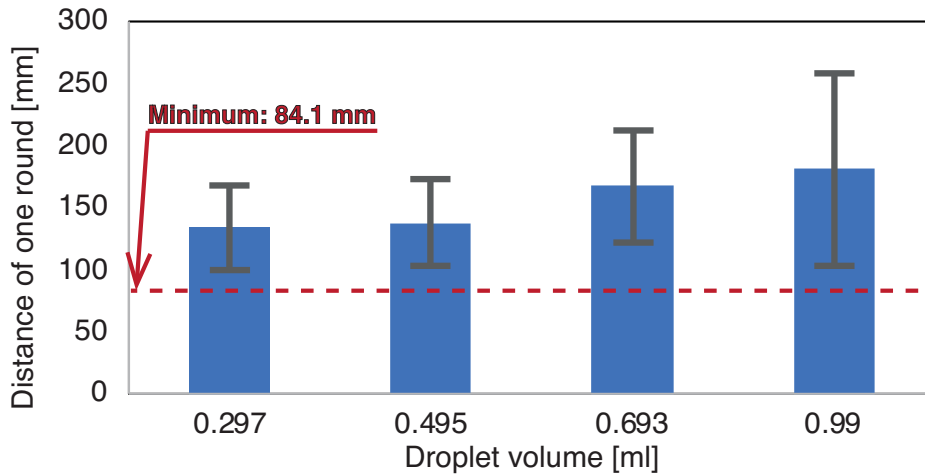


FIGURE 5.10: The average and standard deviation of the distance of one round of the transported droplet with a volume of 0.297, 0.495, 0.693, and 0.990 ml. [ Tone et al., [91], p.2820 ]

experiment was done five times for each volume of droplet and the mean and standard deviation of the distance of one round was calculated.

## Result

The transportable volume range and velocity of the liquid result is shown in Fig. 5.8. By using the proposed method, the droplets with the volume range of 0.186 to 1.114 ml were transported. The target droplet with 0.174 ml was not moved with the ferrofluid deformation and that with 1.211 ml moved out of the robotic sheet.

The trajectories of the transported droplet with the volume of 0.186, 0.396, 0.693, 1.114 ml are shown in Fig. 5.9. This result shows that it was difficult to transport the droplet through the shortest path connecting with 3 goals due to the deformation of the droplet with the increase of the volume of the droplet. This result also shows that even if the shape of the droplet changes, it is possible to transport droplets to the destination by using visual feedback.

The transport accuracy of the droplet with the volume of 0.297, 0.495, 0.693, and 0.990 ml is shown in Fig. 5.10. The shortest path of one round was 84.1 mm. As the droplet volume increased, the average and standard deviation of the distance of one round increased.

These results indicate that as the volume of a droplet increased, the velocity increased and the transportation accuracy decreased due to increasing the average and standard deviation of the distance of one round.



FIGURE 5.11: Initial state of the liquid application experiment. Transportation and mixing are conducted in one sequence. At first, a white droplet moves to a red droplet. After these droplet are combined, the combined droplet are mixed using oscillation. The mixed droplet moves to blue powder, and the droplet and powder is mixed.

### 5.3.3 Liquid application

#### Experiment procedure

Through the liquid mixing and liquid transportation experiments, the result showed that the robotic sheet was able to transport the droplets automatically and realized mixing of the droplets and the mixed droplet and powder on its surface. Based on the results, in this experiment, movement and mixing of droplets are realized in a series of sequences. Also, the effect of surface deformation of the robotic sheet due to transportation of a droplet on the other droplet and the feasibility of mixing of the droplet and powder were verified. This powder was used as non-liquid material. Fig. 5.11 shows the distribution of the droplets and powder. The target droplets were manually moved in this experiment. However, by introducing recognition systems for multiple objects such as [96], multiple object manipulation can be realized. As the target droplets, two types of liquid with a volume of 0.2 ml were used, which were colored white and red at a volume ration of water to paint of 50 : 1. As the power, blue food coloring is used.

#### Result

The results are shown in Fig. 5.12. At first, the white droplet was moved to the red droplet due to the surface deformation of the robotic sheet. After the white and red droplets were combined, vibration at a frequency of 20 Hz was applied to the combined droplet for 260 s, and the combined droplet was mixed. The mixed droplet with a volume of 0.4 ml was moved to the blue food coloring, and vibration at the same frequency was applied to the droplet with food coloring for

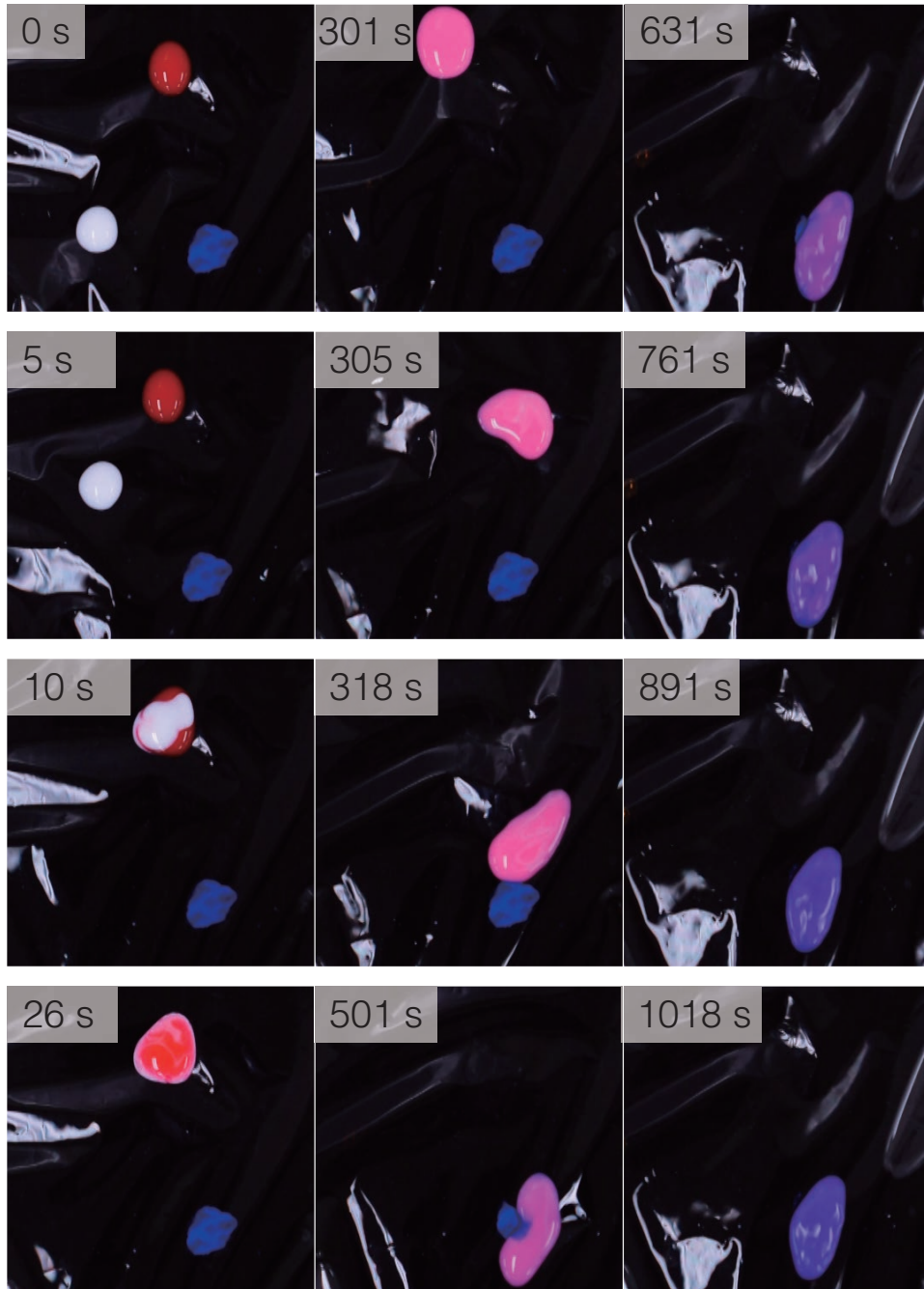


FIGURE 5.12: Liquid transport results. The upper left in each picture shows the experiment time. [ Tone et al., [90], p.780 ]

490 s. Both the transfer of the droplet and the mixing of the droplet and powder were realized as expected.





FIGURE 5.13: Channel transportation route. The robotic sheet is set on channel-like surface. By activating the electromagnets and changing the inner surface of the channel, the ball is moved from right to left. [ Tone et al., [92], p.9 ]

## 5.4 Channel transportation

### Experiment procedure

The transportation of a ball using a channel-like shape of the ferrofluid-based deformable robotic sheet is realized and the feasibility of the transportation is clarified even if the robotic sheet is set to adapt its shape to its surrounding environment. Fig. 5.13 shows the planned path whose length was 120 mm. As the target object, the capsule ball was used as the same ball in the flat transportation experiment. In this section, a pair of electromagnets facing each other is called an electromagnet pair. At first, the ball was set between the adjacent electromagnet pairs. By changing activation of the electromagnet pair one after the other in the moving direction of the ball, the ball was moved.

### Result

The result of this experiment is shown in Fig. 5.14. First, the robotic sheet activated the rightmost electromagnet pair and generated a convexity on each side of the object, as shown in Fig. 5.14. As the convex appeared on each side, the height of the bottom in the groove also increased because the ferrofluid inside the robotic sheet gathered around the activated electromagnet pair. Therefore, the ball moved in the advancing direction, as shown in Fig. 5.14.(2). After the object arrived at the next pair of electromagnets, the electromagnet pairs were switched and the new convexities were generated, as shown in Fig. 5.14.(3). However, the object did not move immediately as a sufficient amount of the ferrofluid did not gather to move the ball. After a few seconds, the object moved as shown in Fig.

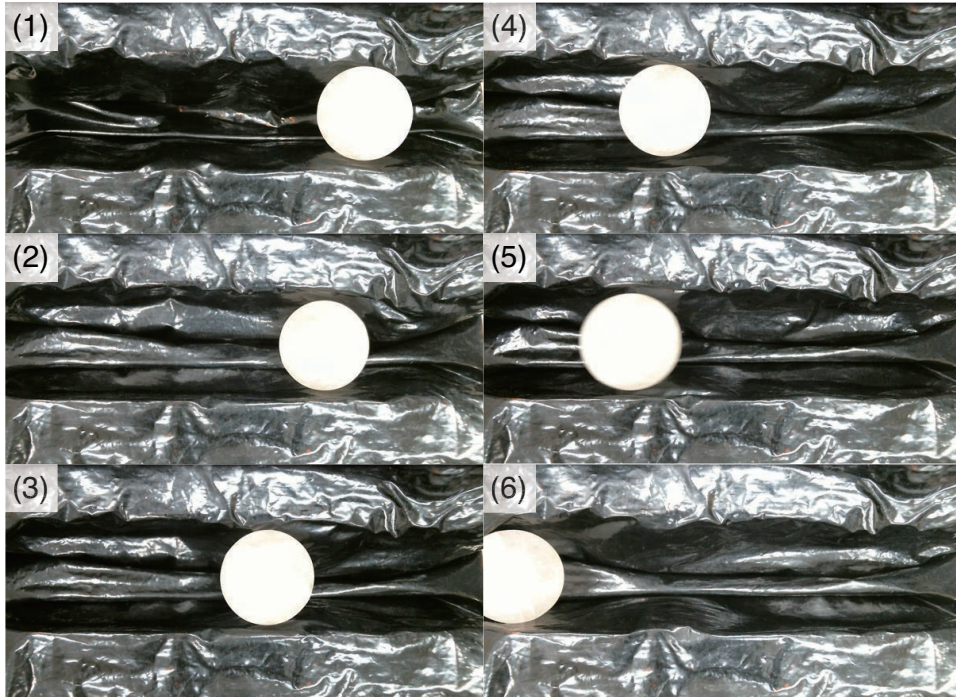


FIGURE 5.14: Ball transportation result through the channel ferrofluid-based robotic sheet. The frames are sequential, starting at "(1)" and ending at "(6)". [ Tone et al., [92], p.10 ]

5.14.(4) after which the robotic sheet completed the object transportation by repeating the proposed method.

# Chapter 6

## Discussion

In this chapter, the conducted experiments and ferrofluid-based deformable robotic sheet are discussed.

### 6.1 Surface deformation

Using 3D-CT, the deformed shape of the robotic sheet under the influence of magnetic field were measured. As the thickness of the polyethylene film increased by 0.1 mm, the mass of the film linearly increased and the ferrofluid could not support the film; thus, the ferrofluid thickness in the robotic sheet gradually decreased around the center of the convexity. The fluid thickness at the center of the convexity is shown in Fig. 4.5. As the ferrofluid thickness decreased and the surface of the robotic sheet approached the activated electromagnet, the intensity of the magnetic field at the fluid surface increased. The magnetic stress (Eq.(2.6)) applied to the film also increased with the decrease in the fluid thickness. The magnetic field is inversely proportional to the square of the length. The relationship between the thickness of the film and fluid is expected to be nonlinear. However, the result showed that this relationship was linear. Therefore, it is assumed that this relationship will be linearly approximated.

The width of the convexity was extended and its gradient was gentle, as shown in Fig. 4.3. Although the thickness of the ferrofluid in the robotic sheet sharply decreased over  $X = 20$  mm, its thickness with the film gradually decreased. The fluid pressure and film stiffness increased with an increase of the film, thus making the gradient gentle. Therefore, it is assumed that the tensile stress of the film affect the ferrofluid shape when a magnetic field is applied. The fluid shape is mainly determined through magnetic field distribution [43, 44]. By approximating the relationship between the thickness of the film and fluid linearly and combining the ferrofluid shape model and the magnetic field distribution, the shape of the robotic sheet can be estimated.

## 6.2 Force of the robotic sheet

The mass range of the object which the robotic sheet lifts up was clarified. The result elucidated that the robotic sheet could lift up the object with the mass of no more than 10 g with the electromagnet activated. This indicates that by activating several electromagnets simultaneously and lifting up the surface, the robotic sheet can lift up the object with the mass of more than 10 g. If the object is raised by activating several electromagnets, the surface area where the robotic sheet contacts the object to be lifted is required to be larger than the surface area raised by activating the electromagnet. Therefore, by measuring the mass and size of an object to be raised in advance, it is possible to estimate the number of activated electromagnets for transporting the object.

Also, the result showed that the relationship between the mass of the object and the displacement of the robotic sheet was linear. When an object is transported on the surface of the robotic sheet, its movement is realized by using the downward gradient of the convex as shown in Chapter 2. As the mass of the object increased, the displacement of the robotic sheet declined, and the surface decreased. The surface decreased by the weight of the object is the actual transport surface on which the object moves. Assuming that the relationship between the displacement of the robotic sheet and the mass of the object is linear at the other points on the surface of the robotic sheet, using the shape model of the robotic sheet, it is possible to estimate the actual transport surface on which the object moves. By using the height and gradient of this transport surface and the transport model shown by Chapter 2, it is possible to estimate the transport possibility, the transport speed, and the transport time of transport objects.

## 6.3 Responsiveness of the robotic sheet

The experiment results showed that the amount of the ferrofluid greatly influenced the magnetic responsiveness of the robotic sheet due to Hagen-Poiseuille flow. The robotic sheet containing 43.9 g of ferrofluid was the largest for displacement magnitude. As the amount of ferrofluid increases, the films wrapping a ferrofluid inhibit the deformation of the ferrofluid because the elastic modulus of the thin film greatly affects deformation. Therefore, by using a film with low elastic modulus it is possible to output large displacement even if it contains more ferrofluid than 43.9 g in the same size robotic sheet. In the magnetic response of the robotic sheet with different numbers of electromagnets, the smaller the number of electromagnets, the more displacement speed increased. The ferrofluid inside the robotic sheet was drawn in the direction of the magnetic field by activating multiple electromagnets simultaneously. The film

wrapping the ferrofluid was also drawn and the thickness of the portion of the robotic sheet where the magnetic field was applied temporarily decreased. The ferrofluid flow was prevented since the flow path narrows. Therefore, the displacement speed decreased. Therefore, the responsiveness of the robotic sheet decreases because the flow path narrows. Even if the number of activating electromagnets was changed, the oscillation amplitude of the robotic sheet after the steady state did not differ greatly. Also, increasing the amount of ferrofluid inside the robotic sheet reduced the flow path problem. From this, it was confirmed that the amount of ferrofluid dominantly affects the magnetic response of the robotic sheet than the number of activating electromagnets, and it was suggested that by using a film with low Young's modulus it is possible to obtain greater displacement and magnetic field responsiveness than the present system.

## 6.4 Flat transportation

On the flat surface, the movement of the object was rotation or slide. In the transportation experiments of the flat transportation, two balls and a thin plates were selected as representative objects to perform these movements. The proposed system moved these object to the destination along the pre-defined transport path by repeating the transportation method. The results suggest that the system has the ability to transport several types of objects. When the robotic sheet handled the spherical objects, the robotic sheet controlled the movement of the objects by using the concave surface and downward slope. Also, when the robotic sheet handled the thin plate, the robotic sheet oscillated the surface and controlled the friction between the object and surface. Flexible objects are deformable and cannot rotate on the surface of the sheet as well as the thin plate while being transported. Therefore, it is assumed that the oscillating method is adopted for the transportation of the flexible objects.

## 6.5 Liquid mixing experiment

This experiment was done by solely using water droplets, and the viscosity of water is approximately 1.0 mPa·s. Mixing of liquids by vibration was realized by stirring the interior of the liquid by vibrations. The stirring inside the liquid depends on the viscosity of the liquid to be mixed. Therefore, liquids such as ethyl acetate having viscosity less than the viscosity of water can be mixed by the proposed method. When the viscosity of the liquid to be mixed increases, the liquid attenuates the influence of vibration as with the damper. In this case, since the magnitude of the amplitude increases by lowering the frequency of the pulsed magnetic field, mixing can

be realized by using low frequencies. As the amount of droplets increases, the contact area between the ferrofluid sheet and the droplets increases. Therefore, in order to apply vibration to the whole contact area, it is necessary to increase the number of electromagnets that output the pulsed magnetic field. Therefore, if the amplitude of the oscillation of the robotic sheet accompanying the increase of the electromagnet has a large difference, the result of mixing of the droplets will be different as the amount of the droplet increases. However, as shown in Fig. 5.6, even if the number of electromagnets is increased, there is almost no change in amplitude of vibration, and it was observed that the frequency of vibration has a greater influence on the result of mixing than the amplitude of vibration. Even if the amount of droplets is increased, similar mixing results can be obtained.

## 6.6 Liquid manipulation experiment

The velocity linearly increased until about 0.6 ml. As the volume of the target droplet increases, the shape of the droplet is collapsed and its diameter is larger than the electromagnet used in the liquid manipulation experiment. The droplets were in a state in which a plurality of droplets is combined into one droplet. The droplets were moved while deforming and the center of gravity of the droplet changed. This affected the velocity and accuracy of the droplet transportation. However, this indicates that although the shape of a droplet changed variously during transportation, the robotic sheet had an ability to transport the droplet to the goals. Also, by introducing visual processing to recognize transparent liquids [97, 98], even if the target reagents are transparent, the proposed system can move them. The frequency of the feedback loop was 30 Hz. The frequency was not a limitation for the droplet velocity. Higher frequency can be achieved by using GPU and parallel processing. An image filter can be implemented in the proposed system for detecting transparent liquids, which may cause the calculation cost to increase. If the calculation cost increases and feed-back loop frequency decreases, by using a GPU and parallel processing, the same feed-back loop frequency can be maintained. Although the wrinkles are required to allow the ferrofluid deformation, they disturb the droplet movement with small volumes. To solve this problem, a thin film which has a low Young's Modulus should be used. Then, by developing such films, development of new robotic sheets can be developed. In the droplet manipulation, there is also adhesive objects in the target transport object, such as blood. By using PTFE film as a thin film of the robotic sheet, it is possible to prevent adhesive substances from sticking to the surface of the robotic sheet.

The relationship to control the liquid movement is addressed. Fig. 6.1 shows the system state while transporting a droplet. A white object is a target droplet. The areas (e 1, e 2, e 3, e 4) surrounded by

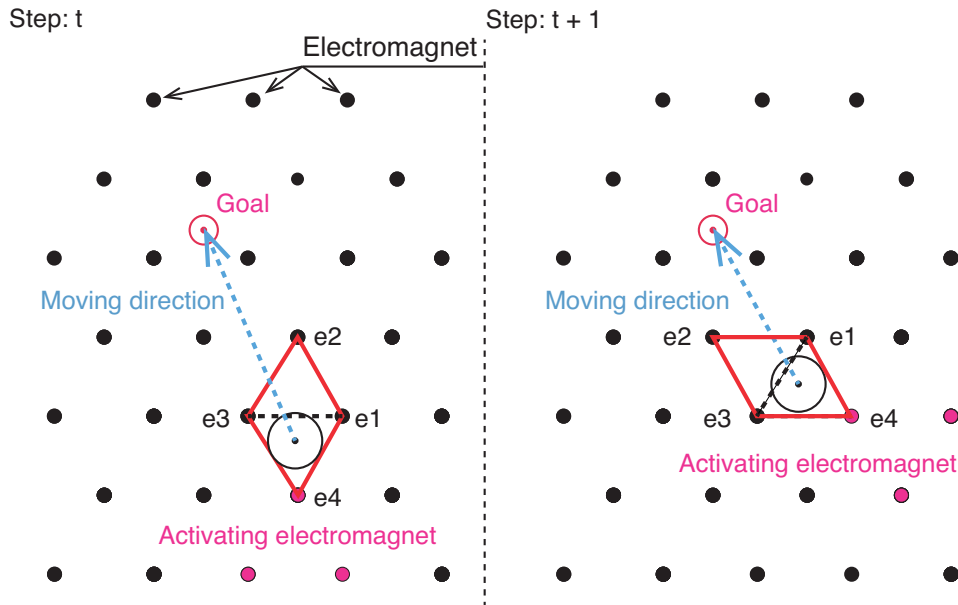


FIGURE 6.1: Left schematic image shows the system state at Step:  $t$ . Right schematic image shows the system state at Step:  $t+1$

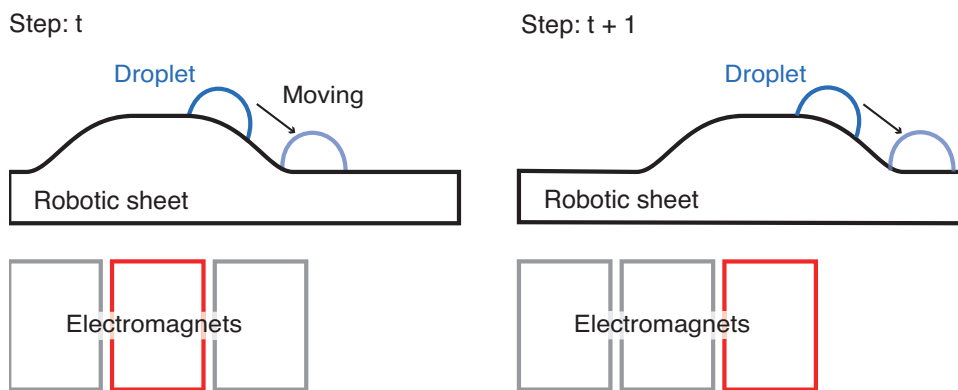


FIGURE 6.2: Object movement on the convex surface of the robotic sheet

the four electromagnets are divided into areas (Area:  $e_1, e_2, e_3$  and Area:  $e_1, e_3, e_4$ ) constituted by three electromagnets. The method of object movement proposed in this study discretely moves the center coordinates of the target object from Area:  $e_1, e_3, e_4$  to Area:  $e_1, e_2, e_3$ . By repeating this process, the object is moved to the target coordinates. The number of areas composed of the three electromagnets required up to Goal is represented by  $N$ . The minimum distance ( $L_{min}$ ) of the object is the straight line distance connecting the initial point of the object and Goal. Using this method, the object moves meandering, and the moving distance increases more than the minimum distance. The moving distance of the object is represented by  $L$ .  $L$  is assumed to be expressed as Eq. 6.1 with a factor  $J(V, \rho)$  multiplied by the volume  $V$  of the object and viscosity ( $\rho$ ) with respect to  $L_{min}$ .

From this, the average of the moving distance of the object by one traveling stroke can be expressed as shown in Eq. 6.2. Also, it is assumed that the shape change of the robotic sheet is a convex surface with no concavity as shown in Fig. 6.2, and the droplet slides down while maintaining a certain contact area with the roboticsheet. The initial state of Step:  $t + 1$  in Fig. 6.2 can be obtained from the equation of motion of the droplet as shown in Eq. 6.3 from the droplet velocity ( $v$ ) and height  $h$  as the initial slope  $\theta$  and frictional force  $R$  of the convex surface and the initial condition.

$$L = VL_{min} \quad (6.1)$$

$$L_{mean} = \frac{L_{min}}{N} \quad (6.2)$$

$$\rho V \frac{dv}{dt} = \rho V g \sin \theta - R \quad (6.3)$$

It is possible to obtain the movement time and the average speed from this motion equation and  $L_{mean}$  to the destination arrival.

## 6.7 Channel transportation

The robotic sheet moved the capsule ball in the channel by changing the inner surface. This result suggests that the system can apply a force to the object three-dimensionally by moving the ferrofluid. Therefore, it is assumed that the system can increase the object elevation by moving the convex surface upward due to the ferrofluid deformation. In this study, the robotic sheet was placed like channel-shape. By rounding the robotic sheet in a tubular shape, the robotic sheet can be a tube-type shape. More than four electromagnets are set around this tube-type robotic sheet for closing the inner space due to the convex surface of the robotic sheet. These electromagnets are named electromagnet group. This electromagnet group is equivalent to the electromagnet pair in the proposed method. If the electromagnet groups are set like the proposed method and activated one after the other in the moving direction of the object, the object in the tube-type robotic sheet is also moved. When one end of the tube-type robotic sheet is set higher than its another end which an object is put, it is possible to move the object through the tube-type robotic sheet. In this state, the system satisfies Eq.(2.15). A research related to this method presented transport systems that transport objects by the expansion and contraction of the inner diameter of a peristaltic pump [59, 99]. The transportation method generates only discrete waves, thus complicating object elevation in the channel because the system cannot generate the convexity between the electromagnets. By using a traveling wave, it is assumed that the continuous wave on the surface can be realized as shown in [61]. There are several research projects that use traveling waves. For this application, it is possible



to decrease the size of our system and still deform the shape of the robotic sheet.

## 6.8 Ferrofluid-based deformable robotic sheet

The characteristics of the robotic sheet was verified and the object manipulation: transportation and mixing was substantiated. From the results of the flat and channel transportation experiments, by applying a magnetic field to the ferrofluid sheet three-dimensionally, the ferrofluid sheet can apply the force to an object three-dimensionally. Therefore, it is assumed that the robotic sheet can be adopted to transport and grab the object such as a conventional manipulator. Owing to the fluidity of the ferrofluid, the robotic sheet does not damage the object and it is appropriate for the robotic sheet to operate the flexible materials.

In the droplet manipulation, the smaller the size of the droplet, the greater the effect of wrinkles on the movement of the droplet. In the current system, wrinkles are left intentionally so as not to disturb the deformation of ferrofluid due to the polytetrafluoroethylene (PTFE) sheet. Therefore, by using a film having Young's modulus smaller than that of PTFE and having water repellency and oil repellency equal to or higher than that of PTFE, it is possible to reduce the influence of wrinkle on the movement of the droplet.

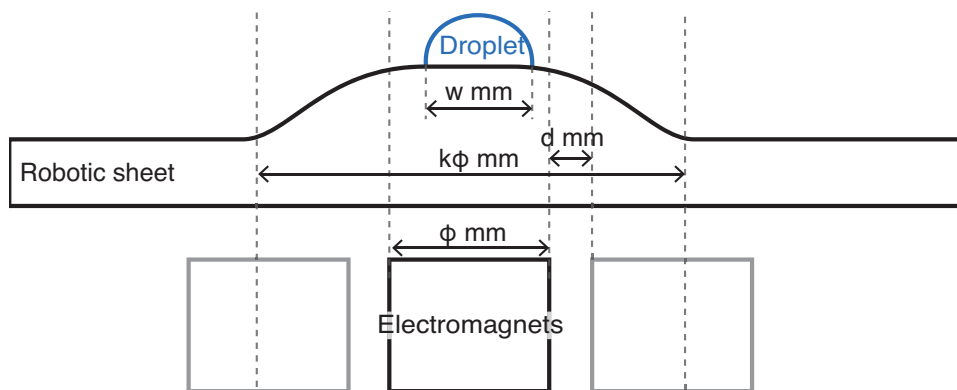


FIGURE 6.3: Schematic diagram of deformation of the robotic sheet

Fig. 6.3 shows the schematic diagram of deformation of the robotic sheet. It is a condition that mixing and movement of the droplet can be performed by one convex surface. The convex shape of the robotic sheet depends on the magnetic field distribution of the electromagnet. Therefore, a strict model is required to clarify the relationship between the electromagnet and the convex shape. At this time, the condition of the figure is simply considered. It is assumed that the diameter of the convex shape is simply  $k$  times the diameter ( $\Phi$  mm) of the electromagnet and the inclination of the convex shape starts from

the edge of the electromagnet. The diameter of the convex plane is  $k\Phi$  mm, the diameter of the contact area between the droplets and the robotic sheet is  $l$  mm, the distance between the electromagnets is  $d$  mm, and  $k$  is a constant.

In order to move an object to an area where an adjacent electromagnet can move the object by changing the surface shape of the robotic sheet, the size of the convex plane needs to be  $k\Phi > 2(\Phi + d)$ . It is assumed that mixing can be given to the droplet by moving the droplet to the central part of the electromagnet using a convex plane and droplet can move by detaching from the center. The influence of friction and surface between droplet and robotic sheet are not considered.

In the proposed system, since  $\Phi$  is 12 mm and  $k\Phi$  is 30 mm,  $k = 2.5$  and  $d = 1$  mm. These values satisfy the above conditions. It is assumed that the minimum size of the target liquid is 30 ml which Yang et al. succeeded in moving [82] and the contact area when the droplet contacts the robotic sheet is a circle. At this time the diameter of the circle is about 0.5 mm. Therefore, in order for the droplet of this size to be mixed and moved, the diameter of the electromagnet can be downsized down to approximately 0.5 mm. Since the magnitude of the magnetic field generated from the electromagnet is simply proportional to the number of turns of the polyurethane wire, by changing the length of the electromagnet, it is also possible to develop an electromagnet having a small diameter as described above. When the size of the system is reduced with keeping  $k = 2.5$ , the diameter of the convex plane is 1.25 mm. In the proposed system of this paper, the distance  $d$  between electromagnets is 1 mm, but in order to satisfy this condition,  $d$  should be smaller than 0.125 mm. The diameter of the polyurethane wire used for the electromagnet is 0.1 mm and the distance  $d$  between the electromagnets can be made smaller than 0.125 mm by installing the part supplying electric power to the electromagnet at the bottom of the electromagnet. Since the direct contact between the electromagnets interferes with the discharge of heat, a space of 0.1 mm is set. As a result, if 30 electromagnets are arranged as in the present situation, the area where the shape of the robotic sheet can be changed by the electromagnet becomes 2.9 mm in width and 3.1 mm in length.

## 6.9 Limitation of a ferrofluid-based deformable robotic sheet

In this paper, the transport object is limited to non-magnetic materials. Magnetic materials react to a magnetic field and stick to the surface of the robotic sheet, and the robotic sheet cannot move them using its deformation. The non-magnetic material includes various

materials, such as cells, blood, and liquid reagents, used in the several fields of chemical or biological analysis. Therefore, even if the target objects is limited to non-magnetic materials, assuming that the application fields of this research is still wide.

Also, In this research, sticky objects is not considered as transport objects of the robotic sheet. The adhesive force of the sticky objects depends on the surface properties of materials which the sticky object contacts with. By using a thin film which can reduce the adhesive force of the sticky object, it is possible to transport it using the proposed transport methods.



## Chapter 7

# Conclusion and Future Directions

In this study, the ferrofluid-based deformable robotic sheet and object manipulation using its deformation characteristics with magnetic field control have been described. Through the object manipulation experiment, the applicability to the droplet manipulation field was verified.

The robotic sheet had a layered structure of a ferrofluid and thin films and its shape was a sheet-type shape. The robotic sheet was flexible and adapted its shape to a target object and its surrounding environment. In the robotic sheet, the ferrofluid freely moved and gathered around a source of magnetic field. A ferrofluid can deform its shape under the influence of a magnetic field generated by the electromagnets. Using this deformation characteristics, the robotic sheet changed its surface shape and a convex appeared on it. An object moved on a downward gradient of the convex. By controlling the activation of the electromagnets, the robotic sheet transported target objects. Two types of the robotic sheet have been proposed. One used the polyethylene films as thin films, and the other used polytetrafluoroethylene (PTFE) films. The former was used for transporting two balls and a thin plate since the polyethylene films have a high robustness against breakage due to contact with the objects. The latter was used for transporting droplets since the PTFE films have a high water and oil repellency. Also, the manipulation methods for a ball, a plate, and a droplet have been proposed.

Since the ferrofluid was encapsulated by thin films, these films affected the ferrofluid deformation characteristics. Therefore, the characteristics of the robotic sheet was verified. Three experiments were conducted: verification of the effect of the thin film on the ferrofluid deformation in the robotic sheet, measurement of the mass range of the object which the robotic sheet lifts up, and measurement of the magnetic responsiveness of the robotic sheet.

In the first experiment, The effect of the polyethylene sheet on the ferrofluid through 3D-CT were verified. It was found that the displacement of the ferrofluid in the robotic sheet under the influence of magnetic field decreased according to increasing thickness of

the polyethylene film. Also, the linear relationship between the ferrofluid displacement and the thickness of the polyethylene films was elucidated.

In the second experiment, the mass range of the object which the robotic sheet raised was measured. The capsule ball was used as the weight and its mass was changed from 3 g to 11 g. It was found that the robotic sheet could raise the object with the mass of no more than 10 g using one convex and the relationship between the object mass and the displacement of the robotic sheet was linearly approximated.

In the third experiment, the magnetic responsiveness of the robotic sheet was verified. The amount of the ferrofluid inside the robotic sheet and the number of the activated electromagnets were focused on, and these effect on the magnetic responsiveness of the robotic sheet were clarified. The amount of ferrofluid dominantly affected the magnetic response of the robotic sheet than the number of activating electromagnets, and it was suggested that by using a film with low Young's modulus, it is possible to obtain greater displacement and magnetic field responsiveness than the present system.

The object manipulation was also realized using the robotic sheet. In this paper, the robotic sheet was set on a flat and channel-like surface, and the object manipulation was realized.

On the flat surface, two balls and a thin plate was transported using the robotic sheet with polyethylene films and a droplet was transported and mixed using the robotic sheet with PTFE films using the proposed methods. Object movements on the robotic sheet are rotation or slides. Therefore, the ball and plate was used as the target object. By realizing these manipulation, it was found that the robotic sheet could handle several types of objects. In the manipulation of a droplet, droplet mixing and droplet transportation were realized. Through the droplet mixing, it was found that the oscillation frequency with 15 Hz was enough to mix colored droplets and the oscillation frequency largely affected the mixing result. Moreover, through the droplet transportation, it was found that colored droplets with the volume range of 0.186 to 1.114 ml were transported, and the transport accuracy decreased as the volume of droplets increased using the proposed method.

On the channel-like surface, a ball was moved through the channel of the robotic sheet with polyethylene films by changing the inner surface of the channel. This indicated that our system can apply force to the object three-dimensionally.

## 7.1 Contribution of this work

### 7.1.1 Contribution to Soft Robotics

Deformable / Inflatable robots such as our proposed system are called soft robots in Soft Robotic, and these soft robots have a high affinity

to its environment due to its softness and flexibility. As artificial intelligence has been developed, robot functions have also been sophisticated. Therefore, consumer robots have been gaining attention. Demand for these robots is not only in daily life but also in various fields such as welfare and medical fields. Therefore, it is assumed that scenes where robots supports our lives will increase. These robots help us by doing some tasks, such as cleaning, talking, and monitoring. However, these robots may cause unintended contact its surroundings. Conventional robots are composed of hard materials and easily damages its surroundings. Avoidance systems has also been researched. However, it is difficult to make a robot avoid unintentional contact completely. Then, a system that reduces the impacts on its surroundings due to the collision is necessary. Soft robots are flexible and have a high affinity to its surrounding environment. Therefore, even if the soft robots collide with its surroundings, the injury and damage can be reduced. However, Soft Robotics are still fundamental research fields. For developing this research fields, many researchers have tried to develop new soft robots by using flexible materials which had not been used for robot components. Through these research, knowledge such as development method and control method of soft robots accumulates. Then, I focused on constructing new materials and developing and control methods among them, and I developed a ferrofluid-based deformable robotic sheet and proposed its control method for object manipulation using its shape deformation. In Soft Robotics, some soft robots using a ferrofluid had already been proposed. However, a method of three-dimensionally handling solids or flexible objects by controlling the shape of the fluid inside the robot had not been elucidated. Therefore, I believe that this study contributes to Soft Robotics by revealing the new method.

In addition, since the robotic sheet was controlled by using a magnetic field generated by the electromagnets, it was possible to separate the robotic sheet from the electromagnet and remotely control it. By introducing these findings to Soft Robotics, this research can contribute to soft robots used in complex environments such as the body and disaster sites. Robots used in complex environments need to adapt their shape according to their environment. Soft robots are flexible and suitable for use in complex environments. On the other hand, it is difficult to separate the power source and the actuator like the conventional robotics, and the working area of the robot is limited. By introducing this method, it is possible to operate the actuator part remotely, and it becomes possible to extend the working area. this study will build a new soft robot technology that three-dimensionally manipulates objects, such as transportation, coalescence, and separation on a substrate. The achievement contributes to the technology for soft robotics and advanced control, opening new aspects for fluid-based three-dimensional manipulations.

### 7.1.2 Contribution to Human Informatics

At first, "Information", "Human information", and "Human Informatics" are defined as follows. "Information" has already been defined in Oxford Dictionaries [100]

**Information:** Facts provided or learned about something or someone.

**Human information:** Facts provided or learned about Human, such as stimuli given to human sense organs, a brain activity processing it, a biological signal, a psychology, an emotion, an action.

**Human informatics:** Academic field in all processes where human information is generated, collected, processed and utilized.

Human Informatics is an academic discipline to handle Human information. Human information includes psychological information which was hard to be used as information. This study has not used Human information. However, this research contributes to Human Informatics through contribution to Soft Robotics. As I explained in the previous section, soft robots have a high affinity to its environment due to its softness and flexibility. The high affinity to the surrounding environment of soft robots is an important function to be introduced for robots used in daily life. Also, since living creatures are composed of flexible materials as well as soft robots, many soft robots referring to the movement of living things have been studied. Softness and creature-like motions can give peace of mind to people, and robots with such functions are actually used in therapy [6, 101–103]. This indicates that soft robots can create peace of mind. Therefore, from the definition of Human Informatics, I assume that Soft robotics are strongly related to Human Informatics. Soft Robotics is still at the stage of basic research. For developing Soft Robotics, the materials, structure, and control methods are required. By developing a new soft robot and clarifying new control methods and operations, this study contributes to Soft Robotics. As the related research to Human Informatics, I believe that this study can also contribute to Human Informatics.

## 7.2 Future Directions

The application field of this study is the droplet manipulation field. The droplet manipulation field is applied to the chemical and biological analysis using droplet reagent for reducing the analysis time and reagent volume. This study elucidated that the robotic sheet can transport solid objects such as balls and a plate and a droplet by controlling its surface deformation. Conventional studies can manipulate and analyze a reagent with only one piece of equipment. A



reagent can be moved in channels on a plate by controlling the repellency of the plate surface or by adding additives such as electrolytes or magnetic powder to the reagent and using magnetic or electric fields [83–87]. The robotic sheet does not require channels or additives and moves droplets and solid objects; therefore, users can freely move a liquid and solid reagent and choose the mixing and analysis area without considering the effect of the additives on the reagent. In addition, since the main components of the proposed system are ferrofluid and electromagnet, simple mechanism for making the surface deformation can be achieved. Also, as I mentioned in Chapter 6, the size of the proposed can be 2.9 mm in width and 3.1 mm in length. By introducing this study to the droplet manipulation field, It is possible to spread reagents usable in droplet manipulation field from liquid to solid and to expand the applicable range of the droplet manipulation field.

Moreover, the robotic sheet can be controlled remotely by using a magnet or an electromagnet capable of generating a larger magnetic field. Although attenuation of a magnetic field should be considered, since it is possible to install only the robotic sheet at the action area, it becomes possible to use it in a complex environment, such as an internal body and disaster area.



# Bibliography

- [1] *Oxford Living Dictionaries. Robot.* <https://en.oxforddictionaries.com/definition/robot>. Accessed: 2018-12-12.
- [2] J. Wallén. *The History of the Industrial Robot*. Linköping, 2008.
- [3] D. Whitney. “Historical perspective and state of the art in robot force control”. In: *Proceedings. 1985 IEEE International Conference on Robotics and Automation*. Vol. 2. 1985, pp. 262–268.
- [4] *Softbank Robotics. Pepper.* <https://www.softbank.jp/robot/pepper/>. Accessed: 2018-12-05.
- [5] *Sony Corporation. Aibo.* <https://aibo.sony.jp>. Accessed: 2018-11-28.
- [6] *GROOVE X, Inc. LOVOT.* <https://lovot.life>. Accessed: 2018-12-22.
- [7] *iRobot Corporation. Roomba.* <https://www.irobot.com>. Accessed: 2018-11-28.
- [8] David Brougham and Jarrod Haar. “Smart Technology, Artificial Intelligence, Robotics, and Algorithms (STARA): Employees’ perceptions of our future workplace”. In: *Journal of Management & Organization* 24.2 (2018), 239–257.
- [9] C. D. Kidd, W. Taggart, and S. Turkle. “A sociable robot to encourage social interaction among the elderly”. In: *Proceedings 2006 IEEE International Conference on Robotics and Automation, 2006. ICRA 2006*. 2006, pp. 3972–3976.
- [10] T. Mukai, S. Hirano, H. Nakashima, Y. Kato, Y. Sakaida, S. Guo, and S. Hosoe. “Development of a nursing-care assistant robot RIBA that can lift a human in its arms”. In: *2010 IEEE/RSJ International Conference on Intelligent Robots and Systems*. 2010, pp. 5996–6001.
- [11] *AIZUK Keipu.* <http://www.aizuk.jp/keipu.php>. Accessed: 2018-12-11.
- [12] Daniel Claes and Karl Tuyls. “Multi robot collision avoidance in a shared workspace”. In: *Autonomous Robots* 42.8 (2018), pp. 1749–1770. ISSN: 1573-7527.
- [13] Marwah Almasri, Khaled Elleithy, and Abrar Alajlan. “Sensor Fusion Based Model for Collision Free Mobile Robot Navigation”. In: *Sensors* 16.1 (2016). ISSN: 1424-8220.

- [14] H. Wada, A. Kanazawa, K. Konada, Y. Wakabayashi, M. Kamioka, S. Kondo, J. Kinugawa, and K. Kosuge. "Dynamic collision avoidance method for co-worker robot using time augmented configuration-space". In: *2016 IEEE International Conference on Mechatronics and Automation*. 2016, pp. 2564–2569.
- [15] Carmel Majidi. "Soft Robotics: A Perspective—Current Trends and Prospects for the Future". In: *Soft Robotics* 1.1 (2014), pp. 5–11.
- [16] Cecilia Laschi, Barbara Mazzolai, and Matteo Cianchetti. "Soft robotics: Technologies and systems pushing the boundaries of robot abilities". In: *Science Robotics* 1.1 (2016).
- [17] J. Rossiter and H. Hauser. "Soft Robotics - The Next Industrial Revolution? [Industrial Activities]". In: *IEEE Robotics Automation Magazine* 23.3 (2016), pp. 17–20. ISSN: 1070-9932.
- [18] David Brougham and Jarrod Haar. "Smart Technology, Artificial Intelligence, Robotics, and Algorithms (STARA): Employees' perceptions of our future workplace". In: *Journal of Management & Organization* 24.2 (2018), 239–257.
- [19] Nicolas Franceschini, Franck Ruffier, and Julien Serres. "A Bio-Inspired Flying Robot Sheds Light on Insect Piloting Abilities". In: *Current Biology* 17.4 (2007), pp. 329–335. ISSN: 0960-9822.
- [20] T Ranzani, G Gerboni, M Cianchetti, and A Menciassi. "A bioinspired soft manipulator for minimally invasive surgery". In: *Bioinspiration & Biomimetics* 10.3 (2015), p. 035008.
- [21] Sangbae Kim, Cecilia Laschi, and Barry Trimmer. "Soft robotics: a bioinspired evolution in robotics". In: *Trends in Biotechnology* 31.5 (2013), pp. 287–294. ISSN: 0167-7799.
- [22] Chiwon Lee, Myungjoon Kim, Yoon Jae Kim, Nhayoung Hong, Seungwan Ryu, H. Jin Kim, and Sungwan Kim. "Soft robot review". In: *International Journal of Control, Automation and Systems* 15.1 (2017), pp. 3–15. ISSN: 2005-4092.
- [23] O. A. Araromi, I. Gavrilovich, J. Shintake, S. Rosset, M. Richard, V. Gass, and H. R. Shea. "Rollable Multisegment Dielectric Elastomer Minimum Energy Structures for a Deployable Microsatellite Gripper". In: *IEEE/ASME Transactions on Mechatronics* 20.1 (2015), pp. 438–446. ISSN: 1083-4435.
- [24] Michael T. Tolley, Robert F. Shepherd, Bobak Mosadegh, Kevin C. Galloway, Michael Wehner, Michael Karpelson, Robert J. Wood, and George M. Whitesides. "A Resilient, Untethered Soft Robot". In: *Soft Robotics* 1.3 (2014), pp. 213–223.

- [25] Robert F. Shepherd, Filip Ilievski, Wonjae Choi, Stephen A. Morin, Adam A. Stokes, Aaron D. Mazzeo, Xin Chen, Michael Wang, and George M. Whitesides. "Multigait soft robot". In: *Proceedings of the National Academy of Sciences* 108.51 (2011), pp. 20400–20403. ISSN: 0027-8424.
- [26] Daehoon Han, Cindy Farino, Chen Yang, Tracy Scott, Daniel Browe, Wonjoon Choi, Joseph W. Freeman, and Howon Lee. "Soft Robotic Manipulation and Locomotion with a 3D Printed Electroactive Hydrogel". In: *ACS Applied Materials & Interfaces* 10.21 (2018), pp. 17512–17518.
- [27] Cecilia Laschi, Matteo Cianchetti, Barbara Mazzolai, Laura Margheri, Maurizio Follador, and Paolo Dario. "Soft Robot Arm Inspired by the Octopus". In: *Advanced Robotics* 26.7 (2012), pp. 709–727.
- [28] P. Glick, S. A. Suresh, D. Ruffatto, M. Cutkosky, M. T. Tolley, and A. Parness. "A Soft Robotic Gripper With Gecko-Inspired Adhesive". In: *IEEE Robotics and Automation Letters* 3.2 (2018), pp. 903–910. ISSN: 2377-3766.
- [29] Eric Brown, Nicholas Rodenberg, John Amend, Annan Mozeika, Erik Steltz, Mitchell R. Zakin, Hod Lipson, and Heinrich M. Jaeger. "Universal robotic gripper based on the jamming of granular material". In: *Proceedings of the National Academy of Sciences* 107.44 (2010), pp. 18809–18814. ISSN: 0027-8424.
- [30] WILLIAM M. KIER and KATHLEEN K. SMITH. "Tongues, tentacles and trunks: the biomechanics of movement in muscular-hydrostats". In: *Zoological Journal of the Linnean Society* 83.4 (1985), pp. 307–324.
- [31] Kellar Autumn, Yiching A. Liang, S. Tonia Hsieh, Wolfgang Zesch, Wai Pang Chan, Thomas W. Kenny, Ronald Fearing, and Robert J. Full. "Adhesive force of a single gecko foot-hair". In: *Nature* 405 (June 2000), 681 EP –.
- [32] T. S. Majmudar, M. Sperl, S. Luding, and R. P. Behringer. "Jamming Transition in Granular Systems". In: *Phys. Rev. Lett.* 98 (5 2007), p. 058001.
- [33] A. Sadeghi, L. Beccai, and B. Mazzolai. "Innovative soft robots based on electro-rheological fluids". In: *2012 IEEE/RSJ International Conference on Intelligent Robots and Systems*. 2012, pp. 4237–4242.
- [34] M. Manti, V. Cacucciolo, and M. Cianchetti. "Stiffening in Soft Robotics: A Review of the State of the Art". In: *IEEE Robotics Automation Magazine* 23.3 (2016), pp. 93–106. ISSN: 1070-9932.

- [35] A. Pettersson, S. Davis, J.O. Gray, T.J. Dodd, and T. Ohlsson. "Design of a magnetorheological robot gripper for handling of delicate food products with varying shapes". In: *Journal of Food Engineering* 98.3 (2010), pp. 332–338. ISSN: 0260-8774.
- [36] B. Chen, Y. Zhu, J. Zhao, and H. Cai. "Design of a prototype of an adaptive soft robot based on ferrofluid". In: *2015 IEEE International Conference on Robotics and Biomimetics (ROBIO)*. 2015, pp. 511–516.
- [37] H. Leon-Rodriguez, V. H. Le, S. Y. Ko, J. Park, and S. Park. "Ferrofluid soft-robot bio-inspired by Amoeba locomotion". In: *2015 15th International Conference on Control, Automation and Systems (ICCAS)*. 2015, pp. 1833–1838.
- [38] R. Stanway. "Smart fluids: current and future developments". In: *Materials Science and Technology* 20.8 (2004), pp. 931–939.
- [39] J. David Carlson and Mark R Jolly. "MR fluid, foam and elastomer devices". In: *Mechatronics* 10.4 (2000), pp. 555–569. ISSN: 0957-4158.
- [40] M Ruzicka. *Electrorheological fluids: modeling and mathematical theory*. Springer Science and Business Media, 2000. ISBN: 9783540413851.
- [41] G.Z. Yao, F.F. Yap, G. Chen, W.H. Li, and S.H. Yeo. "MR damper and its application for semi-active control of vehicle suspension system". In: *Mechatronics* 12.7 (2002), pp. 963–973. ISSN: 0957-4158.
- [42] Seung-Bok Choi, Sung-Ryong Hong, Chae-Cheon Cheong, and Yong-Kun Park. "Comparison of Field-Controlled Characteristics between ER and MR Clutches". In: *Journal of Intelligent Material Systems and Structures* 10.8 (1999), pp. 615–619.
- [43] R.E Rosensweig. *Ferrohydrodynamics*. Cambridge University Press, 1985. ISBN: 0486678342.
- [44] T. B Jones. "Theory and application of ferrofluid seals". In: *B. Berkovsky, ed. (Hemisphere, 1988)* (1988), pp. 255–298.
- [45] C. W. Miller and E. L. Resler. "Magnetic forces and the surface instability in ferromagnetic fluids". In: *The Physics of Fluids* 18.9 (1975), pp. 1112–1118.
- [46] R. Kaiser, R.E. Rosensweig, and Avco Corporation. *Study of Ferromagnetic Liquid*. NASA CR 1407. National Aeronautics and Space Administration, 1969.
- [47] Karim S. Khalil, Seyed Reza Mahmoudi, Numan Abu-dheir, and Kripa K. Varanasi. "Active surfaces: Ferrofluid-impregnated surfaces for active manipulation of droplets". In: *Applied Physics Letters* 105.4 (2014), p. 041604.
- [48] Jie Yao, Jianjun Chang, and Decai Li. "A novel magnetic fluid shock absorber with levitating magnets". In: *Journal of Vibration Engineering* 19 (Feb. 2017), pp. 28–37.

- [49] Koichiro Hayashi, Wataru Sakamoto, and Toshinobu Yogo. "Drug Delivery: Smart Ferrofluid with Quick Gel Transformation in Tumors for MRI-Guided Local Magnetic Thermochemotherapy (Adv. Funct. Mater. 11/2016)". In: *Advanced Functional Materials* 26.11 (2016), pp. 1852–1852.
- [50] Ling-kun Min, Zhi-zheng Wu, Ming-shuang Huang, and Xiang-hui Kong. "A large stroke magnetic fluid deformable mirror for focus control". In: *Optoelectronics Letters* 12 (Mar. 2016), pp. 115–118.
- [51] A. Zeeshan, A. Majeed, and R. Ellahi. "Effect of magnetic dipole on viscous ferro-fluid past a stretching surface with thermal radiation". In: *Journal of Molecular Liquids* 215 (2016), pp. 549–554. ISSN: 0167-7322.
- [52] Hamid Reza Goshayeshi, Marjan Goodarzi, Mohammad Reza Safaei, and Mahidzal Dahari. "Experimental study on the effect of inclination angle on heat transfer enhancement of a ferrofluid in a closed loop oscillating heat pipe under magnetic field". In: *Experimental Thermal and Fluid Science* 74 (2016), pp. 265–270. ISSN: 0894-1777.
- [53] Lianmin Mao, Shengli Pu, Delong Su, Zhaofang Wang, Xianglong Zeng, and Mahieddine Lahoubi. "Magnetic field sensor based on cascaded microfiber coupler with magnetic fluid". In: *Journal of Applied Physics* 120.9 (2016), p. 093102.
- [54] D. E. Weidner. "Drop formation in a magnetic fluid coating a horizontal cylinder carrying an axial electric current". In: *Physics of Fluids* 29.5 (2017), p. 052103.
- [55] L. Wu, J. Cheng, W. Liu, and X. Chen. "Numerical Analysis of Electromagnetically Induced Heating and Bioheat Transfer for Magnetic Fluid Hyperthermia". In: *IEEE Transactions on Magnetics* 51.2 (2015), pp. 1–4. ISSN: 0018-9464.
- [56] Sachiko Kodama. "Dynamic ferrofluid sculpture: Organic shape-changing art forms". In: *Commun. ACM* 51 (June 2008), pp. 79–81.
- [57] Sachiko Kodama. *Kodama, S.* <http://sachikokodama.com/wp-site001/en>. Accessed: 2017-6-4.
- [58] Jun-qiu Wu, Zhi-zheng Wu, Xiang-hui Kong, Zhu Zhang, and Mei Liu. "Magnetic fluid based deformable mirror for aberration correction of liquid telescope". In: *Optoelectronics Letters* 13.2 (2017), pp. 90–94. ISSN: 1993-5013.
- [59] Norihiko Saga and Taro Nakamura. "Development of a peristaltic crawling robot using magnetic fluid on the basis of the locomotion mechanism of the earthworm". In: *Smart Materials and Structures* 13.3 (2004), p. 566.

- [60] K Zimmermann, V A Naletova, I Zeidis, V Böhm, and E Kolev. "Modelling of locomotion systems using deformable magnetizable media". In: *Journal of Physics: Condensed Matter* 18.38 (2006), S2973.
- [61] Koichi Tanaka, Yasushi Ido, and Kunitoshi Takuma. "Dispersive Waves in a Coupled System of Magnetic Fluid and Elastic Membrane." In: *JSME International Journal Series B* 41 (Aug. 1998), pp. 583–589.
- [62] Koichi Tanaka and Itaru Takagi. "Sheet Carrying Mechanisms Using Progressive Waves of a Membrane Sustained by Magnetic Fluids". In: *Transactions of the Japan Society of Mechanical Engineers Series B* 58 (Jan. 1992), pp. 2114–2118.
- [63] Y Ido, K Tanaka, and Y Sugiura. "Fluid transportation mechanisms by a coupled system of elastic membranes and magnetic fluids". In: *Journal of Magnetism and Magnetic Materials* 252 (2002). Proceedings of the 9th International Conference on Magnetic Fluids, pp. 344–346. ISSN: 0304-8853.
- [64] Carmel Majidi. "Soft Robotics : A Perspective — Current Trends and Prospects for the Future". In: 2013.
- [65] Stoll, W. et al. *WaveHandling*. <https://www.festo.com/group/en/cms/10225.htm>. Accessed: 2017-11-14.
- [66] M. Stommel and W. Xu. "Optimal, Efficient Sequential Control of a Soft-Bodied, Peristaltic Sorting Table". In: *IEEE Transactions on Automation Science and Engineering* 13.2 (2016), pp. 858–867. ISSN: 1545-5955.
- [67] M. Stommel and W. Xu. "Learnability of the Moving Surface Profiles of a Soft Robotic Sorting Table". In: *IEEE Transactions on Automation Science and Engineering* 13.4 (2016), pp. 1581–1587. ISSN: 1545-5955.
- [68] M. Stommel, Z. Deng, and W. L. Xu. "Probabilistic Automata Model of a Soft Robot for the Planning of Manipulation Tasks". In: *IEEE Transactions on Automation Science and Engineering* 14.4 (2017), pp. 1722–1730. ISSN: 1545-5955.
- [69] Seppe Terryn, Joost Brancart, Dirk Lefeber, Guy Van Assche, and Bram Vanderborght. "Self-healing soft pneumatic robots". In: *Science Robotics* 2.9 (2017).
- [70] You-you Yao and Jing Liu. "A polarized liquid metal worm squeezing across a localized irregular gap". In: *RSC Adv.* 7 (18 2017), pp. 11049–11056.
- [71] Arthur Hirsch, Hadrien O. Michaud, Aaron P. Gerratt, Séverine de Mulatier, and Stéphanie P. Lacour. "Intrinsically Stretchable Biphasic (Solid–Liquid) Thin Metal Films". In: *Advanced Materials* 28.22 (2016), pp. 4507–4512.



- [72] Rolf Pfeifer and Gabriel Gómez. "Morphological Computation – Connecting Brain, Body, and Environment". In: *Creating Brain-Like Intelligence: From Basic Principles to Complex Intelligent Systems*. Ed. by Bernhard Sendhoff, Edgar Körner, Olaf Sporns, Helge Ritter, and Kenji Doya. Berlin, Heidelberg: Springer Berlin Heidelberg, 2009, pp. 66–83. ISBN: 978-3-642-00616-6.
- [73] Rolf Pfeifer, Fumiya Iida, and Gabriel Gómez. "Morphological computation for adaptive behavior and cognition". In: *International Congress Series 1291 (2006). Brain-Inspired IT II: Decision and Behavioral Choice Organized by Natural and Artificial Brains*. Invited and selected papers of the 2nd International Conference on Brain-inspired Information Technology held in Hibikino, Kitakyushu, Japan between 7 and 9 October 2005, pp. 22–29. ISSN: 0531-5131.
- [74] Vincent C. Müller and Matej Hoffmann. "What Is Morphological Computation? On How the Body Contributes to Cognition and Control". In: *Artificial Life 23.1 (2017)*, pp. 1–24.
- [75] Dario Floreano, Ramon Pericet-Camara, Stéphane Viollet, Franck Ruffier, Andreas Brückner, Robert Leitel, Wolfgang Buss, Mohsine Menouni, Fabien Expert, Raphaël Juston, Michal Dobrzynski, Géraud L'Eplattenier, Fabian Recktenwald, Hanspeter Malhot, and Nicolas Franceschini. "Miniature curved artificial compound eyes". In: *Proceedings of the National Academy of Sciences of the United States of America* 110 (May 2013).
- [76] W. H. Miller, G. D. Bernard, and J. L. Allen. "The Optics of Insect Compound Eyes". In: *Science* 162.3855 (1968), pp. 760–767. ISSN: 0036-8075.
- [77] Jun Kyu Park and Seok Kim. "Droplet manipulation on a structured shape memory polymer surface". In: *Lab Chip* 17 (10 2017), pp. 1793–1801.
- [78] Thomas Schneider, Jason Kreutz, and Daniel T. Chiu. "The Potential Impact of Droplet Microfluidics in Biology". In: *Analytical Chemistry* 85.7 (2013), pp. 3476–3482.
- [79] Sera Shin, Jungmok Seo, Heetak Han, Subin Kang, Hyunchul Kim, and Taeyoon Lee. "Bio-inspired extreme wetting surfaces for biomedical applications". English. In: *Materials* 9.2 (Jan. 2016). ISSN: 1996-1944.
- [80] J. David Smith, Rajeev Dhiman, Sushant Anand, Ernesto Reza-Garduno, Robert E. Cohen, Gareth H. McKinley, and Kripa K. Varanasi. "Droplet mobility on lubricant-impregnated surfaces". In: *Soft Matter* 9 (6 2013), pp. 1772–1780.

- [81] Oliver J. Dressler, Richard M. Maceiczky, Soo-Ik Chang, and Andrew J. deMello. "Droplet-Based Microfluidics: Enabling Impact on Drug Discovery". In: *Journal of Biomolecular Screening* 19.4 (2014), pp. 483–496.
- [82] Xiaolong Yang, Xin Liu, Yao Lu, Jinlong Song, Shuai Huang, Shining Zhou, Zhuji Jin, and Wenji Xu. "Controllable Water Adhesion and Anisotropic Sliding on Patterned Superhydrophobic Surface for Droplet Manipulation". In: *The Journal of Physical Chemistry C* 120.13 (2016), pp. 7233–7240.
- [83] F. Mugele et al. "Microfluidic mixing through electrowetting-induced droplet oscillations". In: *Applied Physics Letters* 88.20 (2006), p. 204106.
- [84] S. Lee et al. "Ultrafast single-droplet bouncing actuator with electrostatic force on superhydrophobic electrodes". In: *RSC Advances* 6.71 (2016), pp. 66729–66737.
- [85] S. and others Padmanabhan. "Controlled droplet discretization and manipulation using membrane displacement traps". In: *Lab on a Chip* 17.21 (2017), pp. 3717–3724.
- [86] G. Huang et al. "Magnetically actuated droplet manipulation and its potential biomedical applications". In: *ACS Applied Materials and Interfaces* 9.2 (2017), pp. 1155–1166.
- [87] S. Damodara et al. "Magnetic field assisted droplet manipulation on a soot-wax coated superhydrophobic surface of a PDMS-iron particle composite substrate". In: *Sensors and Actuators B: Chemical* 239 (2017), pp. 816–823.
- [88] T. Tone, F. Visentin, and K. Suzuki. "Sheet type soft robot with magnetic fluid for object transportation". In: *2014 IEEE International Conference on Automation Science and Engineering (CASE)*. 2014, pp. 852–857.
- [89] T. Tone and K. Suzuki. "Deforming control for object transportation with ferrofluid-based sheet-type soft robot". In: *2015 IEEE International Conference on Automation Science and Engineering (CASE)*. 2015, pp. 1171–1176.
- [90] T. Tone and K. Suzuki. "A ferrofluid-based robotic sheet for liquid manipulation by using vibration control". In: *2017 13th IEEE Conference on Automation Science and Engineering (CASE)*. 2017, pp. 776–781.
- [91] T. Tone and K. Suzuki. "An Automated Liquid Manipulation by Using a Ferrofluid-Based Robotic Sheet". In: *IEEE Robotics and Automation Letters* 3.4 (2018), pp. 2814–2821. ISSN: 2377-3766.

- [92] T. Tone and K. Suzuki. "Surface Deformation Control of a Ferrofluid-Based Robotic Sheet for Object Handling". In: *IEEE Transactions on Automation Science and Engineering* (2018), pp. 1–12. ISSN: 1545-5955.
- [93] G. N. Hounsfield. "Computerized transverse axial scanning (tomography): Part 1. Description of system". In: *The British Journal of Radiology* 46.552 (1973), pp. 1016–1022.
- [94] J. Canny. "A Computational Approach to Edge Detection". In: *IEEE Transactions on Pattern Analysis and Machine Intelligence* PAMI-8.6 (1986), pp. 679–698. ISSN: 0162-8828.
- [95] Alvy Ray Smith. "Color Gamut Transform Pairs". In: *SIG-GRAPH Comput. Graph.* 12.3 (Aug. 1978), pp. 12–19. ISSN: 0097-8930.
- [96] Changjiang Yang, R. Duraiswami, and L. Davis. "Fast multiple object tracking via a hierarchical particle filter". In: *Tenth IEEE International Conference on Computer Vision (ICCV'05) Volume 1*. Vol. 1. 2005, 212–219 Vol. 1.
- [97] Yane Duan, Lars Helge Stien, Anders Thorsen, Ørjan Karlsen, Nina Sandlund, Daoliang Li, Zetian Fu, and Sonnich Meier. "An automatic counting system for transparent pelagic fish eggs based on computer vision". In: *Aquacultural Engineering* 67 (2015), pp. 8–13. ISSN: 0144-8609.
- [98] May Phyto Khaing and Mukunoki Masayuki. "Transparent Object Detection Using Convolutional Neural Network". In: *Big Data Analysis and Deep Learning Applications*. Ed. by Thi Thi Zin and Jerry Chun-Wei Lin. Singapore: Springer Singapore, 2019, pp. 86–93. ISBN: 978-981-13-0869-7.
- [99] Taro Nakamura and Kazuyuki Suzuki. "Development of a Peristaltic Pump Based on Bowel Peristalsis using Artificial Rubber Muscle". In: *Advanced Robotics* 25.3-4 (2011), pp. 371–385.
- [100] *Oxford Living Dictionaries. Information*. <https://en.oxforddictionaries.com/definition/information>. Accessed: 2018-12-27.
- [101] S. Nonaka, K. Inoue, T. Arai, and Y. Mae. "Evaluation of human sense of security for coexisting robots using virtual reality. 1st report: evaluation of pick and place motion of humanoid robots". In: *IEEE International Conference on Robotics and Automation, 2004. Proceedings. ICRA '04. 2004*. Vol. 3. 2004, 2770–2775 Vol.3.

- 
- [102] Neziha Akalin, Andrey Kiselev, Annica Kristoffersson, and Amy Loutfi. "An Evaluation Tool of the Effect of Robots in Eldercare on the Sense of Safety and Security". In: *Social Robotics*. Ed. by Abderrahmane Kheddar, Eiichi Yoshida, Shuzhi Sam Ge, Kenji Suzuki, John-John Cabibihan, Friederike Eyssel, and Hongsheng He. Cham: Springer International Publishing, 2017, pp. 628–637. ISBN: 978-3-319-70022-9.
- [103] T. Shibata. "An overview of human interactive robots for psychological enrichment". In: *Proceedings of the IEEE* 92.11 (2004), pp. 1749–1758. ISSN: 0018-9219.